PROJECT BALDY
AN INVESTIGATION OF AERODYNAMICALLY-INDUCED BALLOON MOTIONS

Prepared For
AEROSPACE ENVIRONMENT OFFICE
AERO-ASTRODYNAMICS LABORATORY
GEORGE C. MARSHALL SPACE FLIGHT CENTER, NASA
HUNTSVILLE, ALABAMA

FINAL REPORT

By: R.R. Rogers and H.G. Camitz

Contract No. NAS8-11140
CAL Report No. VC-1912-P-1
1 April 1965

CORNELL AERONAUTICAL LABORATORY, INC.
OF CORNELL UNIVERSITY, BUFFALO, N. Y. 14221

ERRATA

CAL Report No. VC-1912-P-1
Contract No. NAS8-11140

PROJECT BALDY

AN INVESTIGATION OF AERODYNAMICALLY-INDUCED BALLOON MOTIONS

By

R. R. Rogers

H. G. Camitz

April 1, 1965

Prepared for
AEROSPACE ENVIRONMENT OFFICE
AERO-ASTRODYNAMICS LABORATORY
NASA- GEORGE C. MARSHALL SPACE FLIGHT CENTER
HUNTSVILLE, ALABAMA

1. Pages 43 and 44 have been numbered incorrectly and interchanged. 43 should become 44 and vice versa.

2. On p. 52, in eq. (21), a^2 should be replaced by $(1.7)^2$.

3. On p. 4-3, the words "uniformly in α" should be added after eq. (4.8).

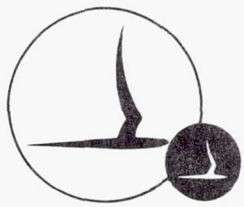

CORNELL AERONAUTICAL LABORATORY, INC.
BUFFALO, NEW YORK 14221

PROJECT BALDY

An Investigation of Aerodynamically-Induced Balloon Motions

FINAL REPORT

CONTRACT NO. NAS8-11140
CAL REPORT NO. VC-1912-P-1

1 APRIL 1965

Prepared by:

R. R. Rogers

R. R. Rogers

H. G. Camnitz

H. G. Camnitz

Approved by:

Roland J. Pilie, Asst. Head
Applied Physics Department

Prepared for:

AEROSPACE ENVIRONMENT OFFICE
AERO-ASTRODYNAMICS LABORATORY
GEORGE C. MARSHALL SPACE FLIGHT CENTER, NASA
HUNTSVILLE, ALABAMA

SUMMARY

Wind velocity data obtained by tracking an ascending balloon are subject to two kinds of error for which the balloon itself is responsible. The first error arises from the balloon's erratic behavior which is excited by aerodynamic forces encountered during ascent. It has been the purpose of the research reported here to measure the character of the erratic motions of several types of balloons and to assess the contribution of these motions to wind measurement error. The particular wind-measurement system considered was the FPS-16 radar/Jimsphere balloon system in use at Cape Kennedy, although the results on balloon behavior are independent of measurement techniques and can be used for assessing the erratic error contribution to any system using balloons as tracers. The second error arises from the inertia of the balloon, which limits its ability to respond to sharp wind changes. This program was not concerned with the second error.

Used in the experiments were Rose-type spherical balloons having diameters of 2 meters, 1 meter, and 2 feet, and Jimspheres with 2-meter diameter. An experiment consisted of releasing a balloon and tracking it during ascent with a Doppler radar. The radial velocity component of the balloon was recorded continuously; this measurement provided the information from which the erratic behavior could be inferred. Most of the data were obtained from the altitude interval between 1 and 6 km.

Velocity records from approximately 50 ascents were subjected to power-spectrum analysis. The spectra usually extended in frequency from 0 cps to about 0.3 cps. In many of these there was a marked separation between low frequency components, extending to about 0.1 cps, and high frequency components, centered at about 0.2 cps. In such cases it was determined that the high frequency components correspond to erratic motions

and the low frequency components are primarily indicative of balloon response to wind variability.

Detailed analysis of the apparently erratic velocity components indicated marked differences in the erratic behavior of the different kinds of balloons tested. No significant dependence on meteorological conditions was found, although the results were biased by the requirement of clear weather for the experiments. It was determined that the high frequency erratic motions of Jimspheres and 2-m Rose balloons are confined primarily to the horizontal plane. The Jimspheres ascend in an orderly helical trajectory while the 2-m Rose balloons have a more irregular behavior. The orbital diameter of the Jimsphere helical trajectory is about 3.5 m; during one complete orbit the balloon ascends approximately 25 m. The rms erratic velocity of the Jimsphere is approximately 1.7 m/sec, while that of the 2-m Rose balloon is approximately 2.6 m/sec within the altitude range of the experiments. It was determined that erratic motions of the Jimsphere would not be detectable with the FPS-16 radar tracking system as used at Cape Kennedy, but that the Rose balloon would contribute approximately 1 m/sec to the rms wind error.

The 2-ft Rose-type balloons were found to have weak erratic motions that are apparently of equal intensity in all directions. This behavior was noted for 1-m Rose-type balloons above an altitude of about 3 km. For lower altitudes, however, the 1-m balloons exhibit generally stronger erratic motions that are primarily horizontal. It is suggested that laminar flow, which is experienced by the 1-m balloons at high altitudes and by the 2-ft balloons, is associated with weak induced motions that are of the same intensity in all directions. Turbulent flow, which characterizes Jimspheres, 2-m balloons, and 1-m balloons at low altitudes, is associated with more intense erratic motions confined primarily to the horizontal.

TABLE OF CONTENTS

LIST OF ILLUSTRATIONS

LIST OF ILLUSTRATIONS (Con't)

LIST OF TABLES

I. INTRODUCTION

Because of the influence of small-scale wind irregularities on the performance of vertically rising vehicles, several techniques have recently been devised for measuring the wind profile with high resolution and accuracy. One such technique, the FPS-16 radar/spherical balloon system*, has been used at Cape Kennedy. In this system a high-precision radar is used to track the position of a pressurized lightweight mylar sphere during ascent. Descriptions of the technique are given by Leviton (1962) and by Scoggins (1963). Balloon position data are acquired at a rapid rate and smoothed over a short time period to remove the effects of possible random tracking errors. The data analysis procedure ultimately gives balloon horizontal velocity as a function of altitude with a height resolution of about 25 m.

The accuracy of the wind measurement with this high resolution system is limited by the radar tracking capability, the inertia of the balloon, and by any laterally-directed aerodynamic forces on the balloon that prevent it from moving exactly with the wind. Scoggins (1964a) showed that wind profiles obtained with the FPS-16/spherical balloon system display a wide scatter of points and that the amount of scatter was strongly dependent on balloon type. It appeared therefore that small scale erratic balloon behavior accounted for a significant portion of the scatter. Thus the ability of the FPS-16 radar to measure balloon motions surpassed the ability of some balloons to trace the wind. The full capability of the radar system cannot be realized until the erratic balloon behavior is understood and corrected.

---

*Smooth spherical balloons are termed Rose balloons and roughened spherical balloons are termed Jimspheres. Both have been used in the system.

The purpose of the research reported here was to describe the erratic behavior of different types of balloons under different meteorological conditions so that the errors which such behavior causes in the FPS-16 radar/balloon system could be evaluated. The approach was experimental, utilizing the CAL Doppler radar to measure the velocity of ascending balloons in the manner reported by McVehil et al. (1965). Jimspheres, 1-m and 2-m Rose-type balloons, and 2-ft spheres were investigated during the program. All were found to have erratic components of motion superimposed on their general response to the wind. The character of these erratic motions varied markedly with balloon type. In fact, the variation with balloon type was stronger than the effect of meteorological situation, at least over the range of conditions encountered in our experiments.

Concurrently with the experiments and data analysis activities, an intensive investigation was conducted of the relationship between erratic velocities and consequent errors in the balloon-measured wind. Results of this investigation made it possible to apply results of the Doppler radar experiments directly to the estimate of errors arising from spurious balloon behavior using either Rose-type balloons or Jimspheres. Additionally, this phase of the work removed many elements of conjecture which might otherwise have been unavoidable in the analysis.

A study of actual balloon dynamics, i.e. the physical processes governing balloon behavior, was not included in this investigation. As pointed out by Scoggins (1964a) and by MacCready and Jex (1964), even the drag coefficients of rising spheres can only be explained by plausibility arguments regarding the flow. It is clear that the erratic motions would be difficult to explain except by similar plausibility arguments. The data and conclusions of this report provide information about balloon kinematics that is necessary for ascertaining the limitations of balloons as wind tracers.

II. BACKGROUND

A useful means of analyzing wind profile data for application to space-vehicle technology is to compute the power spectrum of wind speed, considered as a random function of altitude (Scoggins, 1963). Such a spectrum constitutes a statistical description of the apparent turbulence encountered by a launch vehicle during ascent. The wind-profile spectrum computed from balloon data is different from the actual wind spectrum because of the inability of the balloon to trace the wind exactly. High frequency wind components may be suppressed by balloon inertia; spurious components are introduced by the erratic behavior. Additionally, the high frequency wind components are further suppressed by smoothing operations in the data reduction procedure. Since knowledge of the fine-grain wind structure can be a significant factor in space-vehicle technology, the accuracy and limitations of precise balloon-wind measurements have come under close scrutiny.

The limitations imposed specifically by inertial effects were treated by Reed (1963), who showed that the equation of motion for ascending spherical balloons could be linearized under certain conditions. He found that balloons respond essentially as low-pass filters to the wind field, and that a lag distance (analogous to time constant in circuit theory) can be used to characterize the filtering effect. For a balloon of 2-m diameter (the standard Rose balloon), it was determined that throughout most of the troposphere the lag effect is approximately equivalent to taking a running mean of the wind over a distance of 15 m. In a later analysis, Eckstrom et al. (1965) have shown that 2-m Jimspheres, because of their increased drag, have a considerably shorter lag distance,* corresponding in fact to a running mean distance of only 3 m. Thus, while the data in the FPS-16/balloon system are processed to yield 25 m resolution, the Rose balloon and particularly the Jimsphere balloon could be used for even finer measurements if inertia were the only limiting factor.

* Part of this disparity might also be accounted for by the fact that Eckstrom included an additional term in the equation of balloon motion.

There have been several recent investigations dealing specifically with the (aerodynamically-induced) erratic motions of balloons. Scoggins (1964b) showed the way these motions manifest themselves in wind data as measured using various balloon configurations. By comparing the data with wind measured by the smoke trail technique (Henry, et al., 1961), he obtained estimates of the power spectrum of erratic velocity fluctuations. In wave number space the spectrum was found to extend out to almost 40 cycles/2000 m with the peak component at about 12 cycles/2000 m. The ascent velocity, which for these balloons is about 7 m/sec, can be used to convert the spectrum from wave number space to frequency space. In terms of frequency, the spectrum extends a little beyond 0.1 cps and peaks at about 0.03 cps. Scoggins' analysis showed further that the erratic motions, presumably caused by aerodynamic lift forces and thus normal to the balloon's ascent velocity, have no preferred azimuth and consequently average out to zero over a long enough flight. From the data there were computed curves of drag coefficient versus Reynolds number R_e for the Rose balloons and Jimspheres. Over the Reynolds number range from 5×10^4 to 10^6, the Jimsphere drag coefficient was found to be relatively constant at a value of about 0.5. For the Rose balloon, the drag coefficient decreases rather uniformly from a value of 1 at low Reynolds number to about 0.3 at $R_e = 4 \times 10^5$. Thence the drag coefficient increases gradually until $R_e = 10^6$. It was pointed out that neither of these curves agrees with wind tunnel data on the drag coefficients of spheres. This observation is evidence of the complexity of flow about freely rising spheres. It was inferred that the uniformity of drag coefficient for Jimspheres was connected with their apparent small erratic velocity and large wake.

Additional investigations of drag effects were reported by MacCready and Jex (1964). Observations were made of the mean vertical velocity and the magnitude of the erratic lateral motions as spherical balls and balloons descended and ascended through water and air. In the subcritical Reynolds number regime ($R_e < 2.5 \times 10^5$) the motion was found to be a fairly regular helix with wavelength on the order of 12 times the diameter. In the super-

critical region ($R_e > 3.5 \times 10^5$) the motion tended to be an irregular, meandering spiral. It was concluded that erratic balloon motions could be reduced by operating in the subcritical region with smooth balloons or by operating at higher Reynolds numbers with balloons having surface roughness elements or other attachments.

In a pilot study to the present project, McVehil et al. (1965) measured the fine structure of the velocity fluctuations of two Rose-type balloons during ascent. By using a precision Doppler radar to track an ascending balloon, the velocity component of the balloon in the direction away from the radar was measured and recorded continuously. The short integration time required for these measurements revealed small-scale irregularities in motion that had not been previously observed. Power spectra of the record from a 1-m balloon indicated significant spectral components at frequencies as high as 0.4 cps, corresponding to wavelengths as short as 12 m. The spectrum from a 2-m (standard Rose) balloon extended only to about 0.3 cps, but had a much higher total variance than either of two spectra computed from the 1-m balloon data. The character of the individual spectra and the differences between them suggested that an appreciable part of their high frequency content arose from erratic motions. This observation of erratic velocity components at high frequencies is not inconsistent with Scoggins' observation, mentioned above, of erratic components extending out only to 0.1 cps. In Scoggins' spectrum, 0.1 cps corresponds to a wavelength of about 50 m which is in fact the smallest wavelength measurable in the FPS-16 radar/Jimsphere system. Components having higher frequencies could not be present in spectra measured with this system.* In the spectra given by McVehil, et al., low frequencies are also present but it cannot be readily determined whether they are erratic in origin or representative of real wind variability.

---

*Unless care is taken in data reduction, the high frequency erratic components can contribute at low frequencies in the calculated spectrum because of aliasing.

III. DESCRIPTION OF EXPERIMENTS

Experiments were conducted on 14 days extending from summer to winter, 1964. A total of 51 balloons of several varieties were used. During ascent or, on occasion, while tethered, the balloons were observed with Doppler radar and their velocity behavior was recorded. In this section the equipment, experimental procedure, and method of preliminary data reduction are described. Estimates are given of measurement errors.

A. Equipment

All of the measurements of balloon motions discussed in this report were made by means of a high precision pulse Doppler radar built by CAL. The radar, originally designed for investigating weather targets, is well suited for detailed observations of the motions of radar-reflective balloons in the troposphere. Some of its characteristics are listed in Table 1. For a more complete description of the radar and its associated equipment, the reader is referred to Tripp (1964).

Table 1. Radar Characteristics

Wavelength	3.22 cm
Peak power output	6 kw nominal
Antenna	8-ft parabola
Pulse duration	0.5 μsec
Pulse repetition frequency	5 kc
Beamwidth	0.9 degree

The measurement of balloon velocity proceeds by first isolating the balloon signal from background by means of a range gate. If the distance between balloon and radar is not changing, the frequency of the signal from the balloon will be the same as that of the transmitted signal. If the balloon is moving toward or away from the radar, the Doppler effect causes the balloon signal to be shifted in frequency by an amount f_D. This Doppler shift is related to the velocity V at which the balloon recedes from the radar by

$$f_D = 2V/\lambda$$

where λ is the radar wavelength. The basic measured quantity in the experiments is f_D. Because of the simple Doppler relationship, we can for convenience consider the "Doppler velocity" V to be the basic datum.

A frequency tracker or discriminator which generates a voltage proportional to f_D is used for the basic velocity measurement. This instrument requires a minimum signal of -95 dbm at the receiver for proper operation. In practice this means that 1-m spherical balloons can be tracked to a range of approximately 20 km. Larger balloons can be tracked to correspondingly greater distances.

Photographs of the equipment are shown in Fig. 1. The steps involved in measuring Doppler velocity are illustrated in Fig. 2.

B. Operating procedure

Several experimental runs, in which a balloon was released and tracked as far as possible, were conducted on each day selected for experiments. Tracking was accomplished optically with the aid of a telescope mounted coaxially with the radar antenna. The antenna was positioned manually by an observer at the telescope, as was the range gate position by an observer at the A-scope. Each run required about 30 min for completion. To minimize the effect of wind variability consecutive runs were conducted in quick succession. Usable velocity data were usually obtained in the slant range interval from 1 to 15 km.

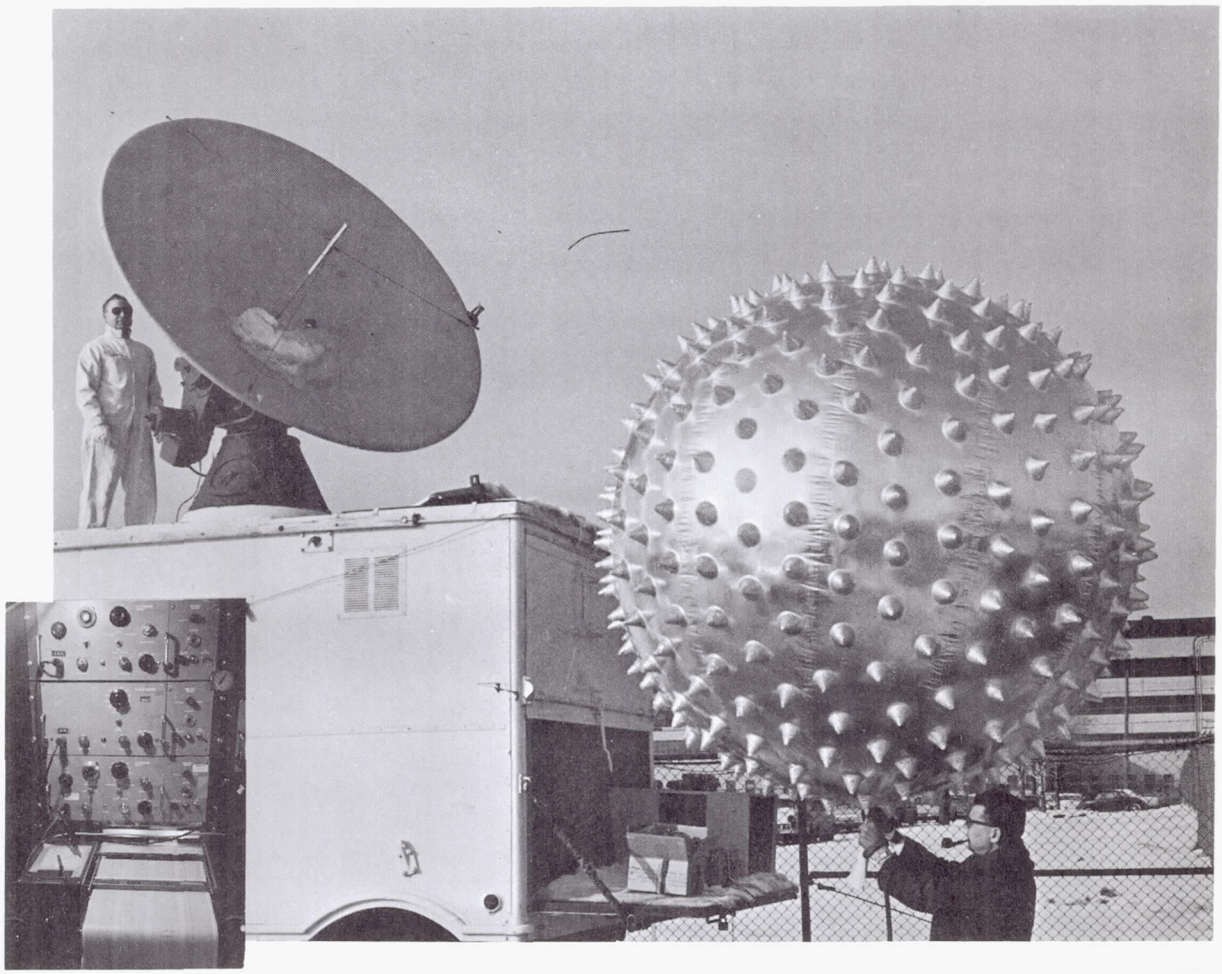

Fig. 1 The radar and associated equipment. Inset is the Sanborn recorder.

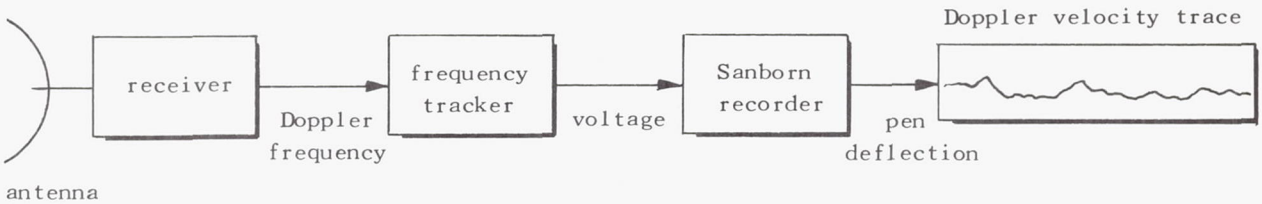

Fig. 2. Schematic diagram of steps in signal processing

The four-channel Sanborn chart constitutes the entire record from a run. Recorded by analog voltages are Doppler velocity, signal intensity, range gate position, and elevation angle. An occasional marginal note of azimuth is entered by the operator at the recorder. Signal intensity is recorded as evidence of radar performance. The balloon's altitude as a function of time was computed from the range gate position and the elevation angle. An example portion of the record from a 1-m balloon run is shown in Fig. 3.

Most of the experiments were designed to enable comparisons of the behavior of different kinds of balloons during ascent. The number of runs in an experiment was not always the same, but on the average was about four. Typically, these four releases might be a 1-m, a 2-m, a Jimsphere, and a 1-m balloon, in that order. This sequence would permit comparison of the behavior of three sizes and the bracketing by 1-m balloons would provide an indication of the importance of meteorological variability over the time of the experiment. Several experiments were designed for investigating a specific characteristic of one balloon rather than for comparative purposes. For example, on occasion balloons were released from a remote site so that radar elevation angle would vary over a wide range during the run. The directional properties of balloon motion were inferred from these runs by investigating the velocity fluctuations as a function of elevation angle. At other times the behavior of balloons on tether lines was observed in connection with certain radar calibration procedures.

C. Initial data reduction

For each balloon ascent, range and elevation angle data were read off the chart at equally spaced time increments of either 50 sec or 1 min. A table was then constructed of elevation angle, range, and computed altitude as a function of time. Additionally, ascent rate was computed from the altitude data. These tables provide an index from which, for any run, an altitude or elevation angle of interest can be located on the record by counting off the appropriate time from release.

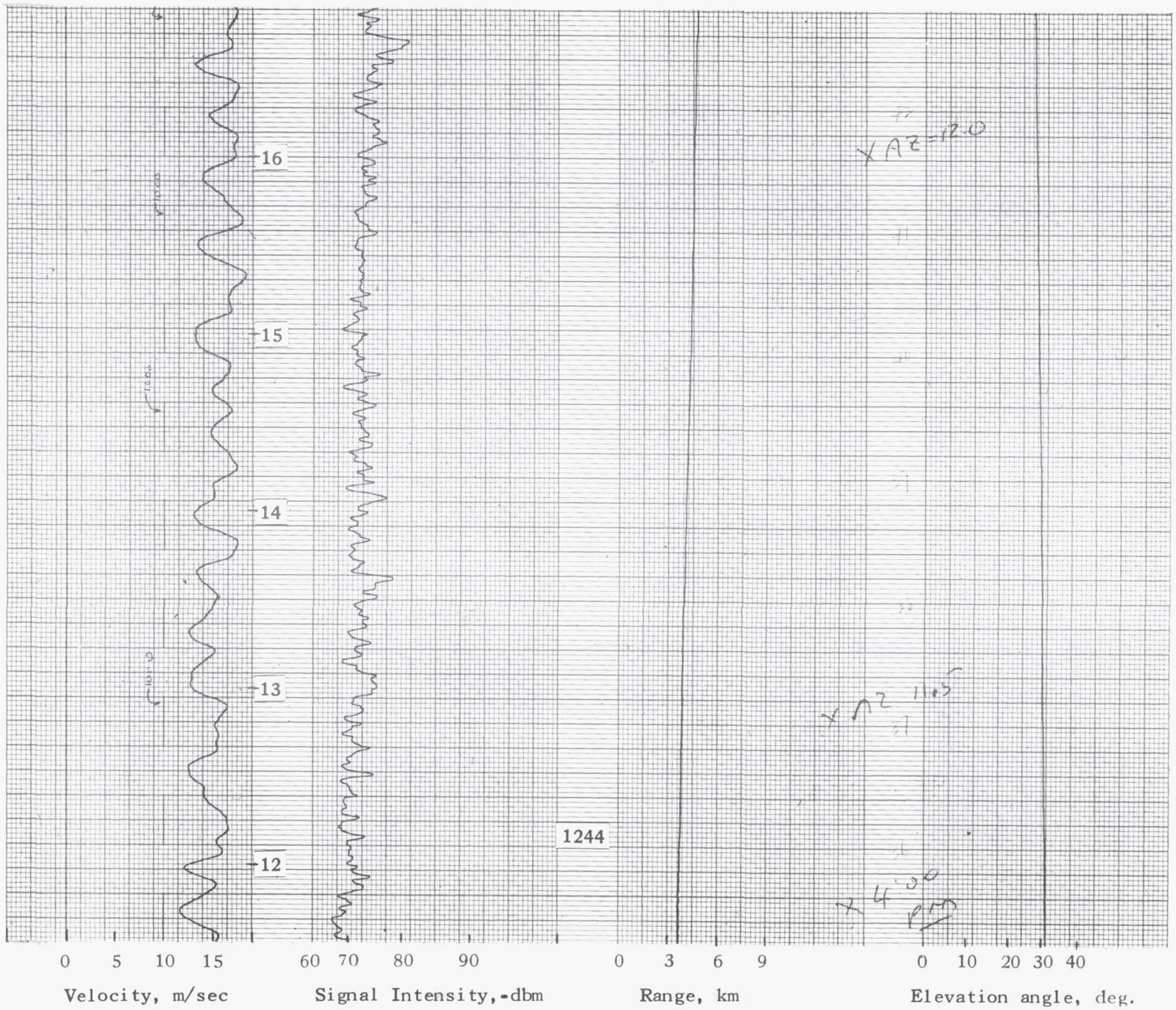

Fig. 3 Example of data record. Nov. 24, 1964, 1-m balloon (code 1244)

The portions of velocity records chosen for detailed statistical analysis were digitized* and stored on IBM cards. Subsequent computations were made on IBM digital electronic computers, initially a model 704 and later a model 7044.

D. Data accuracy

Small errors in the recorded Doppler velocity might be introduced at each step in the signal reduction and recording process. In summary, the error sources are:

1. short-term frequency instability in the radar receiver
2. calibration errors in the frequency tracker and chart recorder
3. errors generated by digitizing the chart record.

For each source of error it is important to distinguish between systematic and random errors. Systematic errors are considered to be those which cause a sequence of measurements of velocity to have a fixed percentage or absolute error. For the purposes of this project the random errors, which introduce apparent fluctuations in velocity, are of more concern because the fluctuations of balloon velocity rather than the mean are under investigation. The different possible errors cannot be analyzed in exact detail, but judgment and due consideration of the experimental procedures can give reasonable estimates of upper bounds on their contributions.

The only potentially significant systematic errors would arise from calibration errors in the frequency tracker and chart recorder. In calibrating each it is necessary to establish a zero and a slope or constant of proportionality relating input to output. Considering the care taken in establishing the calibrations, it is estimated that the error in velocity is less than the sum of 0.5 m/sec (due to possible zero drift) and 2 per cent of the value of velocity (due to possible proportionality errors).

---

*The conversion was performed semiautomatically by means of a Universal Telereader, Telecomputer Corp., Los Angeles.

Random errors, which cause apparent fluctuations in the velocity data, could potentially arise from any of the three sources listed above. It is possible to check the first two experimentally by observing the chart recorder trace as the radar is directed at a fixed, rigid target. Any random errors due to short-term radar instability or noise effects in the frequency tracker and recorder would appear as velocity fluctuations about the mean velocity of zero. In Fig. 4 there is shown a frequency tracker record from a fixed ground target. In the absence of instabilities, this record would be a straight line at zero velocity. It is seen that the record is steady to within the line width of the trace, about 0.2 mm, which for the standard calibration used amounts to 0.1 m/sec.

A final random error is introduced by converting the analog chart record to digital form. This error can amount to no more than the line width of 0.1 m/sec. For convenience the digital data are entered on cards to a precision of two decimal places; thus the final decimal place is essentially a random variable, independent of the balloon's velocity. This round-off error effect can contribute no more than 0.01 $(m/sec)^2$ to the variance of the velocity fluctuations.

In summary, the random errors arising from equipment instability and digitizing are both less than 0.1 m/sec. Since they are independent, the total variance arising from both will be less than 0.02 $(m/sec)^2$.

For certain comparative purposes the altitude of the balloon is required. This altitude will contain an error because of errors in slant range and elevation angle, from which it is computed. The accuracies of both range and elevation data are degraded by errors in calibrating the Sanborn charts. The elevation angle data, moreover, contain any possible antenna boresight or tracking error, and the range can be in error by as much as the radar resolution distance. It is estimated that the error in elevation angle is determined almost entirely by the rather imprecise calibration technique and is less than 2 degrees. The range error on the other hand is determined by the radar resolution ability and can amount to 150 m. The altitude error resulting from these two sources is less than 200 m for most of the geometrical configurations encountered in the experiments.

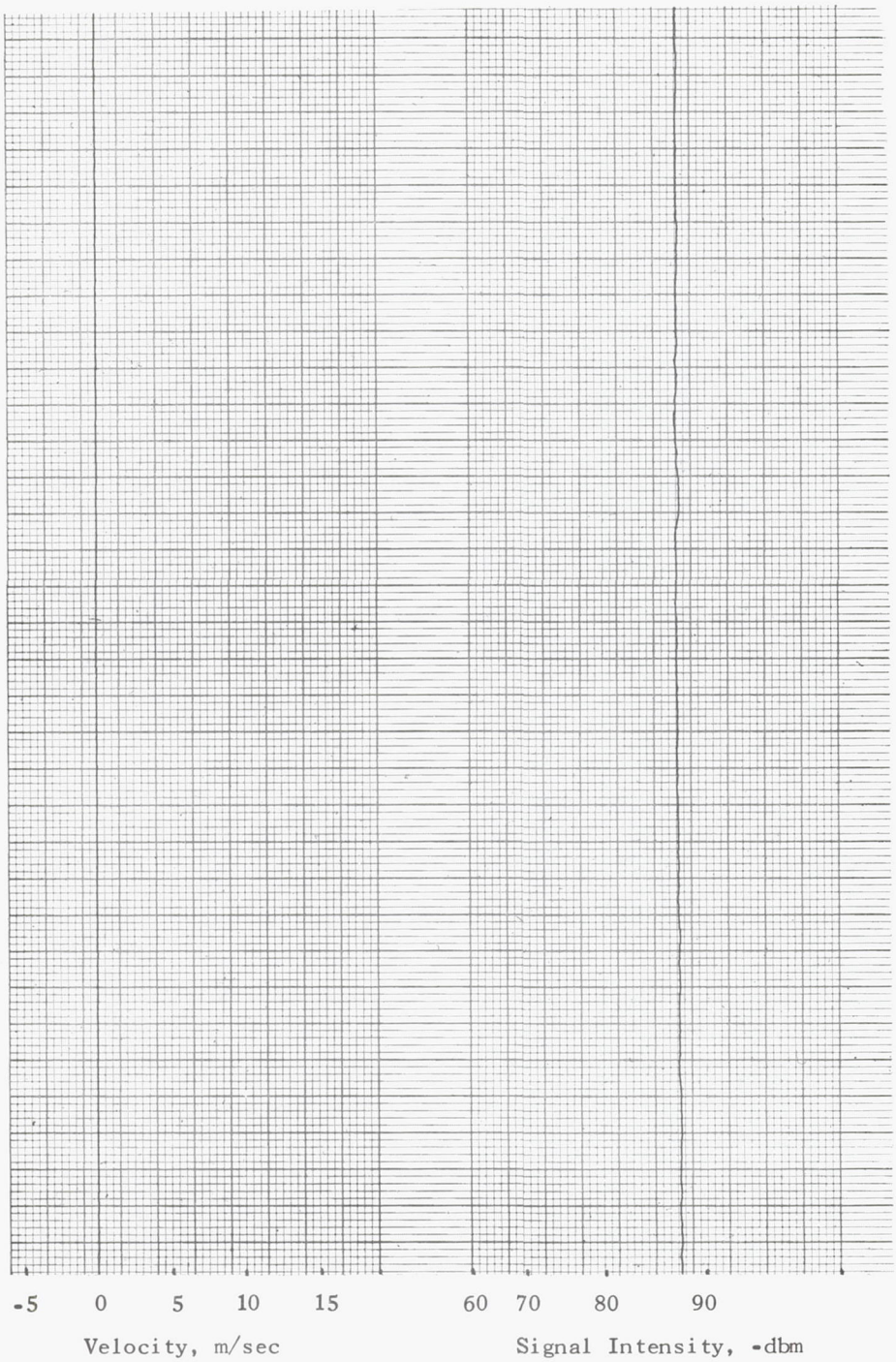

Fig. 4. Record of Doppler velocity and signal intensity from fixed target, 1.8 km range, showing extreme stability of velocity measurement.

IV. DATA AND INTERPRETATION

Important details of the experiments are summarized in Table 2. The code numbers in the table specify the month, day, and run number. The total number of balloon tracking experiments are distributed over sizes as follows:

1-m sphere (22)
2-m sphere (15)
Jimsphere (7)
2-ft sphere (6)
7-ft sphere (1)

Additionally, two 1-m and one Jimsphere balloon were observed while individually tethered on a line approximately 300 m in length.

Almost all of the balloons yielded data useful for the analysis. The few exceptions consist of two balloons that burst soon after release and three for which the data were not useful because of radar malfunction. Presented in this section are the data, a discussion of the behavior of different types of balloons, and implications for wind measurement systems utilizing balloons as tracers.

A. Qualitative appearance of the data

Because the marked fluctuations of velocity during ascent are of interest even in their raw data form, several of the records are shown here to provide an introduction for the quantitative material which follows. In Fig. 5 are displayed velocity records from different balloon types, as indicated. Only the Doppler velocity portions of the four channels of data are shown. These data, all from November 4 within a 1 1/2 hour period, were chosen as representative cases. Each balloon is seen to undergo velocity fluctuations that are more or less erratic, depending upon balloon type. The 2-m balloon

Table 2 Index to Experiments

Code*	Date	Balloon type	Release time (EST)	Altitude max (km)
7011	Jul. 1	2	1322	8.1
7012	"	1	1357	4.3
7013	"	2	1423	7.3
7014	"	1	1448	4.4
7061	Jul. 6	1	1357	3.0
7062	"	2	1419	7.5
7063	"	1	1441	7.5
7064	"	2	1513	3.0
7071	Jul. 7	1	1350	5.6
7072	"	2	1422	4.2
7073	"	1	1450	2.8
7101	Jul. 10	2	1349	6.2
7102	"	1	1412	4.2
7161	Jul. 16	1	0945	5.3
7162	"	2	1017	7.6
7163	"	1	1045	6.1
9281(t)	Sept. 28	1	0839	
9291	Sept. 29	Jim	0924	5.3
9292	"	1	0955	4.2
9293	"	7-ft	1030	1.7
9294	"	1	1049	4.0
9301	Sept. 30	2	0857	5.0
9302	"	1	0918	1.3
0011	Oct. 1	Jim	0839	7.7
0012	"	1	0914	9.1
0013	"	2	0956	10.6
0014(t)	"	1	1250	
0015(t)	"	Jim	1345	
0016(r)	"	1	1359	5.8
0017(r)	"	Jim	1425	1.5
0261	Oct. 26	1	0952	1.9
0262	"	1	1009	2.5
0263	"	Jim	1031	2.5
0264	"	2-ft	1048	0.8
0265	"	2	1109	1.6
0266	"	1	1123	2.3
0267	"	2	1147	2.2
1241(r)	Nov. 24	1	1429	2.8
1242	"	2	1452	3.6
1243	"	Jim	1523	2.0
1244	"	1	1544	2.5
1245	"	2-ft	1607	1.1
2091	Dec. 9	2-ft	1413	1.5
2092	"	2-ft	1427	1.3
2101	Dec. 10	1	1015	4.7
2102	"	1	1038	4.5
2103	"	2	1115	6.1
2104	"	2	1148	1.1
2105	"	2	1207	6.0
2106	"	Jim	1409	5.8
2107	"	Jim	1445	5.0
2108	"	2-ft	1513	1.4
2109	"	2-ft	1536	1.2

*(t) Tethered balloon, 300m alt. (r) Remote release, 2.4 km range
2= 2m sphere 7-ft = 7ft sphere
1= 1m sphere 2-ft = 2ft sphere Jim = Jimsphere

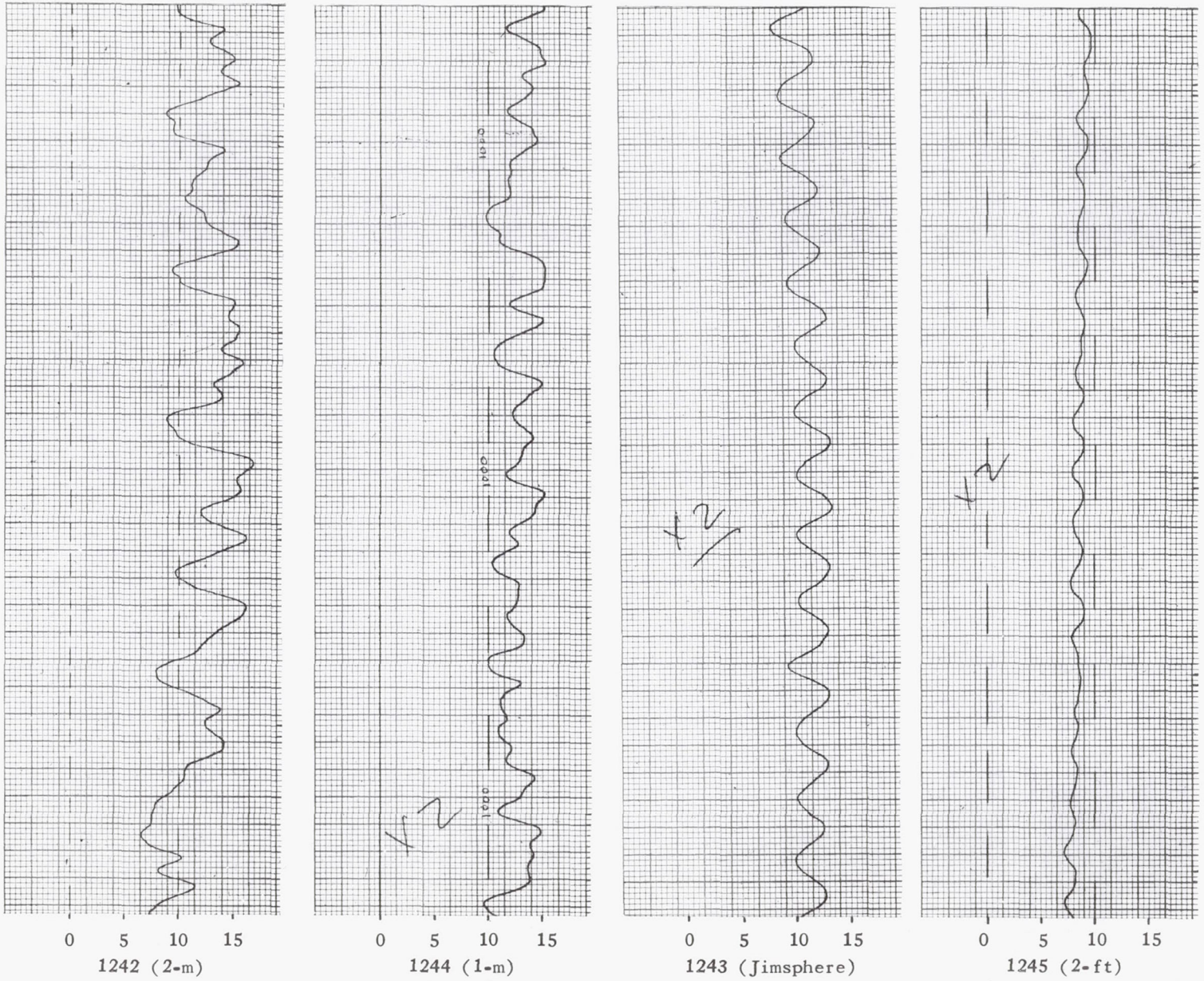

Fig. 5 Velocity records from different balloons, Nov. 24, 1964. Velocity scales indicated on each trace in m/sec. Record lengths are about 66 sec. All runs were conducted within a period of 1½ hours.

undergoes the most extreme fluctuations, with the 1-m balloon exhibiting equally random fluctuations of somewhat reduced amplitude. The Jimsphere is seen to exhibit a remarkably orderly behavior, resulting in an approximate sinusoidal velocity record with peak-to-peak amplitude of about 3 m/sec and period of about 4.5 sec. Finally, the 2-ft balloon fluctuates least and, upon closer inspection, is seen to exhibit a tendency for regular oscillations of about 1m/sec amplitude and 4 sec period.

The fluctuations shown in Fig. 5 are assuredly indications of erratic balloon behavior rather than actual wind irregularities. Wind shear or turbulence of the extent indicated in these records is contrary to results from other wind measurements; furthermore, the appearance of the velocity record from a given balloon was found to depend more heavily on the kind of balloon used than on any other experimental variable. As indicated in Fig. 5, the different balloons behave differently, even under the same meteorological conditions.

That the spurious motions are induced by the relative velocity between ascending balloon and air became apparent from a fortuitous occurrence on October 1. Approximately 2 min after release a Jimsphere (Code 0017) was observed by telescope to be losing helium and developing a flat surface. The leak must have been severe, because only 2 min later, the balloon ceased ascending and gradually lost altitude as it drifted away. Data on this balloon, indicating some effects of the failure, are shown in Fig. 6. In the first few seconds of the data, the usual Jimsphere oscillations of approximately 4-sec period can be observed, At about 150 sec after release however, the oscillations abruptly diminished. By 190 sec the recorded oscillations were completely damped, although the balloon was receding from the radar at a velocity of about 6 m/sec and, as determined by range and elevation angle, was still ascending at 2 m/sec. Some of this change in the character of velocity fluctuations was likely associated with the change in balloon shape. Yet it seems evident that the ascent velocity induced the motions, in any case. The balloon leveled out and started to descend after about 250 seconds. It is

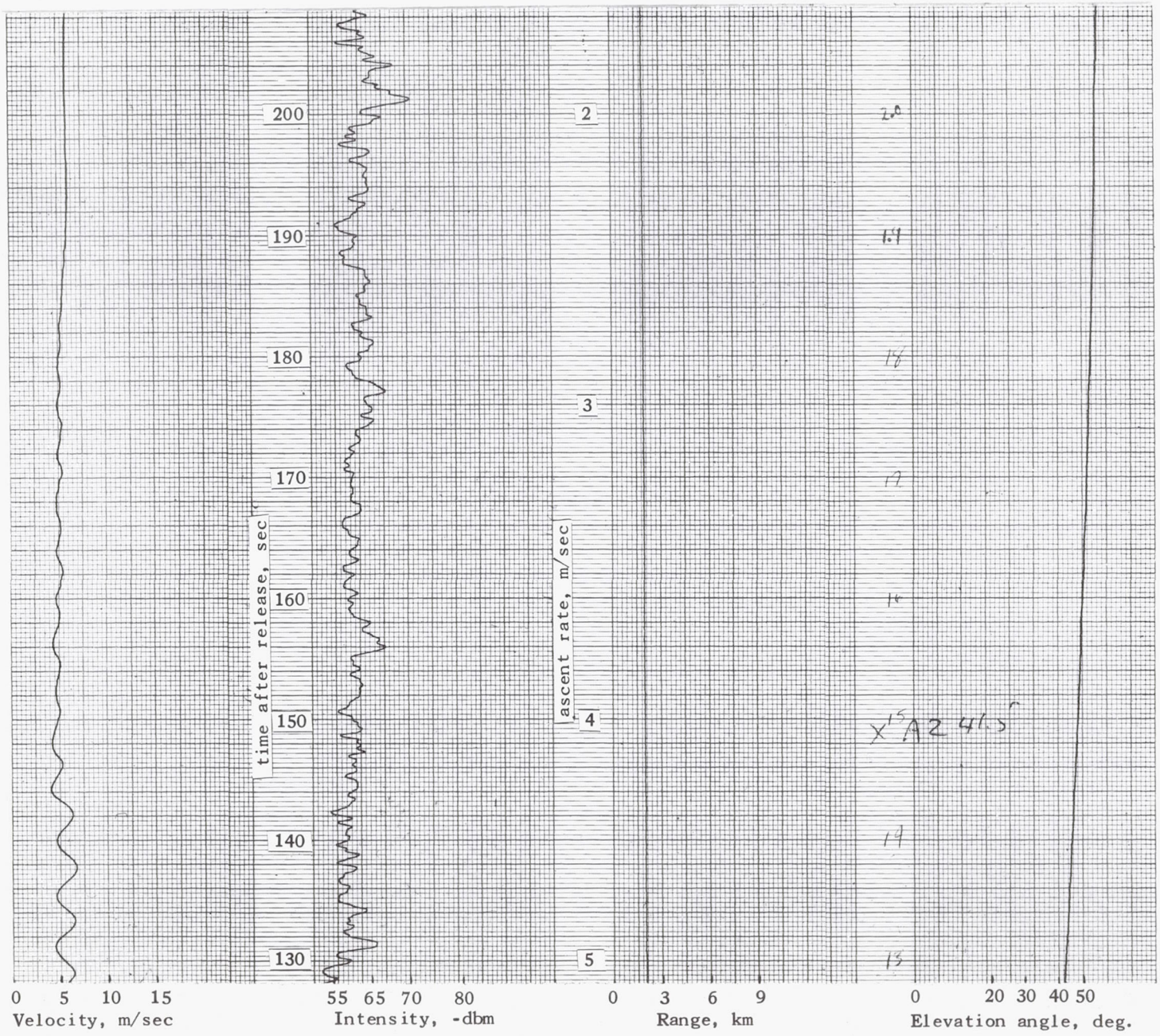

Fig. 6. Record from ascent of damaged Jimsphere. Time after release and ascent velocity indicated.

noteworthy that the oscillations stopped before the ascent velocity became zero, indicating that the relative velocity has to exceed a threshold of about 2 m/sec before the oscillations are initiated. This threshold is evidently not the same for all balloon types, for the 2-ft sphere undergoes small oscillations even though its ascent rate is only about 1.5 m/sec.

During another Jimsphere ascent on October 1 (Code 0011), a significant qualitative aspect of the data was revealed. Because of a change in wind direction with altitude, the balloon, which had been diminishing in elevation angle for several minutes, turned and came back over the radar site. The characteristic 4-sec oscillations quite noticeably became reduced in amplitude as the elevation angle increased. This elevation angle effect is consistent with a helical model for the Jimsphere trajectory. Quantitative aspects of this model have been investigated and are discussed in Section D.

As a summary of the qualitative aspects of the data, we can list the following:

1. All types of balloons tested undergo small scale, erratic movements that are not indicative of actual wind.

2. The motions are more or less random except for the case of Jimspheres, in which the erratic velocity appears as an approximate harmonic function with 4.5 sec period.

3. The motions are associated with the relative velocity of the balloon with respect to air.

4. At least in the case of Jimspheres, the horizontal component of the erratic motion is stronger than the vertical, as revealed by the elevation angle of dependence of the amplitude of oscillation.

5. The amplitude of erratic velocity fluctuations for smooth spherical balloons is positively correlated with balloon size. As ascent rate is also correlated with size, it is not clear whether size, speed or a combination of the two (as in Reynolds number) is the controlling factor in determining the amplitude of oscillations.

With regard to using such balloons for measuring wind, the question now arises: how must one smooth the data to remove the erratic components of motion and be left with only the components indicative of wind? The answer to this question requires quantitative data on balloon behavior and a model relating balloon motions to the wind field.

B. Mathematical formulation

There are generally two fundamental sources of error in the determination of wind velocity with meteorological balloons. One of these is the erratic motion of the balloon which is superimposed upon the direct motion in response to the impetus of the wind. The second source of error is the failure of the balloon to follow the wind perfectly. That is, the balloon velocity, even with random motions averaged out, will not equal the wind velocity if the wind possesses gust components to which the balloon does not respond.

In practice a third source of error creeps into the determination. This error arises since it is usual to smooth the velocity or position data of the balloon before employing it to estimate the wind velocity. The general effect of the smoothing is to reduce the random error, to be sure. However, smoothing the position or velocity data is equivalent to hampering further the ability of the balloon to follow high frequency wind components. In terms of signal theory, we may regard the balloon motion as consisting of signal plus noise (and perhaps signal-noise intermodulation components). Clearly we cannot filter out some of the noise without also filtering out some of the signal and thus smearing or distorting it.

Of the three kinds of error mentioned, the random error is under certain circumstances statistically independent in first order of the other two errors, so the random error may be, under these circumstances, considered as independent of and treated separately from the other errors. Thus the random error may be assessed without assessing the other two errors. Since the other two errors are not statistically independent of each

other, they cannot be independently assessed. Because of this, in the analysis following, the latter errors are lumped together and treated as one error.

Since the experimental technique used on this project is based upon a Doppler radar, the statistical quantities which are most readily determined by data reduction are the autocovariance function and power spectrum of the radial component of balloon velocity. Accordingly, to assess on the basis of project results the random errors in wind velocity determination by any technique employing weather balloons, it is convenient to express the error in terms of the autocovariance function or power spectrum of the relevant component of the erratic velocity. A detailed development leading to the desired expressions is given in Appendix 2. In this section we discuss briefly the salient results of Appendix 2. To relate these results to project data reductions, a derviation is given of a relation between the power spectra of corresponding components of the total velocity, erratic velocity and wind-response velocity.

Let $V(t)$ denote any component of the total balloon velocity and $W(t)$ denote the corresponding component of the sum of the balloon ascent velocity and the wind velocity at the balloon. An estimate of $W(t)$, whether based upon balloon position data or velocity data, will be related to $V(t)$ by a linear transformation, usually a transformation corresponding to low-pass filtering or smoothing. Therefore, as in Appendix 2, this estimate will be denoted by $V_s(t)$, the result of the application of a smoothing or filtering process to $V(t)$. The error in this estimate is just

$$\mathcal{E} = V_s(t) - W(t) \tag{1}$$

The division of this error into a random or erratic part and a non-erratic or systematic part follows naturally from the division of V into erratic and systematic parts. The systematic part of V, which will be denoted by $[\![V]\!]$ may be roughly interpreted as the value of the component V for a somewhat idealized balloon which is free of the erratic response of a real balloon and yet responds to the impetus of the wind in the same way as a real balloon. A more precise definition of $[\![V]\!]$, based upon a suitable representative ensemble, is given in Appendix 1.

The erratic portion of V, which will be denoted by v, is just the deviation of V from its systematic portion $[\![V]\!]$, that is,

$$v = V - [\![V]\!] \tag{2}$$

Rearranging (2), we obtain

$$V = v + [\![V]\!] \tag{3}$$

which expresses V as the sum of an erratic part v and non-erratic (or systematic) part $[\![V]\!]$.

As defined in Appendix 2, the smoothing transformation* which transforms $V(t)$ to $V_s(t)$ may be applied to any integrable function. Since the transformation is linear we have from (3)

$$V_s = v_s + [\![V]\!]_s \tag{4}$$

where v_s denotes the transform of v and $[\![V]\!]_s$ denotes the transform of $[\![V]\!]$.

---

*At this point in the development all sources of smoothing, whether due to numerical filtering or radar characteristics, are included in the smoothing transformation.

Substituting (4) into (1) we have

$$\mathcal{E} = v_S + (\llbracket V \rrbracket_S - W) \tag{5}$$

The relation in (5) expresses the error $\mathcal{E}$ in the estimate of W as the sum of an erratic error v_S and a systematic error $\llbracket V \rrbracket_S - W$.

An expression for the mean-square error is obtained by squaring (5) and averaging over time. On the basis of the discussion in Appendix 2 it is not unreasonable to assume that the cross-product terms in the average vanish. In this case we have the simple relation

$$\langle \mathcal{E}^2 \rangle = \langle v_S^2 \rangle + \langle (\llbracket V \rrbracket_S - W)^2 \rangle \tag{6}$$

where the bent brackets, $\langle\ \rangle$, denote an average over all of time. The relation in (6) expresses the ms (i.e., mean-square) total error as the sum of the ms erratic error and the ms systematic error. Even if the erratic error and systematic error are not uncorrelated, so that (6) is not valid, the quantity $\langle v_S^2 \rangle$ is still a useful measure of the contribution of erratic motion to the error as well as to the spread in a sequence of measurements.

As already observed, it is convenient to express the ms erratic error $\langle v_S^2 \rangle$ in terms of the autocovariance function or power spectrum of v. Clearly,

$$\langle v_S^2 \rangle = \int_0^\infty S_r^S(f)\, df \tag{7}$$

where $S_r^S(f)$ is the power spectrum of v_S. As shown in Appendix 2, the relation between $S_r^S(f)$ and the power spectrum $S_r(f)$ of v is

$$S_r^S(f) = S_r(f)\, T(f) \tag{8}$$

where $T(f)$ is the power transfer function corresponding to the smoothing transformation which transforms V into V_S. $T(f)$ is completely determined

by the measurement process of interest. Therefore the estimation of the ms erratic error $\langle v_s^2 \rangle$ [for arbitrary $T(f)$] depends upon the estimation of the power spectrum $S_r(f)$ of v. Since the power spectrum $S_V(f)$ of V can be obtained directly by reduction of the experimental data but $S_r(f)$ cannot, we derive next the relation connecting $S_V(f)$ and $S_r(f)$. This relation is fundamental to the estimation of $S_r(f)$ on the basis of the experimental data.

The relation connecting $S_r(f)$ and $S_V(f)$ is readily derived from the relation (3). Subtracting the time average of V from (3) we have

$$V - \langle V \rangle = v + \left([\![V]\!] - \langle V \rangle \right) \tag{9}$$

The second member on the right in (9) can be put into a somewhat more meaningful form by employing the relation

$$\langle V \rangle = \langle [\![V]\!] \rangle \tag{10}$$

which follows from equation (1.15) of Appendix 1. Putting

$$\Delta V(t) = V(t) - \langle V \rangle \tag{11}$$

$$\Delta [\![V(t)]\!] = [\![V(t)]\!] - \langle [\![V]\!] \rangle \tag{12}$$

and employing (10), (9) may be written

$$\Delta V(t) = v(t) + \Delta [\![V(t)]\!] \tag{13}$$

(13) expresses the total deviation ΔV in V as the sum of the erratic deviation v and the systematic deviation $\Delta[\![V(t)]\!]$.

The next step in the development is to relate the autocovariance of ΔV to the autocovariance of v. From (13) we obtain

$$\begin{aligned}\langle \Delta V(t)\,\Delta V(t+\tau)\rangle = \langle v(t)\,v(t+\tau)\rangle + \langle \Delta[\![V(t)]\!]\,\Delta[\![V(t+\tau)]\!]\rangle \\ + \langle v(t)\,\Delta[\![V(t+\tau)]\!]\rangle \\ + \langle v(t+\tau)\,\Delta[\![V(t)]\!]\rangle\end{aligned} \tag{14}$$

The first term on the right in (14) is the autocovariance of the erratic velocity and the second term on the right in (14) is the autocovariance of the systematic (nominal wind-response) deviations from the average velocity. The cross terms in (14) represent the first-order coupling or interference between v and $\Delta[\![V]\!]$. Conditions under which the cross terms in (14) vanish are considered briefly in Appendix 2 [see the context of equation (2.19) of Appendix 2]. Alternate conditions, based upon the data reductions are discussed in Section C.

The desired relationship between $S_r(f)$ and $S_V(f)$ is just the cosine Fourier transform of (14), namely,

$$S_V(f) = S_r(f) + S_c(f) + S_{rc}(f) \tag{15}$$

Here $S_V(f)$ denotes the power spectrum of ΔV, $S_r(f)$ denotes the power spectrum of v, $S_c(f)$ denotes the power spectrum of $\Delta[\![V]\!]$, and $S_{rc}(f)$ denotes the cross spectrum for v and $\Delta[\![V]\!]$. The relation (15) serves as the basis for the inference of estimates of $S_r(f)$ from experimentally derived spectra $S_V(f)$ as discussed in Section C.

C. Power spectra of ΔV

In the preceding section, it is shown that power spectra of ΔV are important in the description of spurious balloon behavior. During the course of project effort these spectra have been computed for all Doppler velocity records judged suitable for such analysis. To be considered suitable, the records had to be noise-free for a period of at least several minutes, and all phases of the experiment had to be functioning properly. Since it is desirable to compare the behavior of different types of balloons in similar meteorological conditions, care was also taken in selecting records corresponding to a predetermined altitude interval for the balloon. Spectra from consecutive runs could then be compared on an equal-altitude basis, thus minimizing some of the unavoidable meteorological variability from run to run.

All of the computed spectra are given in Figs. 8-17. These are the spectra $S_V(f)$ of the radial component ΔV of the velocity fluctuations.* The Doppler radar recording equipment actually smooths the velocity $V(t)$ by a small amount. The smoothing has well defined mathematical characteristics, however, (see Appendix 3, equation 3.2) so that the spectrum $S_V^S(f)$ of the smoothed velocity is readily converted to the spectrum $S_V(f)$ corresponding to the unsmoothed velocity. This spectral correction was part of the standard data reduction procedure. On each spectrum appears its identifying code number. To give an idea of the density of computed points and the smoothing used in fitting curves to the points, Fig. 7, an example of a spectrum showing computed points, is included. Computed points are not shown on the spectra in Figs. 8-17. An index to the spectra is given in

*In Section B, V and v denote arbitrary components of the velocities. In the discussion of the data in this and the following sections V and v will denote the radial components of the velocities.

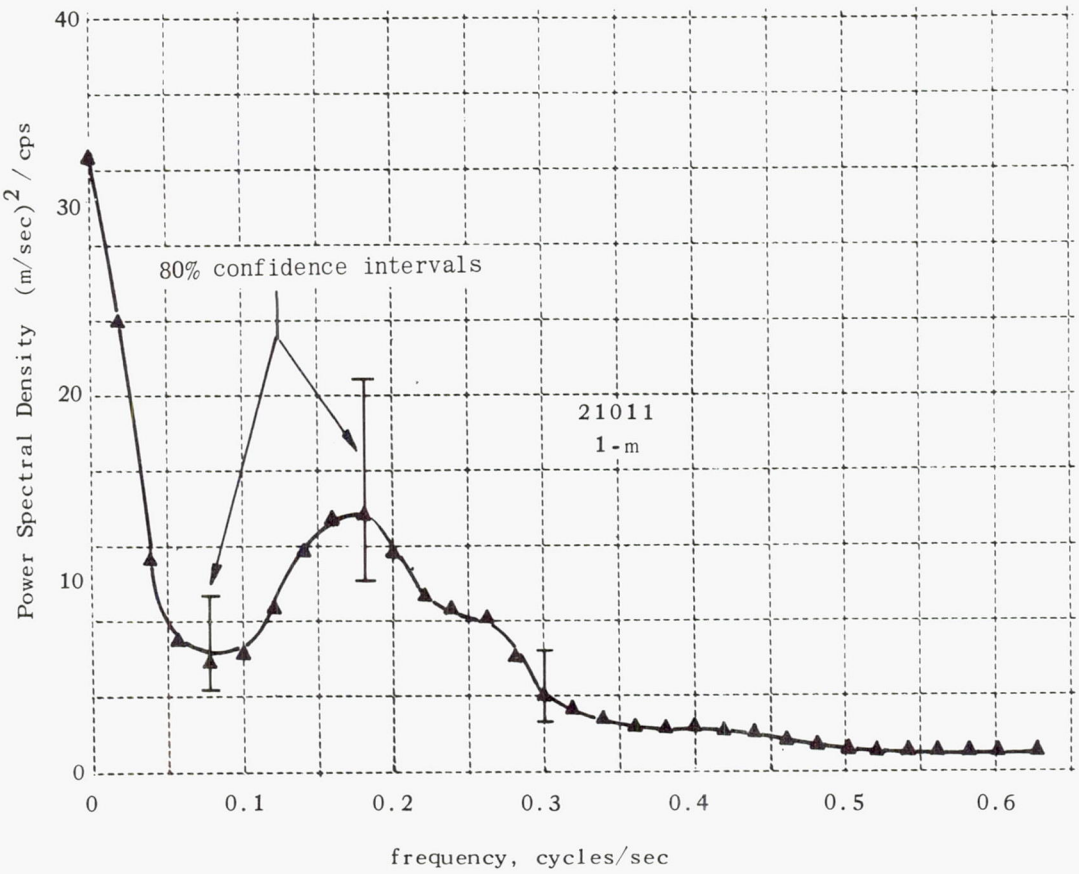

Fig. 7 Example power spectrum of ΔV, showing computed points.

Table 3, which also lists the important associated data. Date, run number, balloon type, and record length are given. Also listed are the total variance* σ_V^2 and the mean velocity $\langle V \rangle$ (both computed over the record length indicated), the height interval corresponding to the record, and a rough estimate of the average elevation angle of the balloon during the analyzed period. The spectra are arranged consecutively according to date and run number. As mentioned in Appendix 3, neither the data sampling rate nor the number of lags used in spectral computations were exactly the same for all cases. For the cases after September 30 (spectra code nos. 00111 ff), the sampling rate of 0.8 sec established the frequency 0.625 cps as the maximum measurable. Although some of the preceding spectra were computed from data at a higher sampling rate and extend therefore to higher frequencies, there are no characteristics of interest beyond about 0.6 cps in any of them. Consequently, for uniformity of presentation, all of the spectra are plotted only to 0.625 cps.

One is impressed in Figs. 8-17 by the extreme variability of spectral shapes. On a given day there is variability between spectra from balloons of different types; for a given balloon type there is day to day variability. Yet the total variances σ_V^2 do change systematically according to balloon type, as close investigation of Table 3 reveals. Large balloons, on the average, have larger total variances than small balloons.

A high degree of nonstationarity was present in some of the velocity data, as indicated by the extremely large components near zero frequency in some of the spectra. No attempt was made to filter out the very low frequencies, because they represent the actual meteorological information. Because of the characteristics of the numerical filter associated with the spectrum analysis computations, the influence of the strong component at $f = 0$ is felt at all the other frequencies. The effective filter power transfer function is shown in Appendix 3, where its effects are discussed in detail.

---

* The ms velocity computed by integrating over all of a spectrum will be called the velocity variance and be denoted σ_V^2.

Table 3. Power Spectra and Associated Data

Code	Date	Run	Balloon Type	Total Variance $(m/sec)^2$	Height Interval (km)	Record Length (sec)	Representative Elevation Angle	$\langle V \rangle$ (m/sec)
70111	July 1	1	2	7.41	1.4 - 3.0	220	40	10.4
70112	July 1	1	2	7.99	3.0 - 8.1	730	40	9.5
70121	July 1	2	1	2.53	0.4 - 2.1	340	35	8.6
70122	July 1	2	1	2.03	2.1 - 4.2	410	35	7.7
70131	July 1	3	2	8.81	0.8 - 2.7	270	45	10.1
70132	July 1	3	2	8.20	2.7 - 7.3	660	40	9.0
70141	July 1	4	1	2.10	0.9 - 2.3	280	35	9.4
70142	July 1	4	1	1.63	2.3 - 4.4	410	35	8.4
7061	July 6	1	1	2.35	0.9 - 2.5	250	65	6.3
70621	July 6	2	2	3.60	1.0 - 2.5	230	60	6.6
70622	July 6	2	2	7.41	2.5 - 5.0	390	55	10.7
70631	July 6	3	1	2.70	0.9 - 2.5	400	45	5.5
70632	July 6	3	1	2.29	2.5 - 4.2	400	45	8.9
7064	July 6	4	2	5.68	1.2 - 2.25	180	65	7.8
70711	July 7	1	1	1.33	1.2 - 4.3	570	70	5.0
70712	July 7	1	1	0.64	4.3 - 5.7	270	70	4.7
7072	July 7	2	2	1.43	1.0 - 4.3	640	70	5.2
7073	July 7	3	1	3.38	0.9 - 2.9	488	55	4.5
7101	July 10	1	2	9.24	0.9 - 4.3	470	45	9.9
7102	July 10	2	1	3.69	0.9 - 4.1	550	45	9.2
7161	July 16	1	1	2.40	1.4 - 5.3	820	50	5.6
7162	July 16	2	2	4.80	2.6 - 5.6	580	60	7.6
7163	July 16	3	1	2.08	1.2 - 5.3	1060	50	5.1
9281	Sept 28	1	1	1.16	———	380	Tethered	———
92911	Sept 29	1	Jim	0.86	1.0 - 2.0	186	70	4.4
92912	Sept 29	1	Jim	4.05	2.8 - 5.3	500	30	11.3
92921	Sept 29	2	1	1.30	1.0 - 2.0	210	60	5.3
92922	Sept 29	2	Jim	4.27	2.5 - 4.2	370	35	14.7
9293	Sept 29	3	7-ft	3.15	0.6 - 1.7	170	70	6.7
92941	Sept 29	4	1	1.72	0.6 - 1.8	210	70	5.4
92942	Sept 29	4	1	4.46	2.5 - 4.2	380	45	14.0

Table 3 (Continued) Power Spectra and Associated Data.

Code	Date	Run	Balloon Type	Total Variance $(m/sec)^2$	Height Interval (km)	Record Length (sec)	Representative Elevation Angle	$\langle V \rangle$ (m/sec)
00111	Oct 1	1	Jim	2.38	1.5 - 4.0	500	60	4.9
00112	Oct 1	1	Jim	1.35	5.5 - 7.5	442	45	7.9
00121	Oct 1	2	1	1.25	1.5 - 3.8	600	55	4.0
00122	Oct 1	2	1	0.58	5.5 - 7.5	300	50	7.1
00131	Oct 1	3	2	4.20	1.5 - 4.0	370	70	7.1
00132	Oct 1	3	2	4.60	5.5 - 7.5	290	60	7.4
0014	Oct 1	4	1	2.08	———	340	Tethered	———
0015	Oct 1	5	Jim	1.14	———	350	Tethered	———
0266	Oct 26	6	1	5.36	0.3 - 1.9	290	25	12.2
0267	Oct 26	7	2	9.85	0.4 - 2.0	214	35	14.2
1242	Nov 24	2	2	11.08	1.0 - 2.5	240	35	14.4
1244	Nov 24	4	1	4.76	1.0 - 2.5	290	30	13.8
1245	Nov 24	5	2-ft	1.98	0.4 - 0.8	260	15	9.7
2091	Dec 9	1	2-ft	0.52	0.8 - 1.3	200	40	3.9
2092	Dec 9	2	2-ft	0.83	0.8 - 1.3	200	45	3.8
2101	Dec 10	1	1	8.58	0.9 - 4.5	690	30	12.3
21011	Dec 10	1	1	3.97	0.9 - 2.7	310	35	10.0
2102	Dec 10	2	1	4.74	0.9 - 2.7	450	30	9.8
2103	Dec 10	3	2	14.28	0.9 - 4.8	480	40	13.7
2105	Dec 10	5	2	12.46	0.9 - 4.8	520	40	13.5
2106	Dec 10	6	Jim	4.79	0.9 - 4.8	750	30	11.3
2107	Dec 10	7	Jim	4.66	0.8 - 4.7	750	30	10.9
2108	Dec 10	8	2-ft	1.99	0.4 - 1.3	650	20	6.6
2109	Dec 10	9	2-ft	1.98	0.3 - 1.2	600	20	7.1

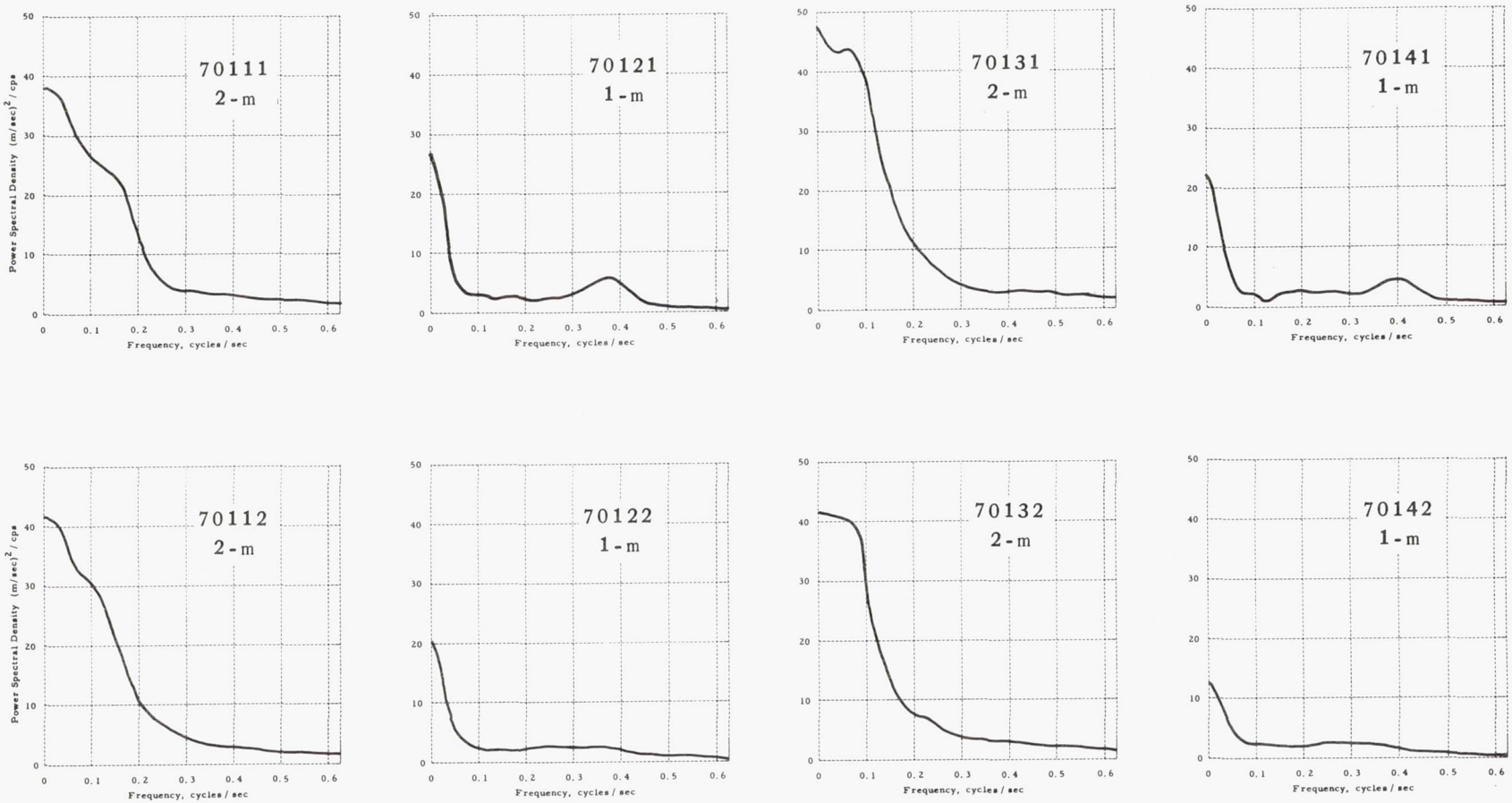

Fig. 8 Experimental spectra of ΔV

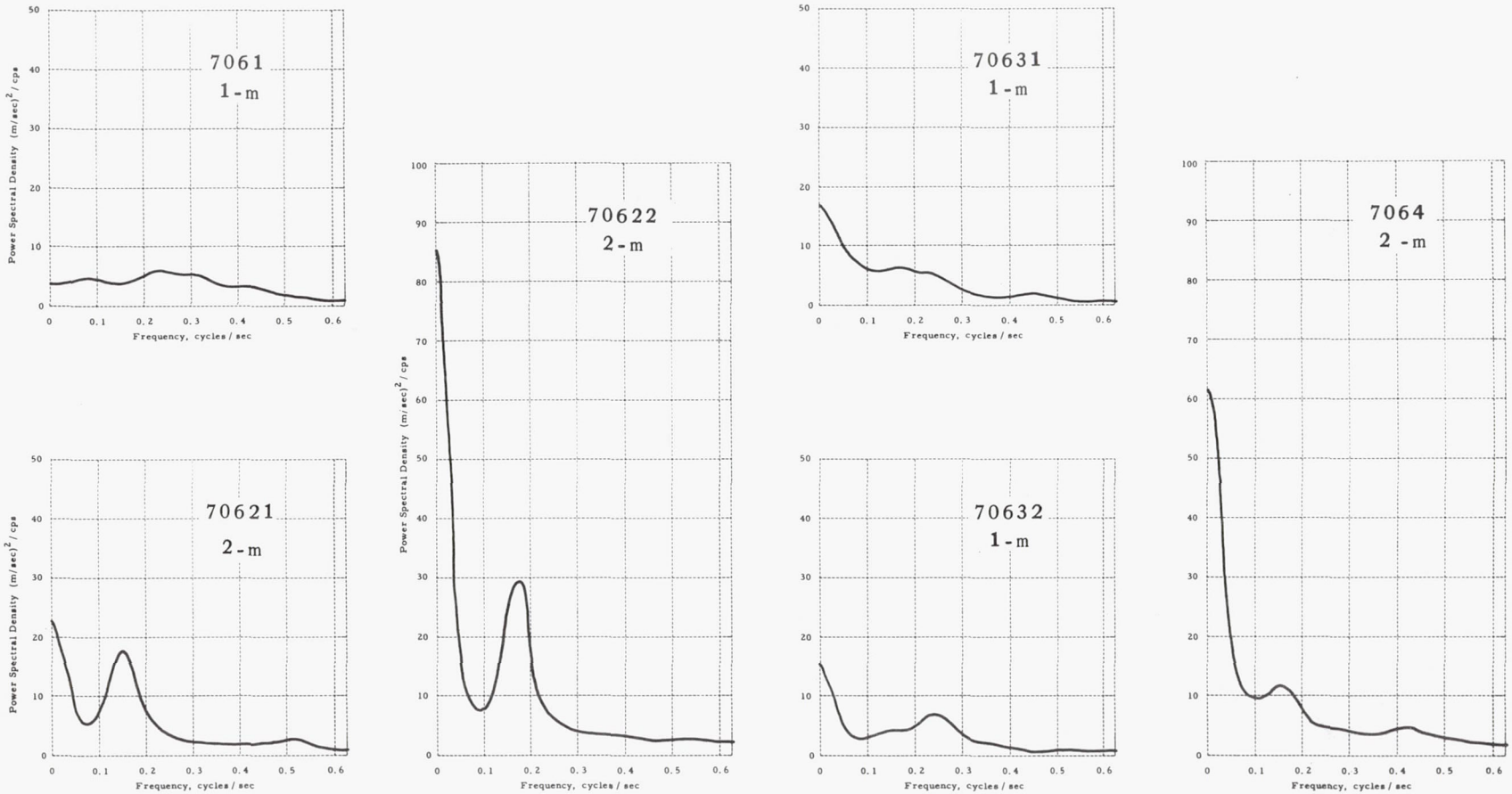

Fig. 9 Experimental spectra of ΔV

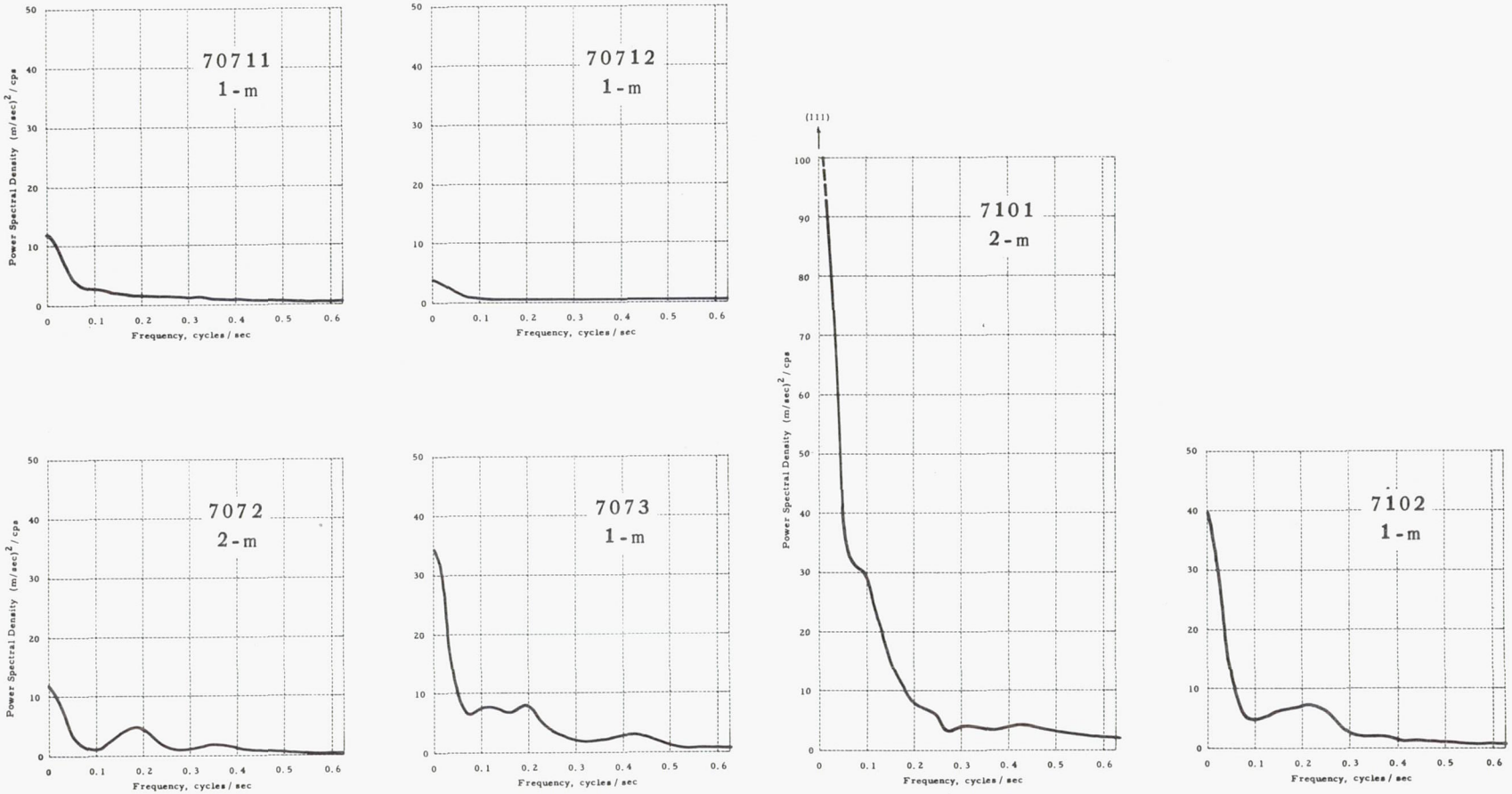

Fig. 10 Experimental spectra of ΔV

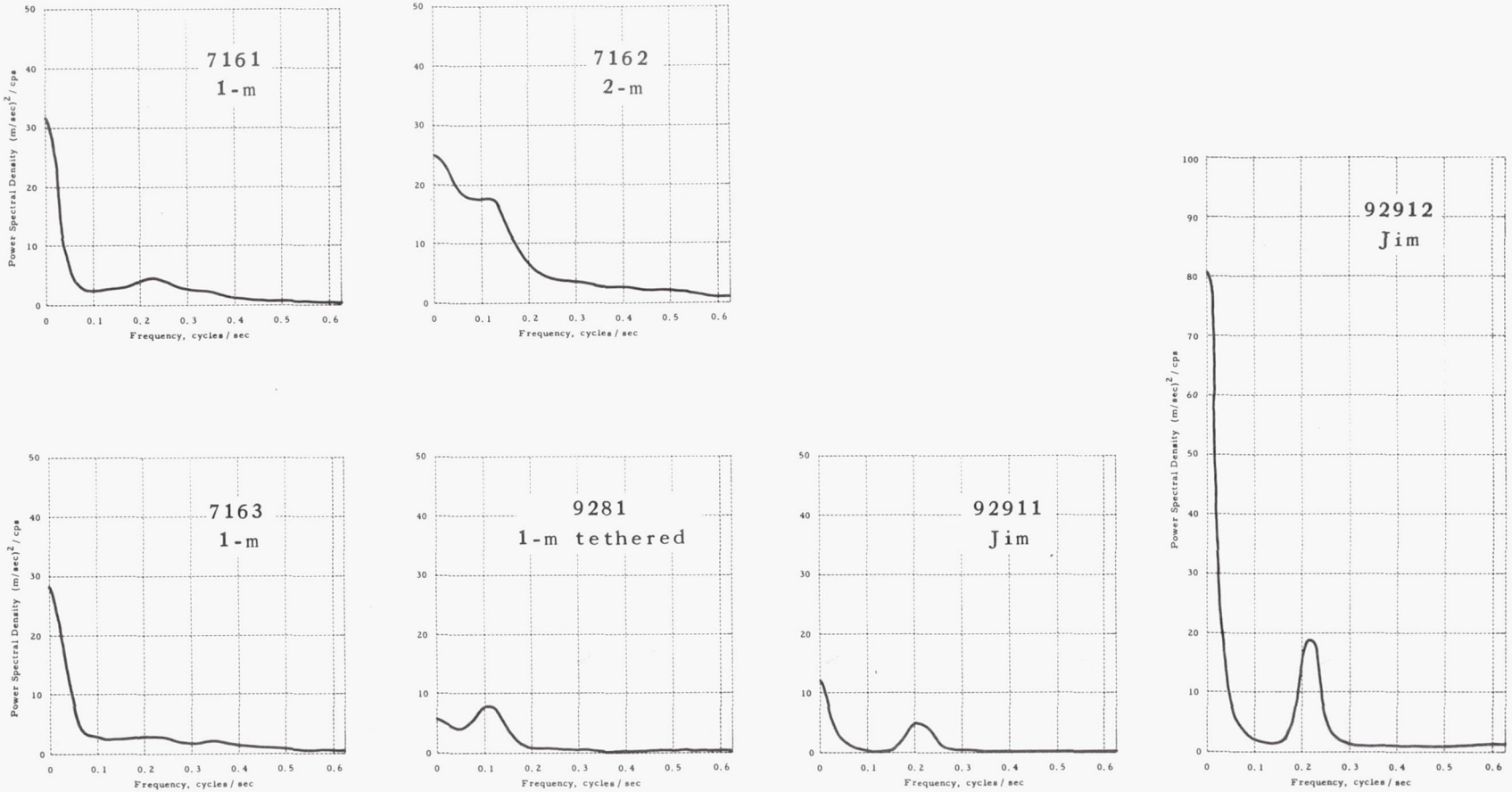

Fig. 11 Experimental spectra of ΔV

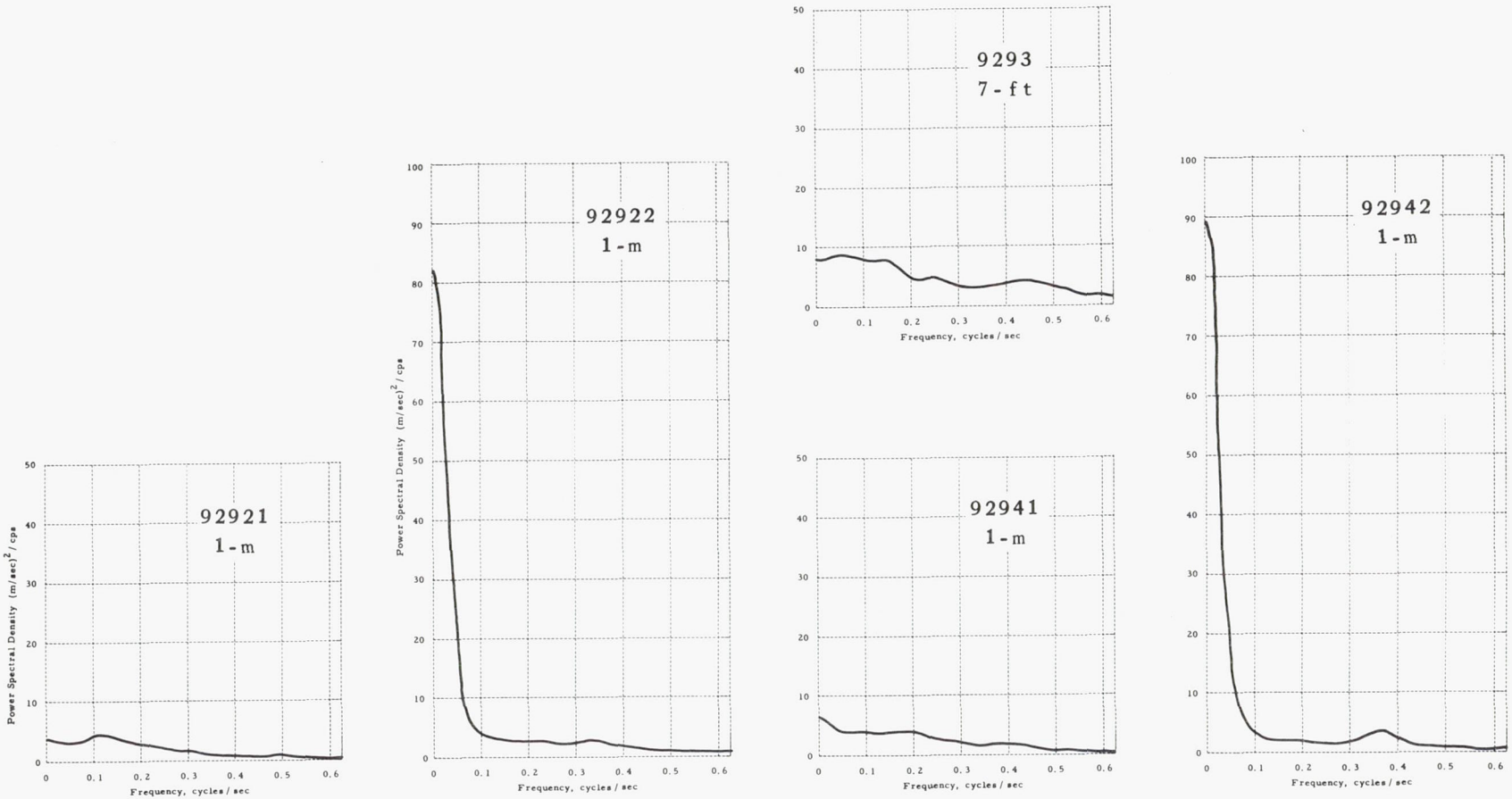

Fig. 12 Experimental spectra of ΔV

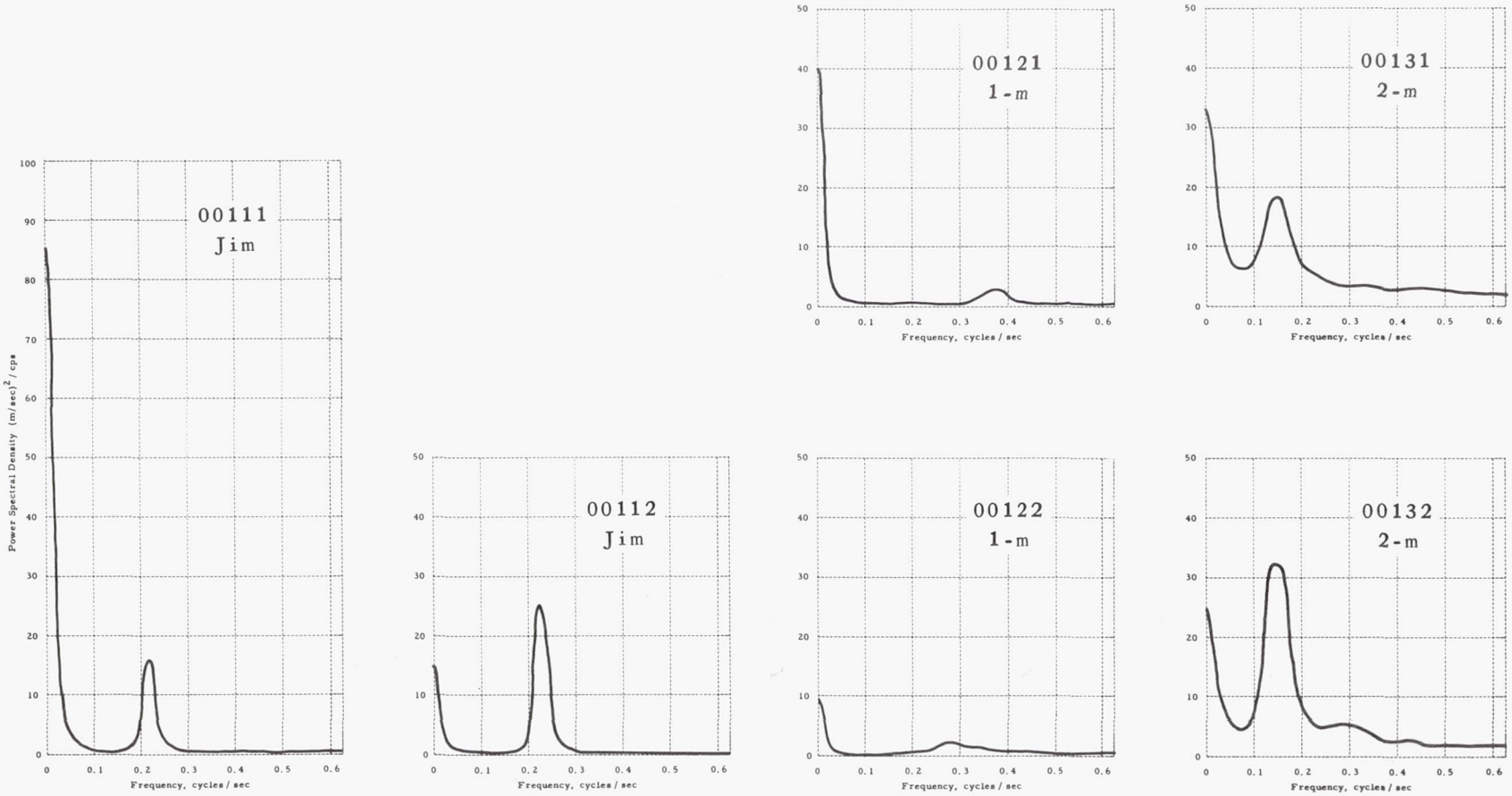

Fig. 13 Experimental spectra of ΔV

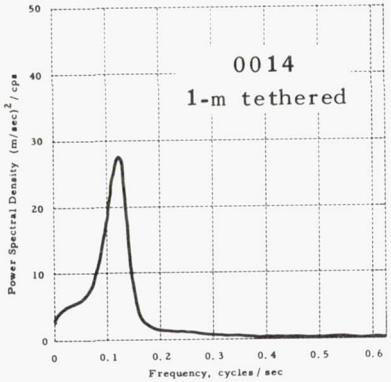

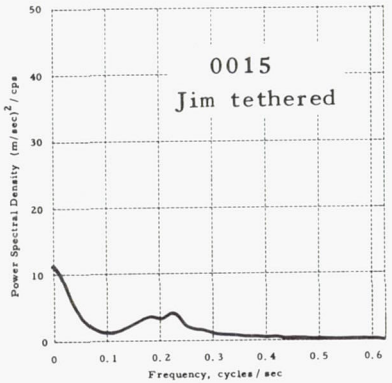

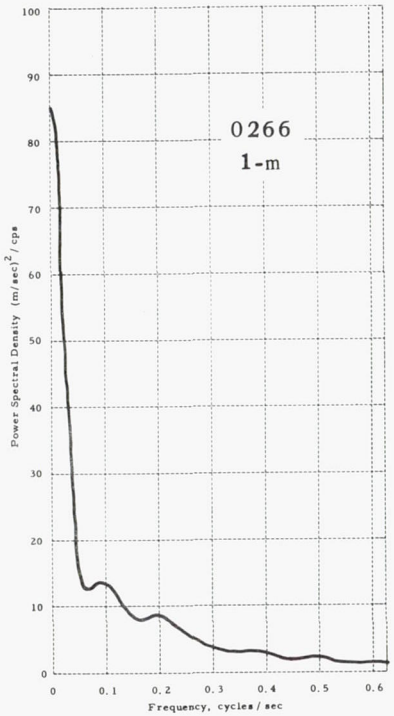

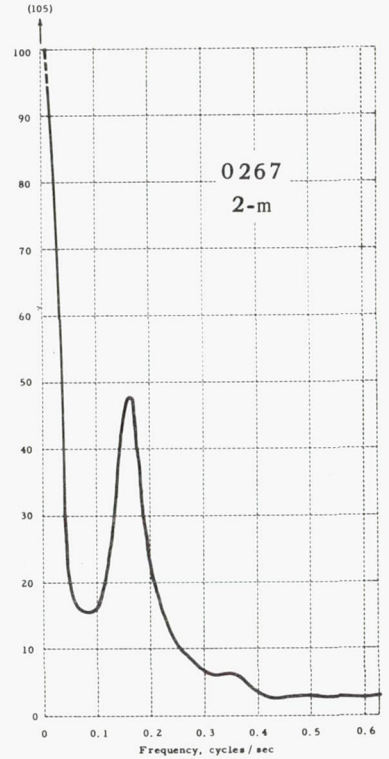

Fig. 14 Experimental spectra of ΔV

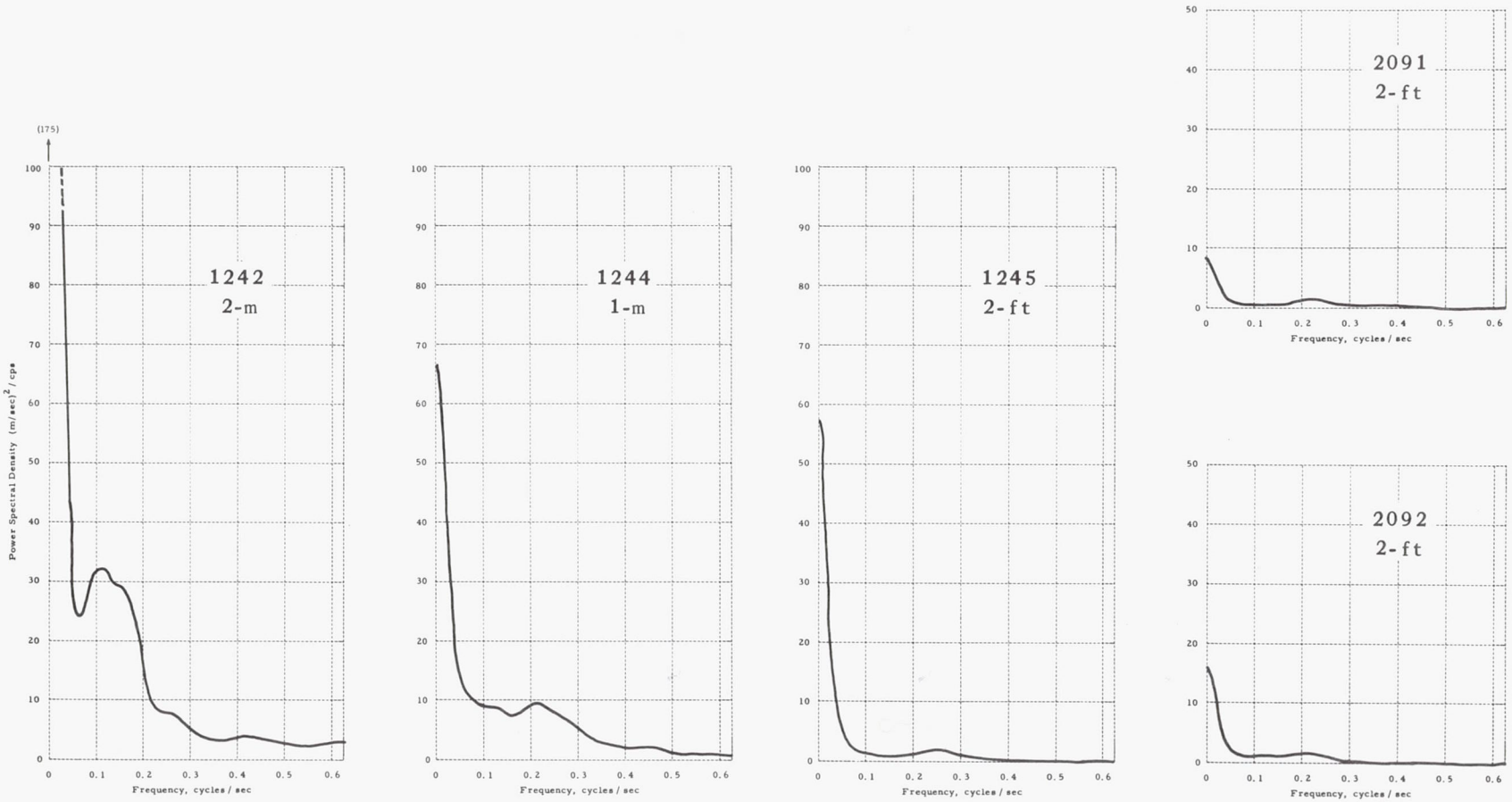

Fig. 15 Experimental spectra of ΔV

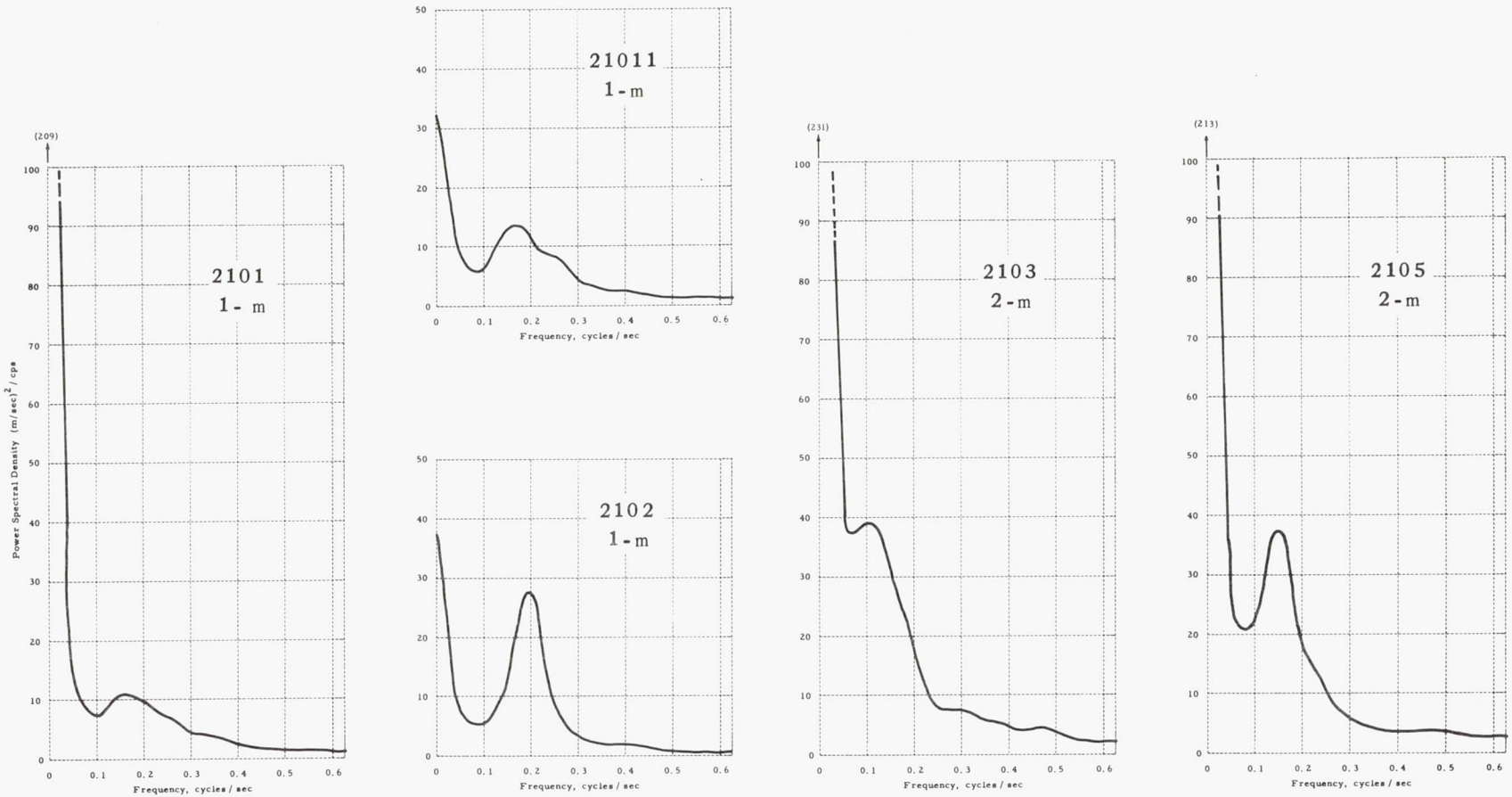

Fig. 16 Experimental spectra of ΔV

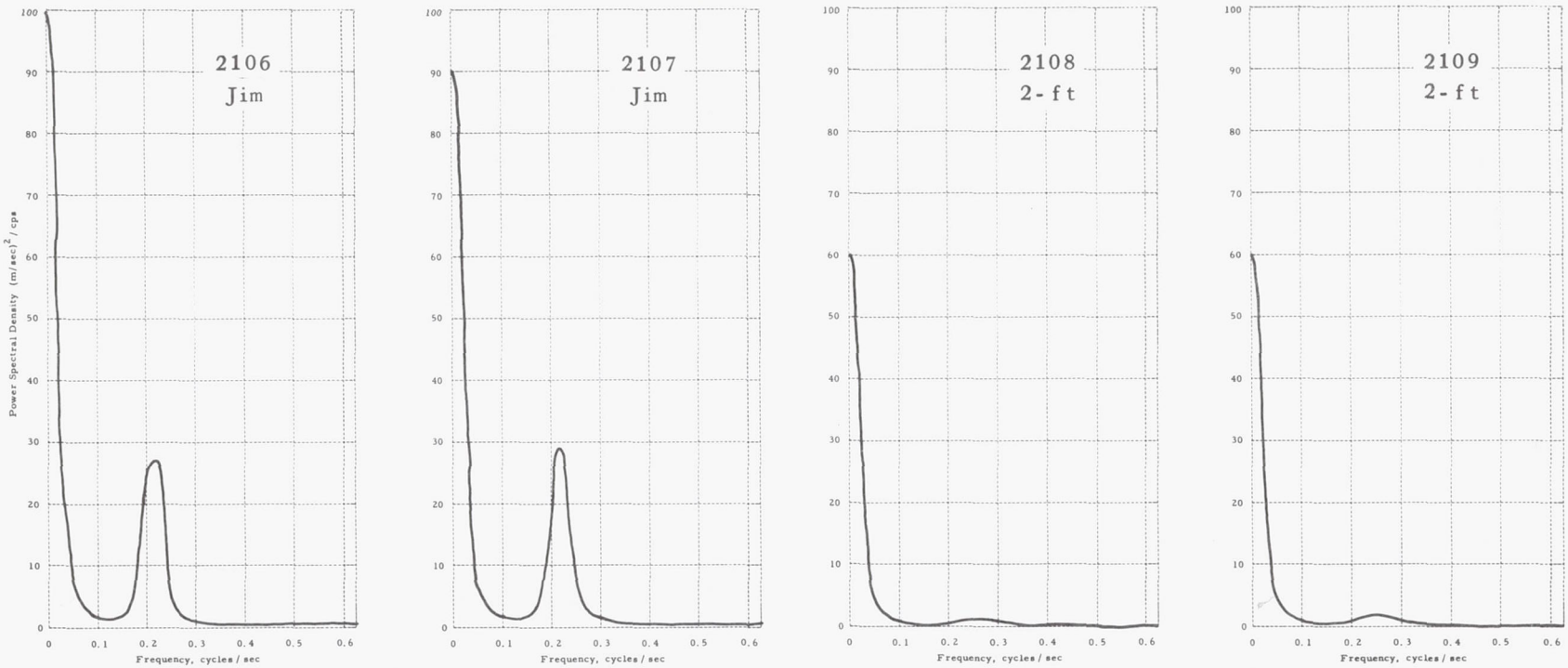

Fig. 17 Experimental spectra of ΔV

It is because of this filter, which limits the dynamic range of spectral estimates, that the noise level at the high frequency end of the spectra tends to be higher in those cases in which there are strong components at low frequencies. These highly nonstationary spectra have not been used in the analyses which depend upon the separation of the spectra into distinct erratic and wind-response portions.

The fundamental relation connecting the wind-response and erratic portions of the spectrum, as derived in section B, is

$$S_V(f) = S_r(f) + S_c(f) + S_{rc}(f) \qquad (16)$$

In (16), $S_r(f)$, the power spectrum of v, is the erratic portion of $S_V(f)$; $S_c(f)$, the power spectrum of the temporal fluctuations in $[\![V]\!]$, is the (nominal) wind-response portion of $S_V(f)$; and $S_{rc}(f)$ is the cross spectrum for v and the fluctuations in $[\![V]\!]$. It is clear from (16) that if there is an appreciable overlap of $S_r(f)$ and $S_c(f)$ in a given sample $S_V(f)$, the inference of $S_r(f)$ from this sample will be impossible without a priori information on $S_c(f)$. Since the only information available on $S_c(f)$ is that which has been inferred from the data reductions themselves, initial estimates of $S_r(f)$ have been based upon samples of $S_V(f)$ that display broad dips or nulls, suggesting a possible division of the spectrum into nonoverlapping portions $S_r(f)$ and $S_c(f)$.

An examination of Figs. 8-17 reveals that many of the spectra do display distinctive dips or nulls. It is in the Jimsphere spectra that these dips, which separate the spectra into distinct high and low frequency portions, are most evident. For this reason, the first estimates of $S_r(f)$ from the spectra $S_V(f)$ were made for Jimspheres. The separation of $S_V(f)$ into high and low frequency portions, when apparent at all, is never as distinct for the smooth balloons as for Jimspheres. Accordingly, interpretations of the spectra and estimates of $S_r(f)$ have generally been more difficult for the smooth balloons than for Jimspheres. For this reason the interpretations of $S_V(f)$ and inferences concerning $S_r(f)$ are discussed first for the Jimsphere in

There is strong justification for the thesis that the spectral content for $f > f_2$ is predominantly or entirely erratic. It seems unlikely that the spectrum of $W(t)$ itself would display a form having a null from f_1 to f_2 and spectral content for $f > f_2$. Therefore, if V were linearly related to $W(t)$ one could conclude that the spectral content for $f > f_2$ is erratic. If the motion involved non-linear coupling effects, wind response-erratic behavior intermodulation components would exist. Such components are neither purely erratic nor purely non-erratic in the sense of the term erratic employed above. However, such effects are clearly spurious and would ideally be assigned to the erratic spectrum. So it is concluded that the spectral content for $f > f_2$ is erratic.*

The final justification for this conclusion is based upon direct observation of time histories of $V(t)$ for Jimspheres. These data (e.g. Fig. 5) indicate a very strong, nearly harmonic spurious behavior in $V(t)$. The frequency of the almost-harmonic erratic variation as measured directly is about .22 cps which lies in the interval from f_1 to f_2 in Fig. 18. This evidence, in conjunction with the above arguments, provides excellent justification for assigning the spectral content for $f > f_2$ to the spectrum $S_r(f)$, i.e.,

$$S_r(f) = S_V(f), \quad f > f_2 \quad \text{(Jimsphere, Fig. 18)} \tag{17}$$

The next question to be considered is whether $S_r(f)$ has content in the region $f < f_1$. Let us say at the outset that we have reached no final conclusion concerning the relative amount of content of $S_r(f)$ in this region. However,

---

*Wind response-erratic behavior intermodulation spectra should not be confused with the cross spectra $S_{rc}(f)$ for v and $[\![V]\!]$. Intermodulation might influence $[\![V]\!]$ as well as v so that the resultant effects might appear in $S_c(f)$ as well as $S_r(f)$. However, since the intermodulation effects are spurious they contribute to the ms error $\langle \varepsilon^2 \rangle$ in any case. Since the systematic error contribution to $\langle \varepsilon^2 \rangle$ is not calculated, the effects of intermodulation on $\langle \varepsilon^2 \rangle$ will be included if its effects on $S_V(f)$ are lumped into $S_r(f)$.

Section D, following. The behavior of smooth balloons is discussed in Section E.

D. The interpretation of Jimsphere velocity spectra

As observed in Section C the spectra $S_V(f)$ for Jimspheres display deep dips or nulls which separate them into distinct high and low frequency portions. The low frequency portion usually extends out to about 0.1 cps. The high frequency portion is a rather narrow spectral peak centered at about 0.22 cps. The forms of the spectra are generally similar to that indicated in Fig. 18.

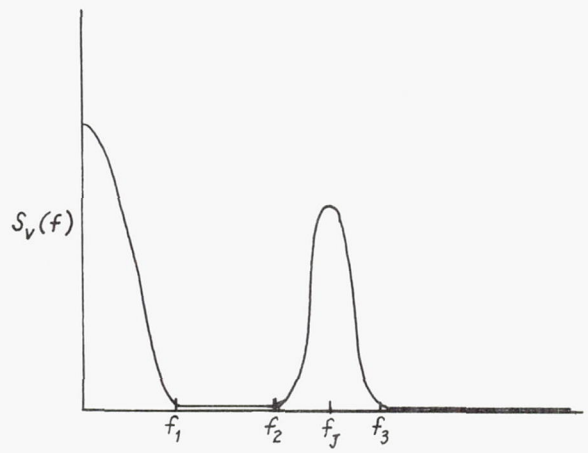

Fig. 18 Idealized spectrum for Jimsphere

This form will be employed in the following discussion regarding estimations of $S_r(f)$ and $S_c(f)$ from the spectra $S_V(f)$.

certain qualified statements can be made, and we shall discuss these at this point.

The observations of quasi-harmonic variations in $V(t)$ for the Jimspheres have led (together with other considerations) in the course of project effort to the helical-trajectory model of the Jimsphere, which is a model providing an approximate description of the erratic behavior of Jimspheres. This model is discussed in detail later. At this point we shall introduce a hypothesis along the same lines but of somewhat more general character. We hypothesize that in the complete absence of any wind $V(t)$ is harmonic at the frequency f_J indicated in Fig. 18. This hypothesis is suggested by the same considerations, discussed later, which lead to the helical-trajectory model. The following discussion, concerning the spectral content of $S_v(f)$ for $f < f_1$, is subject to the validity of this hypothesis.

Consider first a uniform wind field W. Clearly

$$v_0 = V - W$$

is harmonic at frequency f_J and of random phase. Since $[\![v_0]\!]$ is an ensemble average (see Appendix 1) it follows that $[\![v_0]\!] = 0$. Further, from Appendix 1, $W = [\![W]\!]$. Therefore, $v = v_0$ and so $S_v(f)$ has content only at the frequency f_J.

The example just discussed is almost trivial. However, the same conclusions clearly follow for the case of wind fields that are quasi-homogeneous over dimensions of the order of the orbital diameter (~1 meter – see the discussion below of the helical-trajectory model) and which are quasi-stationary over intervals which are long compared to both the period of erratic motion (4 to 5 seconds) and the response time of the balloon. These conclusions are subject to the hypothesis introduced above. If the wind field lacks either the required quasi-stationarity or quasi-homogeneity, strong coupling between v and $[\![V]\!]$ might occur as the result of non-linearities in the balloon response. Since little is known of high frequency balloon dynamics we have no definite conclusions regarding the low-frequency content of $S_v(f)$ in this case.

The lack of satisfaction of the above quasi-stationarity condition does not necessarily mean that $S_r(f)$ has appreciable content for $f < f_1$ even if coupling of wind-response behavior and erratic behavior does occur as the result of non-linear terms in the balloon equation of motion. If the only coupling terms of importance (in a perturbation expansion of the equation of motion) are product terms which are linear in V and W then the coupling will only produce spectral content at frequencies which are sums and differences of wind spectral frequencies and the frequency(s) of the unperturbed erratic balloon motion. Suppose that, in accord with the hypothesis introduced above, the unperturbed motion spectrum consisted only of a single line at $f = f_J$. Then, in the presence of a wind whose spectrum extended from $f = 0$ to f_1, the coupling would produce spurious spectral content at frequencies $f_J \pm f$ with f in the interval $0 < f < f_1$. If $f_1 < f_J - f_1$, this spurious content would be confined to the region $f > f_1$.

On the basis of the simple model just presented, one would expect a simple relation between the width of the hump extending from f_2 to f_3 (see Fig. 18) and the frequency f_1 that is a measure of the lower limit of the spectral null, namely,

$$f_2 = f_J - f_1 \quad , \quad f_3 = f_J + f_1$$

Further, one would expect $S_r(f)$ to have no spectral content for $f < f_1$ (provided $f_1 < f_J - f_1$).

The relations above do appear to fit approximately - though perhaps fortuitously - some of the experimental spectra $S_V(f)$ for Jimspheres, which suggests the possibility of a dependence of the area under the spectrum from f_2 to f_3 on the windfield. By contrast, certain data (see Fig. 20) discussed below indicate that this area is relatively independent of the windfield. There are insufficient data to determine whether there is actually any inconsistency in the latter implication and the relations above between f_2, f_3 and f_J.

Although we do not know the content of $S_r(f)$ in the region $f < f_1$ the foregoing discussion suggests that it is relatively small. Therefore, in the estimations in this report of the erratic error $\langle v_s^2 \rangle$ (see Equation 7) for the case of the Jimsphere we have only included the contributions arising from the erratic spectra $S_r(f)$ as estimated in (17) for $f > f_2$. This course appears preferable to that of assigning an arbitrary fraction of the spectral content for $f < f_2$ to $S_r(f)$, which procedure could result in an overestimation of the erratic error. An approximation for the ms erratic velocity $\langle v^2 \rangle$ in accord with the estimate in (17) for $S_r(f)$ is

$$\langle v^2 \rangle \approx \int_{f_2}^{f_3} S_v(f)\, df \qquad \text{(Jimsphere spectra of form in Fig. 18)} \qquad (18)$$

where f_2 and f_3 can be determined in any case by inspection of the spectrum $S_v(f)$. The results of computation of $\langle v^2 \rangle$ from the experimental Jimsphere spectra, employing the approximation in (18), are listed in Table 4.

Table 4

Mean-Square Erratic Velocities for Jimsphere Ascents, Computed from Spectral Data Employing Equation (18)*

Spectrum	92911	92912	00111	00112	2106	2107
$\langle v^2 \rangle (\text{m/sec})^2$	0.34	1.07	0.58	0,92	1.62	1.70

* The one spectrum from a tethered Jimsphere (0015) is obviously different from the other Jimsphere spectra and has not been used in the Jimsphere analysis. The forces acting on a tethered balloon are not the same as those affecting an ascending balloon; it is anticipated that they would cause different erratic behavior. The wind speed at tether altitude was about 3 m/sec (from USWB pibal data). The spectrum for the tethered balloon, interestingly enough, shows a peak at the characteristic Jimsphere frequency of 0.22 cps.

The appearance of Jimsphere velocity traces (see Fig. 5) and spectra is, as noted above, consistent with a motion which is composed of a wind-response component and an approximately harmonic erratic component. In addition, it is evident from the velocity data that the amplitude of the velocity fluctuations decreased as antenna elevation angle increased. These observations suggest that the Jimsphere motion can be approximately described as the motion resulting from the superposition of a circular motion in a horizontal plane upon the motions of ascent and wind response (see Fig. 19). To test this model which we will term the helical trajectory model, the data from Jimsphere ascents in which the elevation angle varied over an appreciable range were analyzed in detail. Short-term rms erratic velocities (over about 15 sec) were computed from the records at periods of about one minute. Also noted was the average elevation angle over the time interval for which the rms velocity was computed. For convenience these rms velocities were computed by the following expedient: peak-to-peak values of the smoothed velocity fluctuations V_s for several adjacent half-cycles were recorded and then averaged.* If the velocity variation were purely sinusoidal this peak-to-peak velocity fluctuation δV would be related to the rms smoothed velocity $\langle v_s^2 \rangle^{1/2}$ by

$$\langle v_s^2 \rangle^{1/2} = \frac{\delta V}{2\sqrt{2}} = 0.354\,\delta V$$

This relation enables one to convert the measured δV to an rms velocity. The response time of the recording pen as determined by an RC filter is sufficiently long to reduce the recorded amplitudes of Jimsphere erratic velocity fluctuations by a small fraction. This reduction can be corrected for by multiplying the values of $\langle v_s^2 \rangle^{1/2}$ computed from the raw data by

*As observed earlier in this report, the radar recording equipment smooths the velocity V by a small amount. This smoothing has been compensated in the computations.

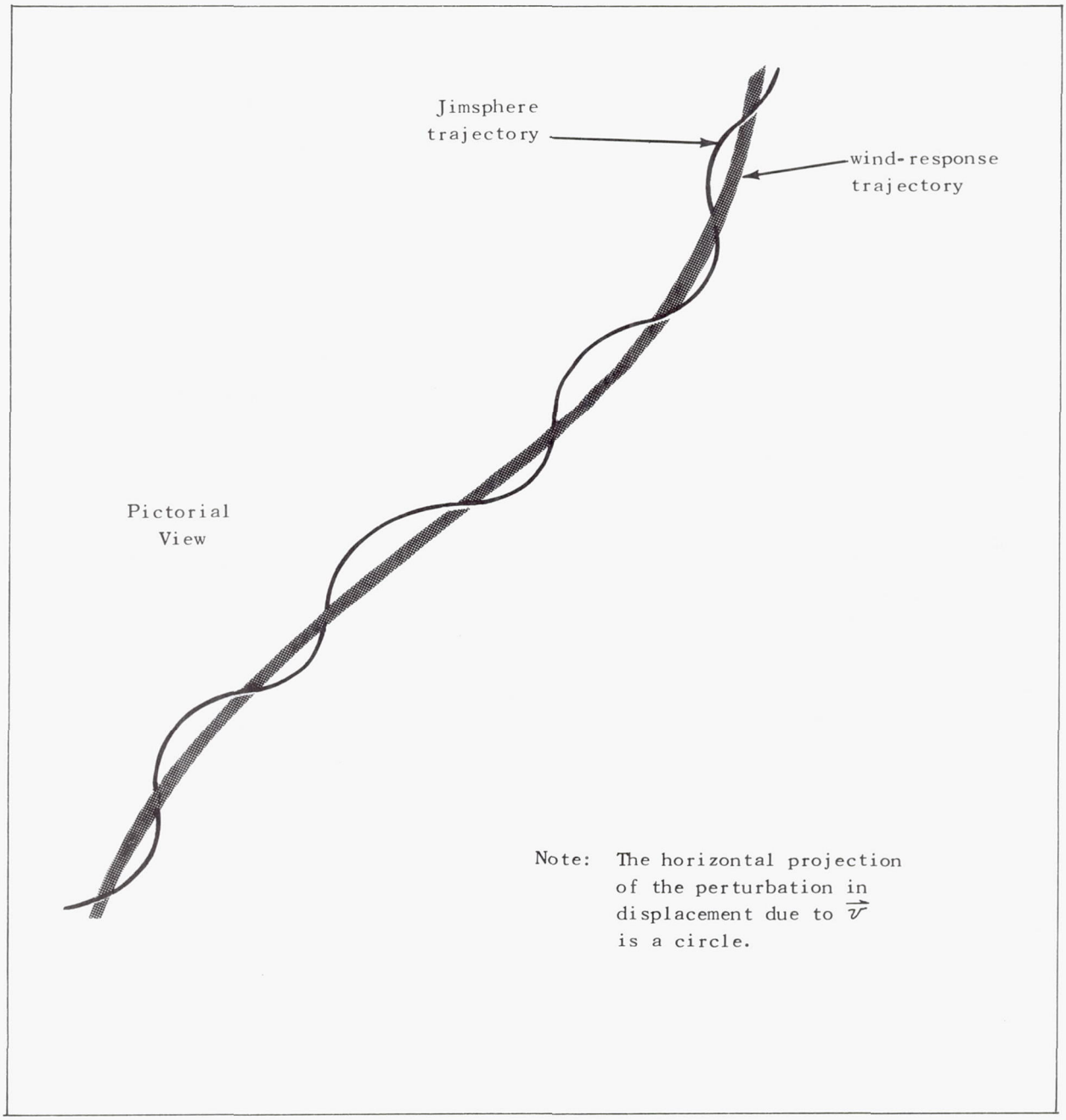

Fig. 19 Model of Jimsphere trajectory

the factor 1.22. This factor is simply the reciprocal of the transfer function of an RC filter with 0.5 sec time constant (which applied at the frequency tracker output), evaluated at $f = 0.22$ cps, the observed frequency of Jimsphere velocity fluctuations. Thus the (unsmoothed) rms erratic velocity is given by

$$\langle v^2 \rangle^{1/2} = 1.22 \langle v_s^2 \rangle^{1/2} = 0.431 \delta V$$

Values of $\langle v^2 \rangle^{1/2}$ computed by the method described are shown plotted in Fig. 20 versus the cosine of the corresponding (observed) elevation angle. While this plot contains points from every Jimsphere run, run 0011 contributed approximately half the total number of points, because of the wide range of elevation angles during the run. An approximate linear relation between the plotted quantities is evident. This linear relationship provides a justification for the "helical-trajectory" model of the Jimsphere motion. It implies that the erratic perturbation is approximately a circular motion, confined primarily to the horizontal plane, and it implies that over the range of conditions encountered in our tests, the rms erratic velocity $\langle \vec{v}^2 \rangle^{1/2}$ is approximately constant and appears to be independent of altitude and of the particular meteorological situation. This magnitude, obtained from the intersection of the best fit straight line in Fig. 20 with the line $\cos \phi = 1.0$, can be seen to have an rms value of about 1.7 m/sec, which corresponds to a peak-to-peak horizontal velocity fluctuation of $1.7/0.354 = 4.8$ m/sec. The erratic velocity component v, observed at arbitrary elevation angle ϕ, can therefore be described by the expression

$$v(t) = a \cos \phi \cos (2\pi t/T_J - \theta) \qquad (19)$$

where $a = 4.8/2 = 2.4$ m/sec

$T_J = 4.5$ sec, the characteristic Jimsphere period

$\theta =$ constant phase angle determined by $v(0)$

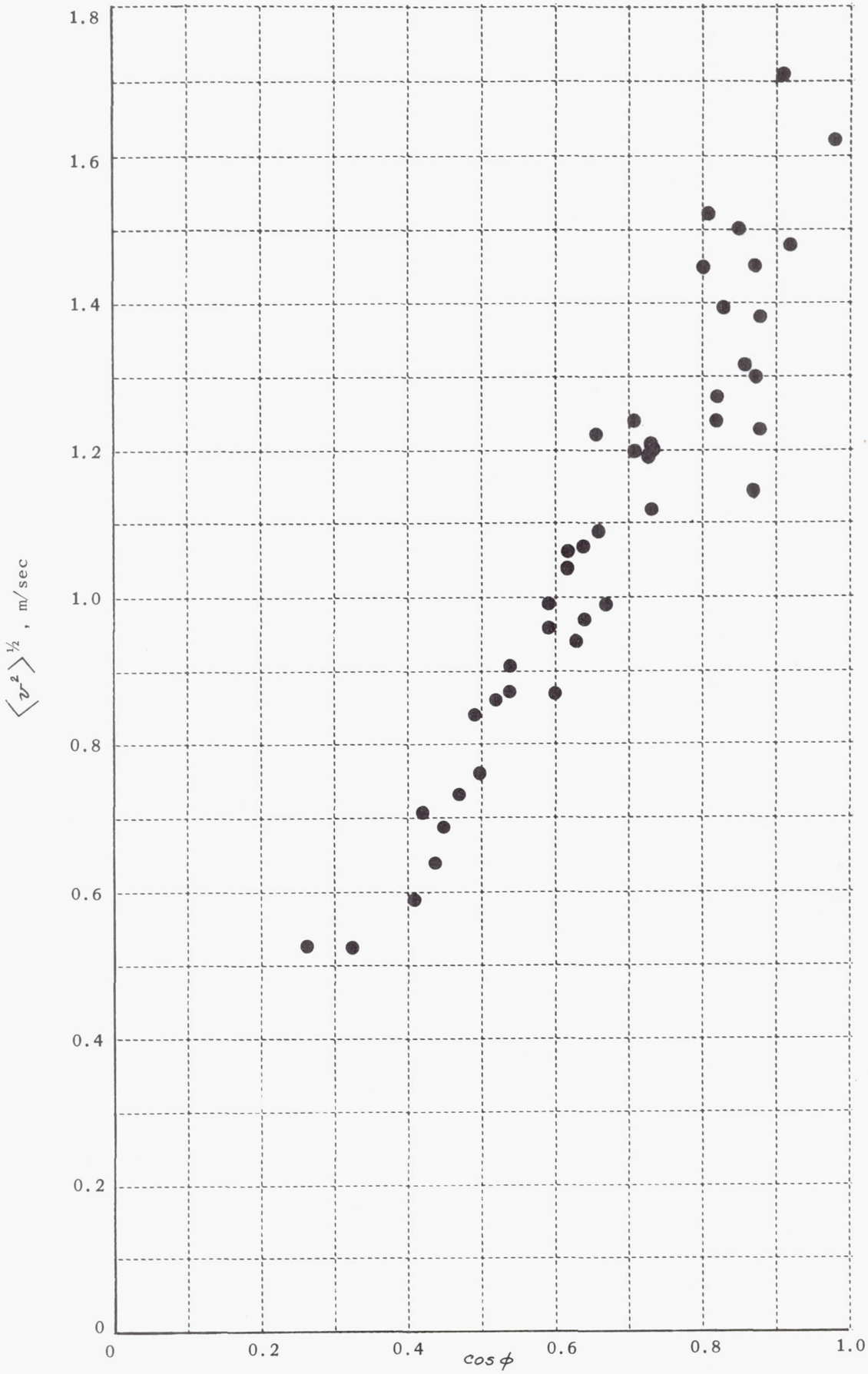

Fig. 20 Viewing angle dependence of Jimsphere erratic velocity fluctuations

It can be shown from (19) that the acceleration vector of the Jimsphere, always directed inward on the erratic orbit, has the magnitude $2\pi a/T_J = 3.3$ m/sec^2, or approximately 0.3g.

The orbital radius of the erratic displacement is found by integration to be 1.72 m. Consequently, the horizontal component of Jimsphere erratic displacement corresponding to $v(t)$ is given by

$$x(t) = 1.72 \sin(2\pi t/T_J - \theta) \tag{20}$$

Equations (19) and (20) are only idealizations of the observed Jimsphere erratic motions. They give rise to a line spectrum for the erratic velocity spectrum, namely,

$$S_r(f) = a^2 \cos^2\phi\, \delta(f - f_J) \tag{21}$$

while actual data show $S_r(f)$ to have a spread of about 0.1 cps around the characteristic Jimsphere frequency f_J (= 0.22 cps). The model defined by (19) and (20), although only an approximation of actually observed Jimsphere motion, is useful in assessing errors in wind data obtained by tracking Jimspheres, as will be seen in Section F.

E. The behavior of Rose balloons

An inspection of the power spectra in Figs. 8-17 shows that Rose (smooth) balloons are not characterized by a well-ordered kind of behavior, as was the case for Jimspheres. Most of the spectra were obtained from experiments designed to permit comparisons between spectral data from balloons of different types under the same meteorological conditions. Thus, sizes were alternated in a series of runs. On December 10 this procedure was modified to investigate the reproducibility of data from each type of balloon individually. Two runs with the same kind of balloon were taken consecutively, and spectra were computed for a height interval common to both. Figs. 16 and 17 contain the

spectra from these experiments. The Jimsphere balloons and 2-ft balloons are seen to yield reproducible data, both in the low frequency ("wind-response") portion of the spectra and in the high frequency ("erratic") portions. The wind-response portions are not expected to be the same for both types, because the altitude intervals that were analyzed are different in the two cases. Further, the ascent rate of the 2-ft balloon is only 1.5 m/sec, less than one-third that of Jimspheres.

Some consistency is also evident in the consecutive runs for 1-m and 2-m Rose balloons (see Fig. 16), particularly in the wind-response portions of the spectra. This observation, especially in the presence of strongly nonstationary data, suggests that 1-m and 2-m balloons respond to the wind in a self-consistent manner, but that their erratic components of motion do not always have the same characteristics. The 2-m balloons usually ascend at 7 m/sec, while the 1-m balloon ascent velocities average 5 m/sec.

Estimates of the mean-square erratic velocities for smooth balloons have been determined by integrating the apparent erratic portions of those spectra $S_v(f)$ in which there is a distinct dip or null - indicating an approximate division of the spectrum into separate erratic and wind-response portions - in accord with the treatment of the Jimsphere spectra. In each of these cases the frequency f_s that separates the two regions was noted, and the frequency f_e which corresponds to the peak amplitude in the erratic spectrum was recorded. The erratic-spectra portions, here estimated as extending from the separation frequency f_s to the high frequency where the spectrum has fallen essentially to the noise level, were integrated numerically to give an estimate of $\langle v^2 \rangle$ for each spectrum. These data are presented in Table 5. For convenience, balloon size, total variance (obtained by integrating the entire spectrum), and the quantity $\sigma^2 - \langle v^2 \rangle$ are also given in the table. The latter is a measure of the intensity of the wind-response components.

Table 5. Intensity of Erratic Velocity Components Obtained from Spectra of Smooth Balloons

Spectrum Code	Balloon Type	Separation freq. (cps)	Erratic Peak freq. (cps)	$\langle v^2 \rangle$	σ^2	$\langle v^2 \rangle^{1/2}$	Altitude Range	$\cos\phi$	$\sigma^2 - \langle v^2 \rangle$
70121	1-m	0.20	0.38	0.90	2.53	0.95	0.4 - 2.1	0.82	1.63
70141	1-m	0.12	0.40	1.03	2.10	1.02	0.9 - 2.3	0.82	1.07
70621	2-m	0.08	0.15	2.34	3.64	1.53	1.0 - 2.5	0.50	1.30
70622	2-m	0.09	0.17	3.10	7.41	1.76	2.5 - 5.0	0.57	4.31
70632	1-m	0.08	0.24	1.30	2.29	1.14	2.5 - 4.2	0.71	0.99
7072	2-m	0.10	0.19	0.84	1.43	0.92	1.0 - 4.3	0.34	0.59
7102	1-m	0.10	0.22	1.46	3.69	1.21	0.9 - 4.1	0.71	2.23
7161	1-m	0.09	0.22	0.98	2.40	0.99	1.4 - 5.3	0.64	1.42
92942	1-m	0.12	0.36	0.62	4.46	0.79	2.5 - 4.2	0.71	3.84
00121	1-m	0.10	0.37	0.31	1.25	0.56	1.5 - 3.8	0.57	0.94
00122	1-m	0.10	0.28	0.32	0.58	0.57	5.5 - 7.5	0.64	0.26
00131	2-m	0.08	0.14	2.16	4.20	1.47	1.5 - 4.0	0.34	2.04
00132	2-m	0.08	0.14	3.16	4.60	1.78	5.5 - 7.5	0.50	1.44
0267	2-m	0.08	0.16	4.59	9.85	2.14	0.4 - 2.0	0.82	5.26
1242	2-m	0.07	0.11	4.73	11.08	2.17	1.0 - 2.5	0.82	7.35
1245	2-ft	0.15	0.25	0.20	1.98	0.45	0.4 - 0.8	0.97	1.78
2091	2-ft	0.10	0.21	0.21	0.52	0.46	0.8 - 1.3	0.77	0.31
21011	1-m	0.09	0.17	2.35	3.97	1.53	0.9 - 2.7	0.82	1.62
2102	1-m	0.09	0.20	3.12	4.74	1.76	0.9 - 2.7	0.87	1.62
2105	2-m	0.08	0.15	4.67	12.46	2.16	0.9 - 4.8	0.77	7.79
2108	2-ft	0.10	0.26	0.16	1.99	0.40	0.4 - 1.3	0.94	1.83
2109	2-ft	0.10	0.25	0.19	1.98	0.44	0.3 - 1.2	0.94	1.79

The data in Table 5 show the dependence of the intensity of erratic velocity fluctuations on balloon size. The four cases of 2-ft balloons have a fairly consistent value of $\langle v^2 \rangle$ which averages about 0.2 $(m/sec)^2$. The peak frequency f_e in the erratic spectra for 2-ft balloons is also fairly consistent at about 0.25 cps. Greater irregularity is evident in the 2-m and 1-m data. For 2-m balloons, $\langle v^2 \rangle$ varies from 0.84 to 4.73 $(m/sec)^2$, while f_e is fairly constant at about 0.15 cps. In 1-m balloons, $\langle v^2 \rangle$ varies from 0.31 to 3.12 $(m/sec)^2$ with f_e ranging from 0.17 to 0.4 cps.

Since the ultimate application of the balloons is the measurement of horizontal wind, it is desirable to determine how the ms erratic velocity $\langle \vec{v}^2 \rangle$ is distributed in direction (i.e., angular or $\hat{k}$ - space distribution). Two distinct cases have been considered for the smooth balloons; both are discussed below.

The first case is that in which the vertical component of the erratic velocity $\vec{v}$ is negligible, and the components of $\vec{v}$ in two orthogonal horizontal directions are uncorrelated, i.e.,

$$v_z \approx 0 \ , \ \langle v_x \, v_y \rangle = 0 \tag{22}$$

For the conditions in (22) one readily obtains the relation*

$$\langle v^2 \rangle^{1/2} = \langle \vec{v}^2 \rangle^{1/2} \cos\phi \tag{23}$$

where ϕ is the radar elevation angle and v, as in Sections C and D, denotes the radial component of $\vec{v}$ (i.e., the component that is observed by the radar). The $\cos\phi$ dependence of $\langle v^2 \rangle^{1/2}$ indicated in (23) has been observed in the Jimsphere data as shown in the discussion of Fig. 20.

---

*In (23) the bent brackets denote an average over an interval of time for which the variation in ϕ is small.

The second case which has been considered is the isotropic erratic velocity case for which

$$\langle v^2 \rangle = \langle v_x^2 \rangle = \langle v_y^2 \rangle = \langle v_z^2 \rangle \tag{24}$$

From (24)

$$\langle v^2 \rangle^{1/2} = \frac{1}{\sqrt{3}} \langle \vec{v}^2 \rangle^{1/2} \tag{25}$$

In contrast to (23), $\langle v^2 \rangle^{1/2}$ in (25) is independent of the elevation angle ϕ. A discussion of the ϕ dependence of $\langle v^2 \rangle^{1/2}$ for the smooth balloons is presented next. From (23) a linear dependence on $\cos\phi$ favors a hypothesis of the validity of the relations (22) whereas ϕ-independence favors the isotropic erratic velocity hypothesis.

Values of $\langle v^2 \rangle^{1/2}$, taken from Table 5 together with their respective corresponding values of $\cos\phi$, are plotted in Fig. 21. The plotted points for balloons of different sizes are distinguished as indicated in the legend for the plot. The grouping of points for particular balloon sizes, quite apparent from the plot, shows that 2-m data were taken, on the average, at higher elevation angles (smaller values of $\cos\phi$) than 1-m data, and that 2-ft data were taken at the lowest elevations. This distribution over elevation angle is a consequence of the faster ascent rates of the larger balloons. The data for 2-m balloons show that high values of $\cos\phi$ are associated with high values of $\langle v^2 \rangle^{1/2}$ in an approximately linear manner, which is consistent with (23), implying thereby, in accord with the above discussion, that the vertical component of the erratic velocity is small compared to its magnitude and that, furthermore, $\langle \vec{v}^2 \rangle$ is approximately constant for the 2-m balloons. Noticeable deviations of the 2-m balloon points from their best-fit straight line can be observed. One reason for these deviations is that the elevation angle occasionally varies over an appreciable range during the length of record required for spectral computations. The values of $\cos\phi$ in Table 5 (which were used in constructing Fig. 21) were estimated for each case as

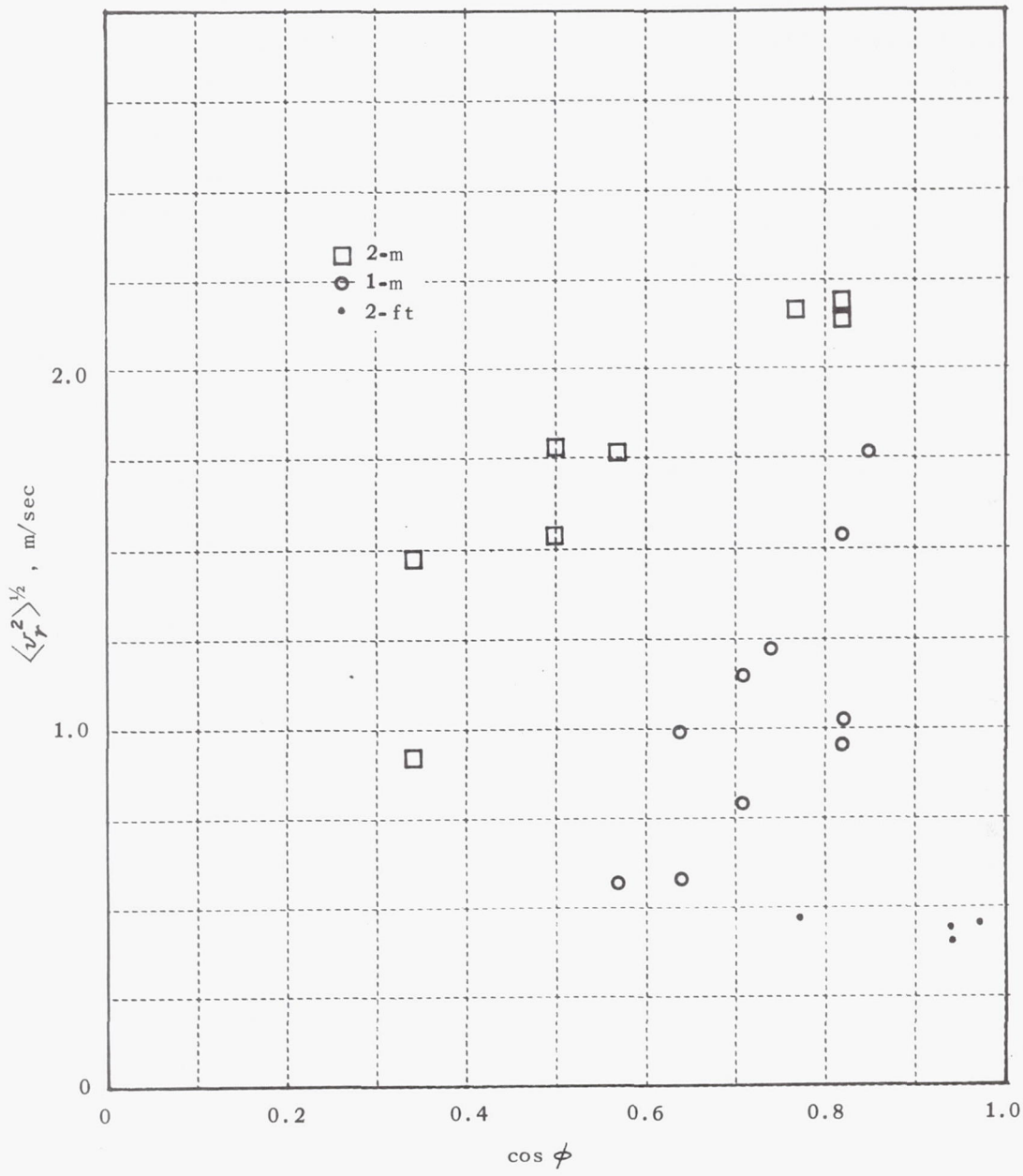

Fig. 21 Viewing angle dependence of erratic velocity fluctuations of smooth balloons.

being representative for the values of ϕ encountered during the case run. Consequently some scatter is to be expected because of the changes in angle during the time of measurement. This was not a problem in the analysis of Jimspheres, for their orderly behavior permitted $\langle v^2 \rangle^{1/2}$ to be estimated from very short lengths of record, over which ϕ was virtually constant. A reasonable estimate of the best-fit straight line for the 2-m data intersects $\cos\phi = 1$ at about 2.6 m/sec. Consequently, for these balloons, the rms erratic velocity is given approximately by

$$\langle v^2 \rangle^{1/2} = (2.6\ m/sec) \cos\phi \ . \tag{26}$$

It will be recalled that the constant appropriate for Jimspheres was found to be about 1.7 m/sec, a figure considerably smaller than the 2.6 m/sec value in (26).

The data for 2-ft balloons, consisting of only four points on Fig. 21, show no elevation angle dependence and can best be characterized by the relation

$$\langle v^2 \rangle^{1/2} = \frac{1}{\sqrt{3}} \langle \vec{v}^{\,2} \rangle^{1/2} \approx 0.45\ m/sec \tag{27}$$

which is the isotropic case.

The 1-m Rose balloon data show a tendency for $\langle v^2 \rangle^{1/2}$ to increase with $\cos\phi$, but there is more scatter than for the 2-m case. Again, the changes in elevation angle during the measurement time could account for some of the scatter. Within the estimated experimental error no straight line from the origin provides a good fit for the data. Consequently neither the "horizontal" model in (23) nor the "isotropic" model in (25) can be used to describe the erratic motions of 1-m balloons adequately.

In an attempt to understand the apparent complexity of the 1-m balloons' erratic behavior, two ascents were analyzed in detail. The ascents were chosen because, in each case, the elevation angle varied over a wide range. An elevation angle effect, if present, should show up in these cases. For both runs, short-term rms velocities were computed at equally spaced intervals on the Doppler velocity record. The intervals between samples were 100 sec for run 92921 and 50 sec for run 0016. The interval was made shorter in the latter case because the elevation angle was changing more rapidly. For both runs the rms velocities were computed for 18 adjacent points on the trace, separated by intervals of 0.8 sec. Eighteen points were chosen for convenience because one IBM card in the format used will accommodate this number of points. The rms values thus were computed from samples approximately 15 seconds in length which, generally speaking, are sensitive to velocity fluctuations having periods shorter than 15 seconds. The spectral data show that components having frequencies higher than 1/15 cps are primarily in the erratic spectrum. It follows that the computed short-term rms velocities are primarily indicative of erratic velocity components. The rms velocities were computed from smoothed data (due to RC filtering) and should be denoted by $\langle v_s^2 \rangle^{1/2}$. Correction for the smoothing would require integration over the erratic velocity range of unsmoothed data. The spectrum of unsmoothed data could be readily computed from the measured spectrum by means of equation (3.2) of Appendix 3 which involves the transfer function of the RC filter. However, since power spectra cannot be computed with any reliability from such short intervals of data as those considered in this particular analysis, a measured value of $\langle v_s^2 \rangle^{1/2}$ cannot be readily modified to yield the unsmoothed rms velocity $\langle v^2 \rangle^{1/2}$. Consequently, the behavior of $\langle v_s^2 \rangle^{1/2}$ must suffice for this analysis. Spectral data indicate that σ_v^2, the total variance of unsmoothed velocity, exceeds σ_{vs}^2 , the total variance of smoothed velocity, by about 60%. In rms terms, this would be only about 30%. It is reasonable therefore that although $\langle v_s^2 \rangle^{1/2}$ will not display the exact behavior of $\langle v^2 \rangle^{1/2}$, it will in any case reflect the more significant characteristics of $\langle v^2 \rangle^{1/2}$.

The data for the two selected runs with 1-m balloons are presented in Table 6. In Fig. 22 are plotted the values of $\langle v_s^2 \rangle^{1/2}$ versus $\cos\phi$ for both runs. The index numbers are entered for the points to make apparent the sequence of data. Curves are sketched through consecutively numbered points to indicate the trajectories of the points representing each balloon in the space determined by coordinates of $\langle v_s^2 \rangle^{1/2}$ and $\cos\phi$. The two trajectories show certain similar characteristics. Both begin by proceeding along a downward path toward the origin. After a certain point is reached along this path, the trajectories curve out toward high values of $\cos\phi$ with considerable oscillation about a more or less horizontal line. In terms of the balloon behavior, they indicate that the measured rms erratic velocities decrease as elevation angle increases in the early portion of each flight. In 0016, the elevation angle reaches its maximum value at point 10 and then starts to decrease. As far as point 13, the erratic velocity retraces its earlier behavior. After point 13, the rms erratic velocity does not increase steadily with $\cos\phi$, but rather tends to oscillate. In 92921, the rms velocity initially decreases with increasing elevation angle. After point 3, where the elevation angle attains its maximum, the rms velocity remains at the value of about 0.5 m/sec rather than increasing in a manner that would indicate a simple elevation effect.

An interpretation of this behavior that is consistent with our analyses of the other types of balloons is as follows: In the early portions of the runs (i.e. at low altitudes) the erratic behavior of these two 1-m balloons can be described by (23), an expression for the case of predominantly horizontal erratic velocity perturbations. In later portions of the runs (corresponding to higher altitudes) the erratic behavior can be approximately described by (25), an expression for the case of isotropic motions. The oscillating character of the trajectories in Fig. 22 for these later portions might be interpreted as a kind of instability in which the character of the erratic component changes between isotropic and predominantly horizontal. The altitude at which the apparent transition occurs is 2.1 km for 92921 and about 3.5 km for 0016. The Reynolds number for a 1-m balloon at these altitudes, assuming an

Table 6. Short-term rms Erratic Velocities for Two Selected 1-m Rose Balloon Runs

Run	Point number	ϕ	$\cos\phi$	$\langle v_{rs}^2 \rangle^{1/2}$ (m/sec)	height (km)
9292	100-sec interval between measurements 1	60	0.50	0.98	1.06
	2	70	0.34	0.74	1.62
	3	72	0.31	0.57	2.10
	4	54	0.59	0.44	2.44
	5	40	0.78	0.44	2.83
	6	35	0.82	0.57	3.44
	7	30	0.87	0.36	3.85
0016	50-sec interval between measurements 1	12	0.98	1.39	0.44
	2	24	0.91	1.22	0.85
	3	34	0.83	1.28	1.12
	4	46	0.69	0.78	1.44
	5	56	0.56	0.49	1.74
	6	66	0.41	0.26	1.92
	7	74	0.28	0.26	2.12
	8	82	0.14	0.20	2.37
	9	87	0.05	0.08	2.49
	10	89	0.02	0.07	2.90
	11	87	0.05	0.10	3.09
	12	84	0.10	0.14	3.28
	13	79	0.19	0.20	3.53
	14	75	0.26	0.10	3.77
	15	70	0.34	0.17	3.95
	16	66	0.41	0.25	4.11
	17	63	0.45	0.25	4.28
	18	61	0.48	0.25	4.45
	19	59	0.51	0.22	4.71
	20	58	0.53	0.37	4.91
	21	56	0.56	0.25	5.06
	22	54	0.59	0.20	5.26
	23	53	0.60	0.32	5.51
	24	51	0.63	0.17	5.60
	25	50	0.64	0.26	5.82

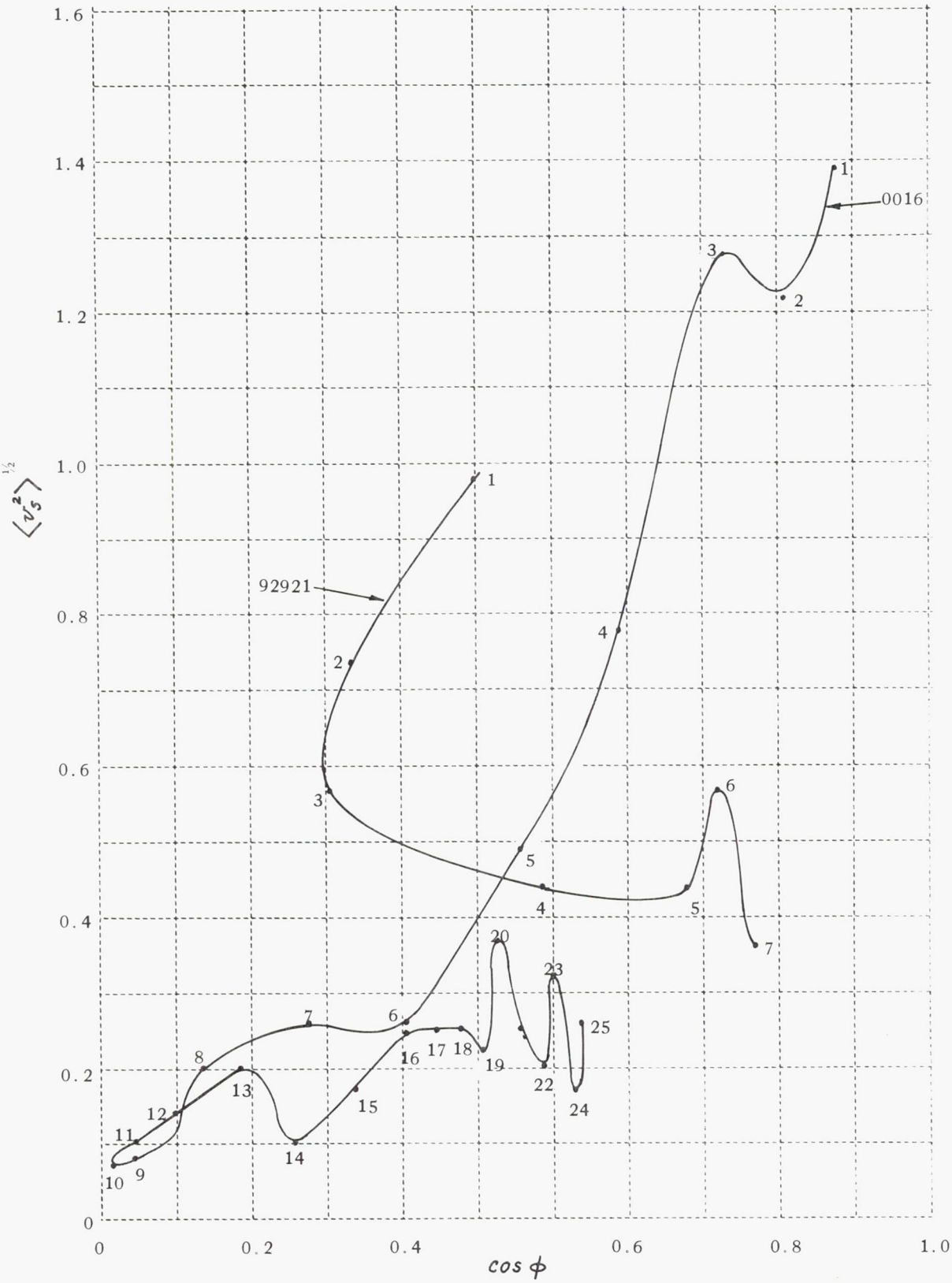

Fig. 22 Elevation angle dependence of short-term rms erratic velocity in two selected 1-m balloon flights.

ascent rate of 5 m/sec, is approximately 2.5×10^5. Wind tunnel data show that a transition in the flow around spheres occurs at a Reynolds number of about 3×10^5. For higher numbers the flow is turbulent; for lower numbers it is laminar. The Reynolds numbers for balloons diminish with altitude. Consequently, on the basis of wind tunnel data, one might expect the flow at low altitudes around a given balloon to be more turbulent than that at high altitudes. Arguing further, one could conclude that the change in character of 1-m balloon erratic velocity data between low and high altitudes is connected with the change in the nature of flow. At altitudes below 2 or 3 km, the Reynolds number is greater than 2.5×10^5, the flow is turbulent, and the erratic behavior fits the horizontal perturbation model. At higher altitudes the flow becomes laminar and the erratic velocity becomes more or less isotropic. This conclusion cannot be stated with certainty because it rests only on two cases and does not explain the reason why the trajectories for even these two cases are not coincident. Yet the conclusion seems reasonable because it is in agreement with the behavior of other kinds of balloons. Thus, Jimspheres and 2-m Rose balloons, about which the flow is always turbulent in our experiments, were observed to fit the horizontal-perturbation model. The 2-ft balloons on the other hand, with their very low Reynolds numbers and consequent laminar flow, were found to fit the isotropic case. The 1-m balloons happen to exhibit both kinds of behavior only because they pass through the transitional region of flow.

On the basis of these conclusions, the model for describing the intensity of 1-m balloon erratic velocity fluctuations would have two forms, depending upon whether the flow was turbulent or laminar. For low altitudes where the flow is turbulent, a suitable expression is of the form

$$\langle v^2 \rangle^{1/2} = \langle \vec{v}^{\,2} \rangle^{1/2} \cos\phi , \qquad (28)$$

where, however, $\langle v^2 \rangle^{1/2}$ cannot be assumed to have the same value for all 1-m balloons since even the very limited evidence of Fig. 22 does not indicate that the 1-m balloons have the same value of $\langle v^2 \rangle^{1/2}$ for a given elevation angle. For the region of laminar flow at higher altitudes, the 1-m rms erratic velocity can be approximated by

$$\langle v^2 \rangle^{1/2} \approx const. \tag{29}$$

The constant cannot be determined from Fig. 22, since values of smoothed rms velocity are plotted rather than $\langle v^2 \rangle^{1/2}$. In general $\langle v^2 \rangle^{1/2} \geq \langle v_s^2 \rangle^{1/2}$. Since a reasonable value of $\langle v_s^2 \rangle^{1/2}$ in the laminar flow region is, from Fig. 22, approximately 0.4 m/sec, we can write in place of (29)

$$\langle v^2 \rangle^{1/2} \geq 0.4 \ m/sec \tag{30}$$

If, as this analysis suggests, stability of the flow around ascending balloons is indeed the critical factor in determining the nature of balloon erratic motions, then one would expect the behavior of 1-m balloons to appear less organized than that of the other balloons tested. Balloons in the free atmosphere should not be expected to exhibit the abrupt transition from laminar to turbulent flow that is found to occur for smooth spheres in wind tunnels. As well as not being perfectly smooth spheres, no two balloons are exactly the same. Small differences in the inflation of these balloons unavoidably makes some relatively smoother than others. Furthermore, the atmosphere itself is not subject to the control of air in wind tunnels. Consequently, when the Reynolds number for a balloon is near the critical (wind tunnel) value of 3×10^5, the balloon might be expected to behave quite irregularly, having neither fully developed turbulent flow nor completely laminar flow. For 1-m balloons in most of our experiments the Reynolds number lies approximately between 2×10^5 and 3×10^5 in the altitude interval 1-5 km. Over this Reynolds number range the flow might be of transitional nature. Since most of the 1-m data come from the 1-5 km height interval, uncertainties would therefore be expected.

The rms erratic velocities of the various balloons tested, and their dependence on viewing angle, characterize the intensity of the erratic behavior. What has been determined about these rms velocities from the data for smooth balloons is given in equations (26), (27), (28), and (30). In order to assess the wind measurement error which arises from the balloon erratic behavior, it is necessary to know the power spectrum of the erratic velocity component in addition to its rms value. The variability of spectral shapes, as seen in Figs. 8-17, indicates that one spectral shape is not sufficient for adequately describing any of the smooth balloon types. This is obviously the case for 1-m balloons, for which even the rms erratic velocity cannot be described precisely by a simple model, apparently because of the complexity of the Reynolds number effect. Yet for those 2-m balloon spectra in which apparent erratic components are separate from the wind-response components (see Table 5), the erratic spectra have an approximate regularity in shape. These spectra are fairly peaked, with the peaks occurring at approximately 0.15 cps. As a rough approximation to the erratic spectra we could use Dirac delta functions, which were adequate for describing Jimsphere erratic spectra. In the case of 2-m balloons, the delta functions would be centered at 0.15 cps and would have intensities such that

$$\langle v^2 \rangle \approx 7\,(m/sec)^2 \times \cos^2\phi \qquad (31)$$

which follows from the expression in (26) for the rms erratic velocity.

The model in (31) does not account for the spread of the erratic spectra, which is obviously more significant for 2-m balloons than for Jimspheres. The erratic spectra for the 2-m cases in Table 5 are seen to extend out to about 0.3 cps, but it is not clear from the spectra how far the erratic portions extend in the low frequency direction.

It would seem that some additional insight into the shape of the 2-m balloon erratic spectra, particularly in the low frequency end, might be gained by comparing the data from consecutive ascents of balloons of different types. The power spectrum $S_v(f)$, computed from the Doppler velocity trace of any balloon during ascent, in general has content due to wind-response velocity fluctuations and content due to erratic velocity fluctuations. It has been found in the foregoing analysis that the erratic components are stronger for 2-m balloons than for the other types tested. One means of assessing the form of the erratic spectrum $S_r(f)$ of the 2-m balloon would be to compare the spectrum $S_v(f)$ of this balloon with the spectrum of a balloon having no erratic components. Assuming that both balloons ascend through the same windfield and respond in the same way to the wind, the wind-response components in both spectra would be identical. Consequently the spectra could be subtracted on a component-by-component basis and the resulting difference spectrum would be just the erratic spectrum $S_r(f)$ of the 2-m balloon.

Although all of the balloons tested in our experiments have erratic spectral content, this spectral content is, from the discussion of Section D, apparently reasonably distinct and separate from the wind-response content in the case of Jimspheres. Thus, it would seem that Jimsphere data, in principle, provide a means of subtracting the wind-response components from 2-m spectra, thereby leaving the erratic velocity spectrum of the 2-m balloon. Experiments were designed with this kind of comparison of spectra in mind. In practice there are several reasons why the wind-response components in 2-m spectra cannot be exactly estimated from Jimsphere data. The ascent rate of Jimspheres is about 5.5 m/sec, while that of 2-m balloons is about 7 m/sec over the altitudes of our experiments. Thus given height variations of the wind will produce slightly lower frequency content in a Jimsphere spectrum than in a 2-m balloon spectrum. This circumstance makes the wind-response spectrum of a Jimsphere slightly narrower than that of the 2-m balloon, for a given windfield. The difference in ascent rate usually leads to lower elevation angles for a Jimsphere than for a 2-m balloon traversing the same height interval. This effect causes a small

difference in the Doppler components for the two balloons. Another discrepancy is introduced by the fact that spectral data cannot be compared exactly on an equal-altitude basis. The unavoidable errors in radar-determined altitude cause some mismatch in altitude intervals that are apparently identical. Probably the most important potential cause of differences between the wind-response components in consecutive runs is time variability of the windfield. During the unavoidable interval between successive ascents, the windfield might undergo changes that significantly modify the wind-response portion of the velocity spectrum. This effect was usually estimated by comparing the wind-response portions from consecutive runs with balloons of the same type. If two such runs reveal only small changes in the wind-response portion of the spectrum, it is reasonable to conclude that time variations in the wind profile were not important.

Bearing in mind all the limitations and qualifications on spectral comparisons, let us now turn to the three cases in which consecutive Jimsphere and 2-m balloon spectra were suitable for comparison. The spectra comprising these cases are as follows:

Case	Jimsphere spectrum	2-m spectrum
1	00111	00131
2	00112	00132
3	2106	2105

It is seen in Table 3 that the height intervals over which spectra were computed were the same for the Jimsphere and the 2-m balloon in each case. The wind-response spectrum for each case is taken to be the low frequency portion of the Jimsphere spectrum. This portion extends from frequency zero out to about 0.15 cps, beyond which the strong erratic spectral content becomes apparent. The wind-response portion, so defined, is then subtracted from the corresponding 2-m balloon spectrum to yield a difference spectrum. For the ideal situation, this difference spectrum would be identical to the erratic spectrum of the 2-m balloon.

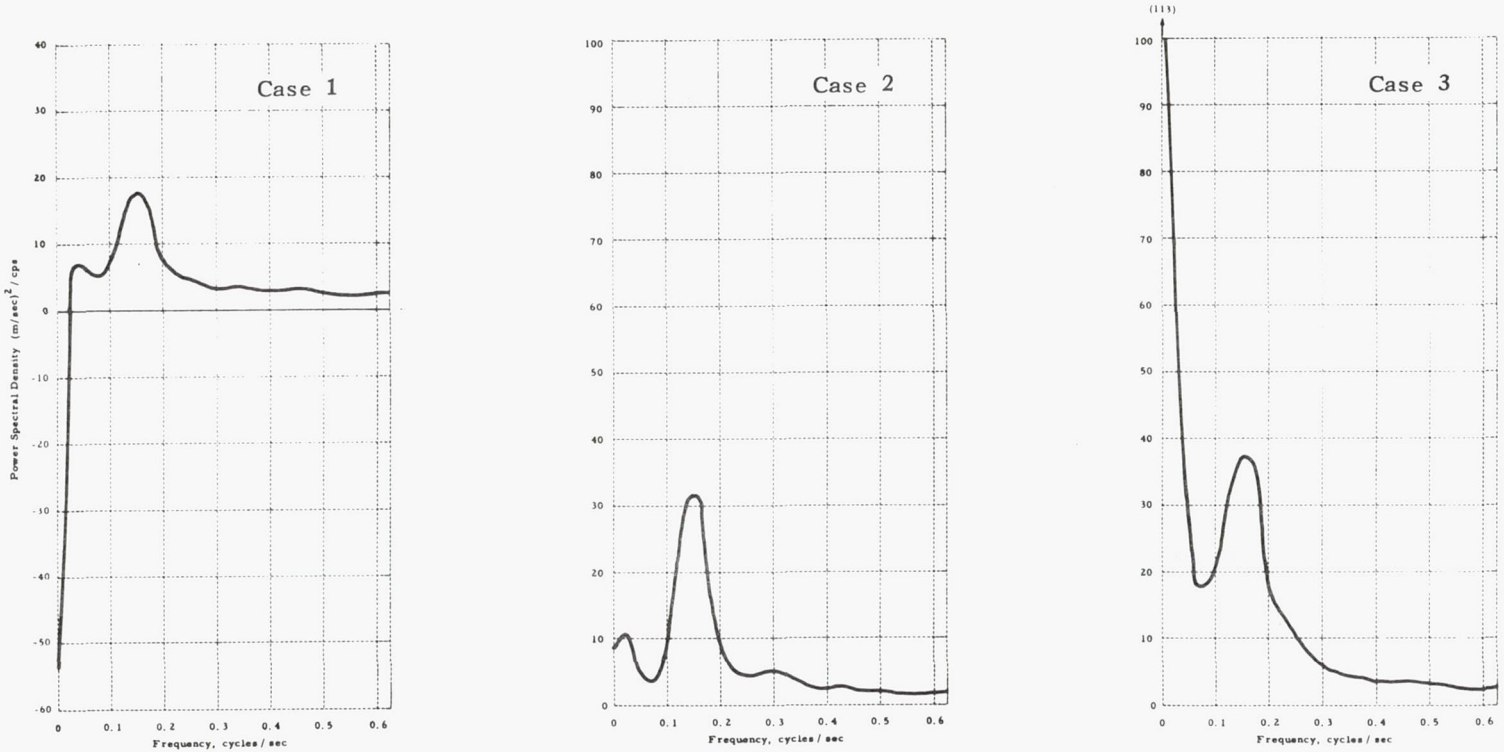

Fig. 23 Difference spectra for three selected 2-m balloon flights

Difference spectra for the three cases above are plotted in Fig. 23. In each there is a consistent peak at 0.15 cps which falls to the noise level by about 0.3 cps. The low frequency portions have different characteristics in each case. Although in principle the procedure of forming difference spectra can lead to better estimates of the erratic components at low frequencies, no particular improvement in our understanding of these low frequency components accrues from the three cases studied here. It seems evident that the erratic components extend to frequencies as low as 0.08 cps, but it cannot be determined from the data what the appropriate spectral amplitude is at this frequency or whether the erratic components extend to significantly lower frequencies. It might be that there is no single spectral form that will adequately represent all 2-m erratic spectra in the low frequency range. In any case, it is reasonable to assume that the differences in the three spectra of Fig. 23 at the low frequencies are primarily due to the errors mentioned above.

Allowing for the uncertainty in the erratic spectral content at low frequencies, some definite characteristics of 2-m balloon behavior have been established by the analysis: There is appreciable erratic spectral content extending in frequency from 0.08 to 0.3 cps and peaking consistently at 0.15 cps. The shape of the spectrum in this range is usually of the general form shown in Fig. 24. These high frequency components arise primarily from horizontal erratic velocity perturbations having an rms value of about 2.6 m/sec.

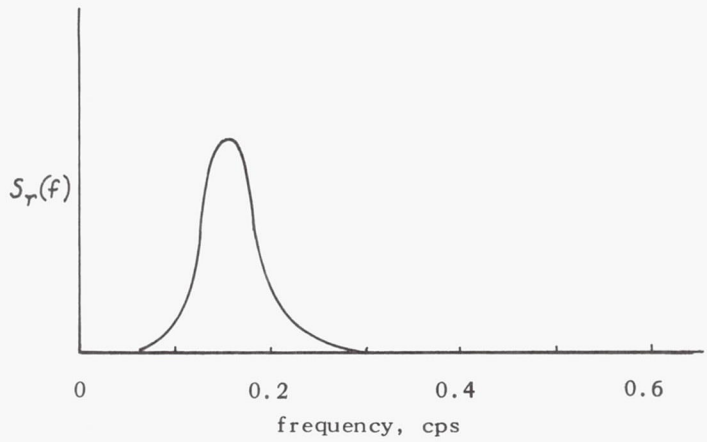

Fig. 24 Suggested model for 2-m Rose balloon high-frequency erratic spectrum

A convenient analytic form which approximates the erratic spectrum of Fig. 24, and which embodies the correct rms value, is

$$S_r(f) = \langle v^2 \rangle \frac{1}{\sqrt{2\pi}\,\sigma} \exp\left[\frac{-(f-f_o)^2}{2\sigma^2}\right] \qquad (32)$$

where $\langle v^2 \rangle$ is given by (31), f_o = 0.15 cps, and $\sigma \approx 0.03$ cps. This value of σ seems to provide a reasonable fit to the curve in Fig. 24. Estimates of errors in the FPS-16 radar/Jimsphere system which are based upon (32) are limited to errors arising from erratic velocity variations having frequencies higher than 0.08 cps. Contributions from erratic spectral content at lower frequencies are not included.

F. Wind errors in the Rose Sounding System caused by erratic balloon motions

The characteristics of erratic motions of the different balloons tested are described in preceding sections. The influence of these motions upon balloon-wind data is determined by the extent to which they are smoothed out by data reduction procedures in a given system. It is shown in Appendix 2 that two kinds of smoothing arise in the Rose Sounding System. The first of these, characterized by the filter function $T(f)$, arises because the rapidly acquired balloon position data are averaged over a short time interval δt to give an average balloon position. The second smoothing results from computing the balloon's velocity from the difference in two such positions separated by time Δt. Its filtering effect is denoted by $Q(f)$. The total filtering effect of the system is given by $T(f) \cdot Q(f)$.

In Appendix 2, $Q(f)$ is shown to have the form

$$Q(f) = \left(\frac{\sin \pi f \Delta t}{\pi f \Delta t}\right)^2 \qquad (33)$$

The position data are apparently averaged by a simple running mean over δt (Scoggins, 1963), from which it turns out that

$$T(f) = \left(\frac{\sin \pi f \delta t}{\pi f \delta t}\right)^2 \quad , \tag{34}$$

a relation also derived in Appendix 2. Both Δt and δt in the FPS-16/spherical balloon system are approximately 3.6 sec. Consequently the combined filter effect of the system is given by

$$T(f)\,Q(f) = \left(\frac{\sin 3.6\pi f}{3.6\pi f}\right)^4 \quad ,$$

with f in cps. This transfer function is plotted in Fig. 25, which shows that the system strongly suppresses balloon velocity fluctuations with frequencies higher than 0.2 cps. This is consistent with the 25 m height resolution of the system, since 0.2 cps corresponds to 25 m for a balloon ascending at 5 m/sec. (For the 7 m/sec ascent rate of 2-m Rose balloons, a frequency of 0.2 cps actually corresponds to an irregularity with a length scale of 35 m. Thus although the data are processed to yield a resolution of 25 m, the system almost completely suppresses wavelengths shorter than 35 m when 2-m Rose balloons are used.)

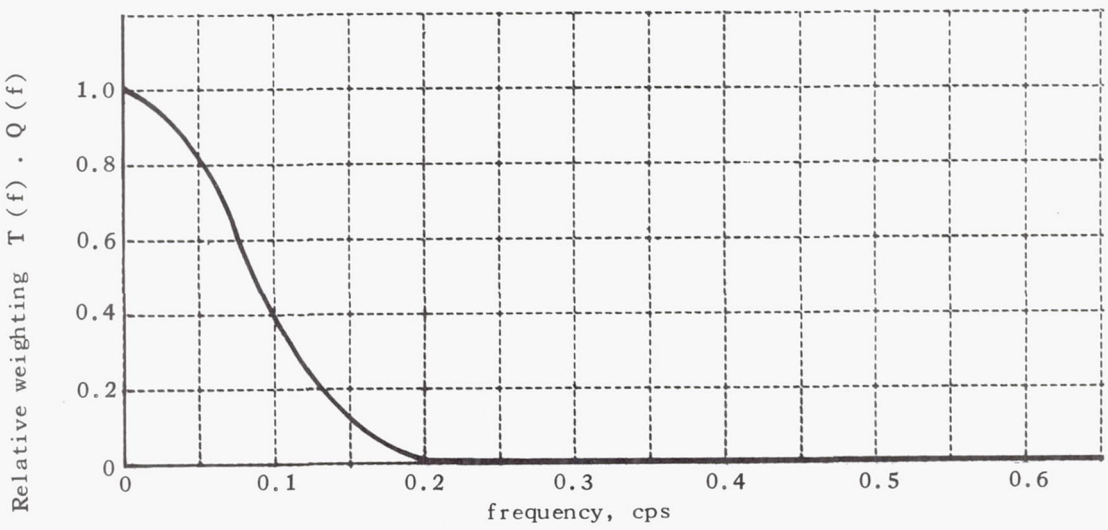

Fig. 25 Response function characterizing FPS/16 spherical balloon system

Since the system is characterized by a linear filter, the spectrum $S_r(f)$ of erratic velocity of a given balloon can be taken as the input to the system, with the output (measured) spectrum given by

$$S_r(f)\,T(f)\,Q(f)$$

The mean-square wind velocity error due to erratic motions is then simply, from Appendix 2,

$$\langle(\mathcal{E}_r')^2\rangle = \int_0^\infty S_r(f)\,T(f)\,Q(f)\,df. \qquad (35)$$

This formula for the wind error can be evaluated for Jimspheres and 2-m Rose balloons by using the appropriate forms for $S_r(f)$.

Utilizing (21) to characterize the Jimsphere erratic velocity spectrum, it is readily determined from (35) that the Jimsphere erratic behavior contributes only negligibly to the error in the wind velocity measured by the FPS-16/Jimsphere system. On the other hand, the erratic behavior of the 2-m Rose balloon, described approximately by (32), causes an rms wind-velocity error of 1.0 m/sec, as obtained by graphical integration of (35). It is worth noting here that the error expression (35) is not strongly sensitive to the choice of σ in the model (32) for the 2-m balloon erratic spectrum. Indeed, for σ = 0.05 m/sec, it turns out that

$$\langle(\mathcal{E}_r')^2\rangle^{1/2} = 1.1\ m/sec$$

and in the case of the very narrow erratic spectrum corresponding to the limiting case of (32) as $\sigma \to 0$,

$$\langle(\mathcal{E}_r')^2\rangle^{1/2} = 0.9\ m/sec$$

Consequently, for 2-m Rose balloons an estimate of the rms wind velocity error due to high frequency erratic behavior is 1 m/sec, more or less independently of the exact value of σ in the approximate expression (32) for $S_r(f)$.

V. CONCLUSIONS AND RECOMMENDATIONS

All of the balloons tested exhibit aerodynamically-induced motions which produce erratic fluctuations in the Doppler velocity records. The experiments were well suited for analyzing the small-scale erratic components of balloon motions, in particular those which are readily distinguishable from actual wind-response motions. In many of the computed velocity spectra the content at frequencies higher than about 0.1 cps is apparently erratic in origin, while content at lower frequencies appears to be primarily due to wind-response motions. It cannot be determined from the data whether erratic components are present in the apparent wind-response region below 0.1 cps. Strong components are present at these low frequencies, but they could be entirely accounted for by wind-response motions and the nonstationary character of the data. In any case, the analysis of erratic motions was based on those components having frequencies greater than approximately 0.1 cps.

For Rose-type balloons (smooth and spherical) the intensity of erratic motions is greater for large balloons than for small ones over the altitude range of the experiments. For those balloons around which the airflow is turbulent (Reynolds numbers greater than 3×10^5) the erratic motions are confined primarily to the horizontal plane. In the case of laminar flow (Reynolds numbers less than 2×10^5) the erratic motions are weaker and are apparently of the same intensity in all directions. Jimspheres exhibit a remarkably regular behavior, having an orbital erratic component that gives rise to helical ascent trajectory.

As a consequence of the data smoothing in the FPS-16 radar/spherical balloon system the orbital erratic component of Jimspheres is undetected; it does not contribute to wind measurement errors in this system. The high frequency erratic behavior of 2-m Rose balloons, however, contributes about 1 m/sec to the rms wind error. Thus the Jimsphere represents a solution

to the problem of wind errors caused by erratic motions of balloons in the FPS-16 system used at Cape Kennedy. Wind errors resulting from using 1-m Rose-type balloons cannot be accurately assessed because of the relatively complex behavior of these balloons. Over much of the altitude range of our experiments these balloons are in the critical flow region that is neither fully developed turbulent nor laminar. It is nevertheless clear that the 1-m Rose balloons are more accurate wind sensors than the 2-m Rose balloons, for which the erratic motions are considerably more intense.

Relationships have not been found between balloon erratic behavior and meteorological conditions. This does not imply that the erratic motions are independent of meteorological conditions, but only that any such relations were masked by other variability in the data. Moreover, the requirement of tracking the balloons optically restricted the experiments to clear days and might have biased the results.

Since it is the purpose of the FPS-16/spherical balloon system to measure the wind profile with high resolution, the evidence in this report suggests that the smoothing imposed by data processing in the system is more severe than need be for Jimspheres. The inertial damping of these balloons, as determined by Eckstrom, et al. (1965), is equivalent to a running mean smoothing over about 3 m. Thus the effective cut-off of the Jimsphere as a wind tracer would be at 3 m or, in frequency terms, at about 1.8 cps. It would seem desirable on the basis of inertial considerations alone, therefore, assuming that very high resolution is required, to compute Jimsphere-measured wind profile spectra out to frequencies exceeding 1 cps. The analysis of erratic motions has shown, of course, that spectra extending this far would not be representative of wind because of the strong characteristic Jimsphere component at 0.22 cps. In the present system, this erratic component is suppressed, but not by a very efficient kind of filter. Because of the very narrow band of erratic components in a Jimsphere spectrum, it would be necessary to filter out only the components around 0.22 cps. The response of the system, however, as shown in Fig. 25, is down by 60% at frequencies

as low as 0.1 cps. Full advantage could be taken of the Jimsphere as a precise wind sensor by using a sharp numerical filter on the data which would suppress frequencies beyond 0.2 cps while admitting components at lower frequencies.

ACKNOWLEDGMENT

The balloon-tracking experiments were conducted by a team made up of Messrs. C. C. Easterbrook, W. C. Kocmond, R. L. Peace, and G. A. Zigrossi, whose cooperation is gratefully acknowledged. The balloons were kindly furnished by Mr. James R. Scoggins of the George C. Marshall Space Flight Center. The analog records were digitized by the Flight Research Department of CAL under the supervision of Mr. W. H. Shed. Programming for the digital computer was handled very efficiently by Mr. H. Selib of the Computer Services Department. We benefited from discussions with Mr. R. J. Pilié and Dr. G. E. McVehil of CAL and with Mr. Scoggins of NASA/MSFC.

REFERENCES

Blackman, R. B., and J. W. Tukey, 1958: The measurement of power spectra. Dover Publications, New York. (see pp. 21ff)

Eckstrom, C. V., and R. E. Albrecht, 1965: Theoretical study and engineering development of Jimsphere sensor. Monthly Progress Report No. 11. G. T. Schjeldahl Co., Northfield, Minn.

Henry, Robert M. et al., 1961: The smoke trail method for obtaining detailed measurements of the vertical wind profile for application to missile-dynamic-response problems. NASA TN D-976.

MacCready, Paul B. and Henry R. Jex, 1964: Study of sphere motion and balloon wind sensors. NASA TMX-53089.

McVehil, G. E., et al., 1965: Some measurements of balloon motions with Doppler radar. To be published in J. Appl. Meteor.

Reed, Wilmer H. III, 1963: Dynamic response of rising and falling balloon wind sensors with application to estimates of wind loads on launch vehicles. NASA TN D-1821.

Scoggins, James R., 1963: An evaluation of detail wind data as measured by the FPS-16 Radar/Spherical Balloon Technique. NASA TN D-1572.

———————, 1964a: Aerodynamics of spherical balloon wind sensors. J. Geophys. Res. 69, 591-598.

Scoggins, James R., 1964b: Spherical balloon wind sensor behavior. Paper presented at AMS 5th Conf. on Appl. Meteor., Atlantic City, N. J.

Tripp, B. R., 1964: The CAL pulse Doppler radar. Proc. 1964 World Conference on Radio Meteorology, Boulder, Colo., pp. 332-337. (See also, with same title, CAL Report No. 133, Dec. 1963).

APPENDIX 1

The Definition and Properties of the Average $[\![F]\!]$ of a Function F of Balloon Position and Velocity Coordinates

Balloon data analysis is facilitated by a division of the balloon velocity into two portions, one portion which nominally represents wind-response and is non-erratic in character, and a second portion which represents the erratic or random deviation of the total velocity from the nominal wind-response velocity.

This division can be based formally upon a statistical average of the balloon velocity $\vec{V}$ which tends to remove spurious behavior contributions to $\vec{V}$ while retaining gross wind-response contributions. The desired character of this average, which is denoted by $[\![\vec{V}]\!]$, can be achieved by defining it in terms of an ensemble chosen on the basis of a consideration of the requisite ensemble properties. The requisite properties can in turn be inferred from a consideration of the desired character of $[\![\vec{V}]\!]$. The definition of the average $[\![F]\!]$ of any function F of balloon coordinates then follows from the definition of the ensemble.

Since the ensemble average $[\![\vec{V}]\!]$ is to be representative of the instantaneous wind-response portion of the velocity of a given balloon in a given local wind field, it is clear that every member balloon of the representative ensemble should be subjected to the same local wind field. This condition, a requisite property, will be satisfied provided the local wind field is equal to its ensemble average.

The ensemble average $[\![\vec{V}]\!]$ should be free of spurious behavior while retaining the gross wind-response contributions. Both of these conditions can be satisfied if the ensemble has a uniform distribution of phase points (i.e. members) throughout the physically admissable portion of phase space.

In the following we shall first introduce an emsemble, $\mathcal{E}$, which is suitable for describing a given balloon experiment. This ensemble, $\mathcal{E}$, will then serve as a point of departure for the introduction of the ensemble upon which the average $[\![F]\!]$ is based.

Consider a representative ensemble, $\mathcal{E}$, which corresponds to a hypothetical set of many samples of data obtained under identical weather conditions. Each member of the ensemble represents data on one particular balloon. It is further assumed that all balloons were released from the same point and at corresponding times, that is,

$$\vec{X}_k(t_o) = \overline{\vec{X}}(t_o) \tag{1.1}$$

where $\vec{X}_k(t)$ denotes the position vector at time t for the kth member of the ensemble $\mathcal{E}$, the overbar denotes an average over $\mathcal{E}$, and t_o denotes the balloon launch time. The atmospheric wind field is the same for each member of $\mathcal{E}$ so that

$$\vec{W}_k[\vec{X}, t] = \overline{\vec{W}}[\vec{X}, t] \equiv \vec{W}[\vec{X}, t] \tag{1.2}$$

where $\vec{W}_k[\vec{X}, t]$ denotes, for the kth member of $\mathcal{E}$, the sum of the wind velocity and the mean balloon ascent velocity at the point $\vec{X}$ and time t.

If $\mathcal{E}$ has N member balloons, the average of F over $\mathcal{E}$ may be expressed

$$\overline{F} = \frac{1}{N}\sum_{k=1}^{N} F_k \tag{1.3}$$

where F_k denotes F evaluated for the k th member (balloon) of the ensemble.

The average $[\![F]\!]$ of F is defined, as discussed above, on an ensemble with certain requisite properties. These properties can be realized in a subensemble of E which is constructed utilizing the cell method of statistical physics. Consider all of space to be divided into equal cubical cells. The cell size shall be small enough so that

$$\vec{W}[\vec{X}_1, t] = \vec{W}[\vec{X}_2, t] \qquad \text{if } \vec{X}_1 \text{ and } \vec{X}_2 \text{ are in the same cell} \qquad (1.4)$$

where $\vec{W}[\vec{X}, t]$ denotes, as in the above, the sum of the wind velocity and the mean balloon ascent velocity at the point $\vec{X}$ and time t. The merit of the condition (1.4) will be brought out shortly.

Now, employing the cell formalism, the average of F can be expressed somewhat differently. At any time t each cell will contain a given number of balloons (equal to or greater than zero). Hence at any time t we can label the balloons in each cell and employ the labeling (i, j, t) to denote the i th balloon in the j th cell at time t. In particular, we may employ the triple labeling on F: F_{ijt} denotes F evaluated for the coordinates of the balloon which was the i th balloon in cell j at time t. Letting N_{jt} denote the occupation number for the j th cell at time t we have

$$\bar{F} = \frac{1}{N} \sum_{j=1}^{\infty} \sum_{i=1}^{N_{jt}} F_{ijt} \qquad (1.5)$$

$$N = \sum_{j=1}^{\infty} N_{jt} \qquad (1.6)$$

Let us now express E as the union of subensembles E_{jt} of E as follows: There will be an emsemble E_{jt} corresponding to each cell j and composed of those members of E with position coordinates in cell j at time t. Clearly an ensemble E_{jt} depends both upon the specification of j and t. An average over the ensemble E_{jt} is given by

$$[\![F]\!]_{jt} = \frac{1}{N_{jt}} \sum_{i=1}^{N_{jt}} F_{ijt} \tag{1.7}$$

where the subscripts t and j on the brackets indicate that the ensemble average depends both upon j and t.

The expression in (1.7) is applicable to any function, F, of the coordinates of a single balloon at one or more times. As an example, consider a function of the velocity component V for two times t_1 and t_2:

$$F = F[V(t_1), V(t_2)] \tag{1.8}$$

In this case

$$F_{ijt} = F[V_{ijt}(t_1), V_{ijt}(t_2)] \tag{1.9}$$

where the symbol $V_{ijt}(t')$ denotes the velocity at time t' of the balloon which was the ith balloon in cell j at time t. In (1.9) t is not necessarily equal to either t_1 or t_2. The average $[\![F]\!]_{jt}$ of a function F of the form in (1.8) is obtained by substituting (1.9) into the right member of (1.7). The application of (1.7) to more general functions, F, is straightforward.

We are now in a position to consider the definition of the average $[\![F]\!]$ of F. The definition will be given for functions F of the form in (1.8). The generalization to more general functions is straightforward.

The average of F expressed symbolically by $[\![F]\!]$ has two distinct interpretations. In the first interpretation, $[\![F]\!]$ does not refer to or depend upon a particular balloon but is to be regarded as a function of position $\vec{X}$ as well as a function of one or more times. In the second interpretation, the position $\vec{X}$, upon which $[\![F]\!]$ depends is to be understood to be replaced by the position $\vec{X}(t)$ of a given balloon at time t. In other words, to obtain the second interpretation of $[\![F]\!]$ the argument $\vec{X}$ of $[\![F]\!]$ is to be replaced by the dependent variable $\vec{X}(t)$ so that $[\![F]\!]$ refers to a particular balloon rather than a fixed position in space. This ambiguity in the definition of $[\![F]\!]$ should cause no difficulty since wherever the symbol $[\![F]\!]$ is employed in this report, the interpretation to be given to the symbol is evident from the context.

To evaluate $[\![F]\!]$ for functions of the form in (1.8) put

$$[\![F]\!] = [\![F]\!]_{jt} \tag{1.10}$$

where the right member is given by (1.7) and j and t are defined as follows: If the desired interpretation of $[\![F]\!]$ is the position (i.e. $\vec{X}$) dependent interpretation, then j in (1.10) is evaluated for the cell which contains the point $\vec{X}$. If, on the other hand, $[\![F]\!]$ refers to a particular balloon, then j in (1.10) refers to the cell which contains this particular balloon at time t. t in (1.10) would usually be equated to the largest value of time on which F depends. For example, if F has the form in (1.9), $t = t_2$ if $t_2 > t_1$ and $t = t_1$ if $t_1 > t_2$. This choice of t is somewhat arbitrary but suits the applications given in this report. The evaluation of the right member of (1.10) has already been discussed. The generalization of the definition of $[\![F]\!]$ to more general forms of F than that in (1.8) is clear.

We shall now prove the useful relation

$$\overline{[\![F]\!]} = \overline{F} \tag{1.11}$$

Since (1.5) is valid for any function F of the coordinates of a balloon (at one or more times) it is valid if F is replaced by $[\![F]\!]$ (and we interpret $[\![F]\!]$ as referring to a particular balloon). Therefore

$$\overline{[\![F]\!]} = \frac{1}{N}\sum_{j=1}^{\infty}\sum_{i=1}^{N_{jt}}[\![F]\!]_{ijt} \tag{1.12}$$

From (1.10) and the definition of F_{ijt} it is clear that

$$[\![F]\!]_{ijt} = [\![F]\!]_{jt}$$

so (1.12) becomes

$$\overline{[\![F]\!]} = \frac{1}{N}\sum_{j=1}^{\infty} N_{jt}[\![F]\!]_{jt}$$

Substituting for $[\![F]\!]_{jt}$ from (1.7) we obtain

$$\overline{[\![F]\!]} = \frac{1}{N}\sum_{j=1}^{\infty}\sum_{i=1}^{N_{jt}} F_{ijt} \tag{1.13}$$

(1.11) follows immediately from (1.13) and (1.5).

Employing (1.11) and the relation

$$\langle F\rangle = \langle \overline{F}\rangle \tag{1.14}$$

discussed in Appendix 4 we readily obtain

$$\langle [\![F]\!]\rangle = \langle F\rangle \tag{1.15}$$

(1.15) is subject to the validity of (1.14), which is proved in Appendix 4.

A consequence of the property (1.4) of the cells is the relation

$$\vec{W}(t) = [\![\vec{W}(t)]\!] \tag{1.16}$$

where

$$\vec{W}(t) = \vec{W}[\![\vec{X}(t), t]\!] \tag{1.17}$$

The relation (1.16) is a requisite property as discussed above. Another desirable characteristic of the average, $[\![\ ]\!]$, as discussed, is the characteristic that the spurious behavior of $\vec{V}$ should be absent in the average $[\![\vec{V}]\!]$. As observed above this condition can be satisfied if the ensemble of interest (E_{jt}) has a uniform distribution of phase points throughout physically admissable portions of velocity space. It is quite apparent that ensembles E_{jt} which are situated in regions of low balloon density for balloons of the ensemble E will not satisfy this condition. However, if the ensemble E contains a uniform distribution of states of member balloons over all physical states which are consistent with the conditions (1.1) and (1.2) then this condition should be satisfied for ensembles E_{jt} which are in the interior of the ascending cloud of balloons of the ensemble E . The partial satisfaction of this desired condition is entirely adequate since the balloon of interest will most likely be found in the interior of the ascending cloud.

APPENDIX 2

The Effect on Measurement Error of Smoothing Balloon Position Data or Velocity Data

In this report we consider the effects of smoothing of certain time functions by linear smoothing or filtering. We can express the smoothing transformation by an impulse response function $h(\alpha)$. After smoothing, an arbitrary function $F(t)$ becomes

$$F_s(t) = \int_0^t F(t-\alpha)\, h(\alpha)\, d\alpha \tag{2.1}$$

where $h(\alpha)$ is normalized so that

$$\int_0^\infty h(\alpha)\, d\alpha = 1. \tag{2.2}$$

For convenience it is assumed that

$$F(t) = 0\,, \quad t < 0 \tag{2.3}$$

so that (2.1) can be written

$$F_s(t) = \int_0^\infty F(t-\alpha)\, h(\alpha)\, d\alpha. \tag{2.4}$$

Thus the result of smoothing a component V of the balloon's velocity is expressed by

$$V_s(t) = \int_0^\infty V(t-\alpha)\, h(\alpha)\, d\alpha\,. \tag{2.5}$$

Corresponding to $V(t)$ is the displacement

$$X(t) = \int_0^t V(t')\,dt' . \tag{2.6}$$

The smoothed displacement is then given by

$$X_s(t) = \int_0^\infty X(t-\alpha)\,h(\alpha)\,d\alpha. \tag{2.7}$$

From the foregoing, it is readily shown that

$$X_s(t) = \int_0^t V_s(t)\,dt. \tag{2.8}$$

Suppose now that the quantity

$$\frac{X_s(t+\Delta t) - X_s(t)}{\Delta t} \tag{2.9}$$

is employed as an estimate of the component $W(t)$ of the sum of the wind velocity and balloon ascent velocity. The error ε' in this estimate is the difference between the estimate and $W(t)$, that is,

$$\varepsilon' = \frac{X_s(t+\Delta t) - X_s(t)}{\Delta t} - W\left(t+\frac{\Delta t}{2}\right) \tag{2.10}$$

To relate (2.10) to the velocity component V we observe from (2.8) that

$$\frac{X_s(t+\Delta t) - X_s(t)}{\Delta t} = \frac{1}{\Delta t}\int_t^{t+\Delta t} V_s(t)\,dt \tag{2.11}$$

Substituting into (2.10) we have

$$\varepsilon' = \frac{1}{\Delta t}\int_t^{t+\Delta t} V_s(t)\,dt - W\left(t+\frac{\Delta t}{2}\right) . \tag{2.12}$$

To analyze the error ε' we shall re-express it as the sum of an erratic or random error and a consistent error. This re-expression will be based upon the division of V into erratic and nonerratic parts as discussed in Appendix 1. On the basis of that discussion, the quantity

$$v = V - [\![V]\!] \tag{2.13}$$

is the deviation of the velocity component V from the nomial wind-response velocity $[\![V]\!]$. From (2.13)

$$v_s = V_s - [\![V]\!]_s$$

or

$$V_s = v_s + [\![V]\!]_s \tag{2.14}$$

where the definition of $[\![V]\!]_s$ is obtained by setting $F(t) = [\![V(t)]\!]$ in (2.4.). Substituting (2.14) into (2.12) we have

$$\varepsilon' = \frac{1}{\Delta t}\int_t^{t+\Delta t} v_s(\bar{t})\,d\bar{t} + \left[\frac{1}{\Delta t}\int_t^{t+\Delta t} [\![V]\!]_s\,d\bar{t} - W\left(t+\frac{\Delta t}{2}\right)\right] \tag{2.15}$$

The first member on the right in (2.15) may be regarded as the erratic error and the second term on the right as the non-erratic error contribution. There is, of course, some degree of arbitrariness in the division of ε' into erratic and non-erratic portions. An alternate division can be obtained by replacing $[\![V]\!]_s$ by $[\![V_s]\!]$ in (2.15). The merit of the particular division in (2.15), as will become apparent, is that it leads to a direct relationship between the mean-square random error and the power spectrum of the random velocity defined in (2.13).

Putting $\bar{t} = t + \alpha$, (2.15) becomes

$$\varepsilon' = \frac{1}{\Delta t}\int_0^{\Delta t} v_s(t+\alpha)\, d\alpha + \left[\frac{1}{\Delta t}\int_0^{\Delta t} [\![V(t+\alpha)]\!]_s\, d\alpha - W\left(t+\frac{\Delta t}{2}\right)\right] \tag{2.16}$$

Squaring (2.16) and averaging over time we have

$$\left\langle (\varepsilon')^2 \right\rangle = \frac{1}{(\Delta t)^2}\int_0^{\Delta t}\int_0^{\Delta t} \left\langle v_s(t+\alpha)\, v_s(t+\beta)\right\rangle d\alpha\, d\beta \tag{2.17}$$

$$+ \left\langle \left[\frac{1}{\Delta t}\int_0^{\Delta t} [\![V(t+\alpha)]\!]_s\, d\alpha - W\left(t+\frac{\Delta t}{2}\right)\right]^2 \right\rangle$$

$$+ \frac{2}{(\Delta t)^2}\int_0^{\Delta t} \left\langle v_s(t+\alpha)\, [\![V(t+\beta)]\!]_s \right\rangle d\alpha\, d\beta$$

$$- \frac{2}{\Delta t}\int_0^{\Delta t} \left\langle v_s(t+\alpha)\, W\left(t+\frac{\Delta t}{2}\right)\right\rangle d\alpha$$

In (2.17) the bent brackets denote an average over all of time, that is,

$$\langle F \rangle = \lim_{T\to\infty} \frac{1}{T}\int_0^T F(t)\, dt \tag{2.18}$$

for any function $F(t)$. The first term on the right in (2.17) is the mean-square erratic error, and the second term on the right is the mean-square non-erratic (or wind-response velocity) error. The third and fourth terms on the right in (2.17) are the cross-product terms.

The cross-product terms in (2.17) will vanish provided

$$\langle v(t+\alpha)[\![V(t)]\!]\rangle = 0 \qquad \text{all } \alpha \tag{2.19}$$

$$\langle v(t+\alpha)\, W(t)\rangle = 0 \qquad \text{all } \alpha \tag{2.20}$$

We shall disgress briefly to consider the conditions under which (2.19) and (2.20) are satisfied.

Inspections of Project Baldy data reveal oscillatory behavior in V with relatively short periods, (e.g. $\sim$ 5 seconds for the Jimsphere). This situation suggests that

$$\frac{1}{\delta t}\int_t^{t+\delta t} v(\bar{t})\, d\bar{t}$$

should vanish for relatively short averaging times δt (δt may vary with t). If $[\![V(t)]\!]$ does not vary appreciably during the interval δt then

$$\frac{1}{\delta t}\int_t^{t+\delta t} v(\bar{t}+\alpha)[\![V(\bar{t})]\!]\, d\bar{t} \tag{2.21}$$

will vanish for a short averaging time δt. In this case (2.19) is satisfied. It seems reasonable that the rates of change of $[\![V(t)]\!]$ are of the order of (or less than) the rates of change of $W(t)$. Therefore, if $W(t)$ is slowly varying compared to $v(t)$, (2.19) and (2.20) should be satisfied.

(2.19) will also be satisfied even though $W(t)$ is not slowly varying compared to $v(t)$ if the distributions of the relative phases of corresponding Fourier components of v and $[\![V]\!]$ are uniform, and the complex exponentials of the relative phases are uncorrelated with the Fourier moduli. When the relative phases have these properties they are popularly termed "random phases." Corresponding conditions on $W(t)$ lead to (2.20).

When the cross terms in (2.17) vanish, we have

(2.22)

$$\left\langle (\mathcal{E}')^2 \right\rangle = \left\langle (\mathcal{E}'_r)^2 \right\rangle + \left\langle \left[\frac{1}{\Delta t} \int_0^{\Delta t} [\![V(t+\alpha)]\!]_s \, d\alpha - W\left(t + \frac{\Delta t}{2}\right) \right]^2 \right\rangle$$

where

$$\left\langle (\mathcal{E}'_r)^2 \right\rangle = \frac{1}{(\Delta t)^2} \int_0^{\Delta t} \int_0^{\Delta t} \left\langle v_s(t+\alpha)\, v_s(t+\beta) \right\rangle d\alpha \, d\beta \qquad (2.23)$$

is the ms (mean-square) erratic error.

To simplify (2.23) let us introduce the erratic-velocity autocovariance function

$$\psi(\tau) = \left\langle v(t)\, v(t+\tau) \right\rangle \qquad (2.24)$$

and the autocovariance of the smoothed erratic velocities

$$\psi^s(\tau) = \langle v_s(t)\, v_s(t+\tau)\rangle \tag{2.25}$$

Before proceeding with (2.23) we shall express ψ^s in terms of ψ and $h(\alpha)$. Utilizing

$$v_s(t) = \int_0^\infty v(t-\alpha)\, h(\alpha)\, d\alpha \tag{2.26}$$

and assuming a time average $\langle\ \rangle$ commutes with integrations over α and β we readily obtain

$$\langle v_s(t)\, v_s(t+\tau)\rangle = \int_0^\infty\int_0^\infty \langle v(t-\alpha)\, v(t+\tau-\beta)\rangle h(\alpha)h(\beta)\, d\alpha\, d\beta \tag{2.27}$$

whence from (2.24) and (2.25)

$$\psi^s(\tau) = \int_0^\infty\int_0^\infty \psi(\tau+\alpha-\beta)h(\alpha)h(\beta)\, d\beta\, d\alpha \tag{2.28}$$

Putting $\beta=\alpha-\gamma$, (2.28) becomes

$$\psi^s(\tau) = \int_0^\infty\int_{-\infty}^{\alpha} \psi(\tau+\gamma)h(\alpha)h(\alpha-\gamma)\, d\gamma\, d\alpha \tag{2.29}$$

It is convenient to introduce the causality condition

$$h(\beta) = 0 \qquad \beta<0 \tag{2.30}$$

Then $h(\alpha-\gamma)=0$ if $\alpha-\gamma<0$ or $\gamma>\alpha$. Accordingly, the integrand in (2.29) vanishes for $\gamma>\alpha$ so that we may replace the upper limit α by ∞ :

$$\psi^s(\tau) = \int_0^\infty\int_{-\infty}^{\infty} \psi(\tau+\gamma)h(\alpha)h(\alpha-\gamma)\, d\gamma\, d\alpha$$

Interchanging the order of integration we obtain

$$\psi^s(\tau) = \int_{-\infty}^{\infty} \psi(\tau+\gamma)\, G(\gamma)\, d\gamma \tag{2.31}$$

where

$$G(\gamma) = \int_{-\infty}^{\infty} h(\alpha)\, h(\alpha-\gamma)\, d\alpha \tag{2.32}$$

Utilizing (2.30) it is readily shown that

$$G(\gamma) = G(-\gamma) \tag{2.33}$$

Employing (2.33) and the symmetry $\psi(\tau)=\psi(-\tau)$ it can be shown that

$$\psi^s(\tau) = \psi^s(-\tau) \tag{2.34}$$

Going back to (2.23) and substituting from (2.25) we have for the ms erratic error

$$\langle (\varepsilon_r')^2 \rangle = \frac{1}{(\Delta t)^2} \int_0^{\Delta t}\int_0^{\Delta t} \psi^s(\beta-\alpha)\, d\beta\, d\alpha \tag{2.35}$$

Passing to the limit as $\Delta t \to 0$ and observing (2.23) we conclude

$$\langle v_s^2 \rangle = \psi^s(0) \tag{2.36}$$

Putting $\beta = \alpha+\gamma$, (2.35) becomes

$$\langle (\varepsilon_r')^2 \rangle = \frac{1}{(\Delta t)^2} \int_0^{\Delta t}\int_{-\alpha}^{\Delta t-\alpha} \psi^s(\gamma)\, d\gamma\, d\alpha \tag{2.37}$$

Integrating by parts and employing (2.34) we readily obtain

$$\langle (\mathcal{E}_r')^2 \rangle = \frac{2}{(\Delta t)^2} \int_0^{\Delta t} [\Delta t - \alpha] \psi^s(\alpha) \, d\alpha \tag{2.38}$$

which cannot be simplified any further.

We shall proceed to express $\langle (\mathcal{E}_r')^2 \rangle$ in terms of the power spectrum of v and the power transfer functions representing the processing of the data The expression for $\langle (\mathcal{E}_r')^2 \rangle$ in terms of the spectrum will appear somewhat more meaningful than (2.38) and will be more readily applicable to the data.

The relationship between the autocovariance function $\psi(\tau)$ of v and the power spectrum $S_r(f)$ of v is given by

$$\psi(\tau) = \int_0^\infty S_r(f) \cos 2\pi f t \, df \tag{2.39}$$

or the inverse relation

$$S_r(f) = 4 \int_0^\infty \psi(\tau) \cos 2\pi f \tau \, d\tau \tag{2.40}$$

To determine the relationship between $S_r(f)$ and the power spectrum $S_r^s(f)$ of v_s we put, from (2.39)

$$\psi(\tau + \gamma) = \int_0^\infty S_r(f) \cos 2\pi f (\tau + \gamma) \, df \tag{2.41}$$

Multiplying (2.41) by $G(\gamma)$ and integrating with respect to γ from $-\infty$ to ∞ yields the desired relationship (see 2.31). Observing the evenness of $G(\gamma)$ and the oddness of $\sin 2\pi f \gamma$ we readily obtain

$$\psi^s(\tau) = \int_0^\infty S_r^s(f) \cos 2\pi f \tau \, df \tag{2.42}$$

where

$$S_r^s(f) = S_r(f)\,T(f) \tag{2.43}$$

and

$$T(f) = \int_{-\infty}^{\infty} G(\tau)\cos 2\pi f \tau \, d\tau \tag{2.44}$$

is the power transfer function representing the effect of the smoothing on the power spectrum $S_r(f)$.

Substituting (2.42) into (2.38) and reversing the order of integration we obtain

$$\langle (\mathcal{E}_r')^2 \rangle = \int_0^{\infty} S_r^s(f)\,Q(f)\,df \tag{2.45}$$

where

$$Q(f) = \frac{2}{(\Delta t)^2} \int_0^{\Delta t} [\Delta t - \alpha] \cos 2\pi f \alpha \, d\alpha ,$$

that is,

$$Q(f) = \left(\frac{\sin \pi f \Delta t}{\pi f \Delta t} \right) \tag{2.46}$$

Utilizing (2.43), (2.45) may be re-expressed

$$\langle (\mathcal{E}_r')^2 \rangle = \int_0^{\infty} S_r(f)\,T(f)\,Q(f)\,df \tag{2.47}$$

From (2.36) and (2.42)

$$\langle v_s^2 \rangle = \int_0^\infty S_r(f)\, T(f)\, df \tag{2.48}$$

from which (for $T(f) = 1$, that is, no smoothing)

$$\langle v^2 \rangle = \int_0^\infty S_r(f)\, df \tag{2.49}$$

$Q(f)$ in (2.46) is identical to the power transfer function corresponding to a local time averaging (running-mean smoothing) with interval Δt . To prove this, consider

$$\begin{aligned} h(\alpha) &= 1/\delta t \qquad 0 \le \alpha < \delta t \\ &= 0 \qquad \text{otherwise} \end{aligned} \tag{2.50}$$

Substituting (2.50) into (2.26) we obtain

$$v_s(t) = \frac{1}{\delta t} \int_t^{t+\delta t} v(\bar{t})\, d\bar{t} \qquad \text{(for running-mean smoothing)} \tag{2.51}$$

So (2.50) represents running-mean smoothing with averaging interval δt. Substituting (2.50) into (2.32) we obtain

$$\left.\begin{aligned} G(\tau) &= \frac{\delta t - |\tau|}{(\delta t)^2} \qquad |\tau| < \delta t \\ &= 0 \qquad \text{otherwise} \end{aligned}\right\} \text{(for running-mean smoothing)} \tag{2.52}$$

Substituting (2.52) into (2.44) we obtain the power transfer function for running-mean smoothing:

$$T(f) = \left(\frac{\sin \pi \delta t}{\pi f \delta t}\right)^2 \qquad \text{(for running-mean smoothing)} \tag{2.53}$$

Clearly (2.53) is identical to (2.46) when $\delta t = \Delta t$, which suggests that the operation $\frac{X(t+\Delta t) - X(t)}{\Delta t}$ is equivalent to a running-mean smoothing of $V(t)$. The exact equivalence of the two operations is evident from a comparison of (2.51) and (2.11). Thus, the estimate for $W(t)$ in (2.9) is equivalent to the estimate obtained by smoothing $V(t)$ twice, the first smoothing having an impulse-response function $h(\alpha)$ and the second smoothing having an impulse-response function as given by (2.50) with $\delta t = \Delta t$.

In addition to the running-mean smoothing discussed above one commonly encounters the exponential impulse-response smoothing arising from RC low-pass filtering. The impulse response is given by

$$h(\alpha) = \frac{1}{T} e^{-\alpha/T} \qquad \text{(for RC filter)} \tag{2.54}$$

where $T = RC$ is the time constant. It follows that

$$G(\gamma) = \frac{1}{2T} e^{-|\gamma|/T} \qquad \text{(for RC filter)} \tag{2.55}$$

and

$$T(f) = \frac{1}{1 + 4\pi^2 T^2 f^2} \,. \tag{2.56}$$

APPENDIX 3

Computational Details

During the course of project effort long portions of raw velocity records were digitized. These data or subsets thereof were subsequently used for power spectrum and total variance calculations. Initially in the program, the records were digitized at a sampling interval of 0.4 sec. This interval establishes a folding frequency of $(2 \times 0.4)^{-1} = 1.25$ cps. Since the computed spectra showed no significant content at frequencies greater than about 0.5 cps, the sampling period was extended to 0.8 sec (giving a folding frequency of 0.625 cps) for all data taken after Sept. 29. The number of lags used in power spectrum calculations was either 50 or 31, which, in connection with the sampling periods used, gave spectral estimates at frequency intervals varying between .0125 and .025 cps. After October 1, all spectra were computed with 31 lags, yielding estimates at an interval of .02 cps.

The accuracy (or statistical confidence) of a given spectral estimate depends upon the length of record and the total number of lags used. According to Blackman and Tukey (1958), a spectral estimate can be thought of as a chi-square variate with the number of degrees of freedom k given approximately by

$$k = 2T_n / T_m \qquad (3.1)$$

where T_n is the length of record used in the analysis and T_m is the maximum lag. For a given case, the greater k, the less is the statistical uncertainty associated with the estimate. For all the data analyzed in this program, k ranges approximately between 15 and 50 but rarely is less than 20. Taking 30 as a fairly typical value for the data, we find that a random variable with this number of degrees of freedom will lie within the limits from 75% to 145% of its estimated value with 80% confidence. These bounds are useful in the interpretations of computed power spectra.

One spectral estimate is influenced by its neighbors because the numerical filter used in the program does not have an infinitesimally narrow width. The shape of the filter is plotted in Fig. A1. The influence of an estimate on the adjacent point is seen to be down by a factor of about 10; on an estimate two points away it is down by about 180. For distant points, the effect levels out and has an amplitude about 1/500 of the maximum. Although this effect is small, it can be significant in the case of spectra from severely nonstationary records. For such spectra the strong component at zero is felt for all frequencies and tends to raise the noise level at the high frequency end of the spectra. This effect becomes apparent when a power spectrum $S_V^s(f)$ of measured velocity fluctuations ΔV_s is converted to the spectrum $S_r(f)$ corresponding to unsmoothed velocity fluctuations.

Owing to some noise in the output of the frequency tracker, which is the instrument that converts Doppler frequency to a voltage, a small degree of R-C filtering is required. Up until October 26, the time constant of this circuit was set at 0.94 sec, a value greater than actually required to eliminate noise and which introduced unnecessary smoothing in the velocity data. The smoothing was corrected for by multiplying the spectrum by the inverse of the transfer function of the filter. From the results in Appendix 2, the unsmoothed spectrum is given by

$$S_V(f) = \frac{S_V^s(f)}{T(f)} = \left[1 + (2\pi f T)^2\right] S_V^s(f), \qquad (3.2)$$

where τ is the time constant of the circuit and $S_v^s(f)$ is the spectrum computed from $\Delta V_s(t)$. The factor $\left[1+(2\pi f t)^2\right]$ is plotted in Fig. A2. As seen in the figure, this factor becomes quite large at high frequencies for the 0.94 sec time constant. When applied to $S_v^s(f)$, this correction magnifies the high frequency spectral components, which might be predominantly noise with amplitudes down by a factor of about 500 from the maximum amplitude in the spectrum. From October 26 onward, the time constant of the filter circuit was set at 0.5 sec. The spectra were still corrected by the inverse of the filter, but in this case the corrections were quite small. The only complication in the correction procedure occurred for the spectra up to September 30. For these, lags of 0.4 sec had been used and as a result the spectra extended all the way out to 1.25 cps, well beyond the highest frequency actually present in the velocity fluctuations. The high frequency portion of the spectra decayed to very low values but not absolutely to zero because of round-off errors and the effect of the numerical filter. Upon multiplication by the inverse filter function, these high frequency components were greatly magnified and assumed significant proportions. An example of this effect is shown in Fig. A3. A more accurate spectral representation is obtained by deleting the magnified tail from all further consideration. The spectra were considered valid out to 0.8 cps, a frequency beyond which for all the corrected spectra the noise effect is important. Unsmoothed mean-square velocities (variances) were computed by integrating the corrected spectra out to 0.8 cps. For the data up to September 30, the unsmoothed variances were about 60% greater than the variances of the (smoothed) raw data. The omitted portion of the spectra beyond 0.8 cps would generally add an additional 15% onto the value of the corrected variance.

The correction for the effect of smoothing of data obtained after October 26, when the time constant was decreased, is relatively minor. The effect of the correction on variances usually amounted to an average increase of less than 20%, and there was no problem connected with amplification of high frequency noise, partly because these later spectra only extended to a frequency of 0.625 cps, as established from the 0.8 sec sampling rate.

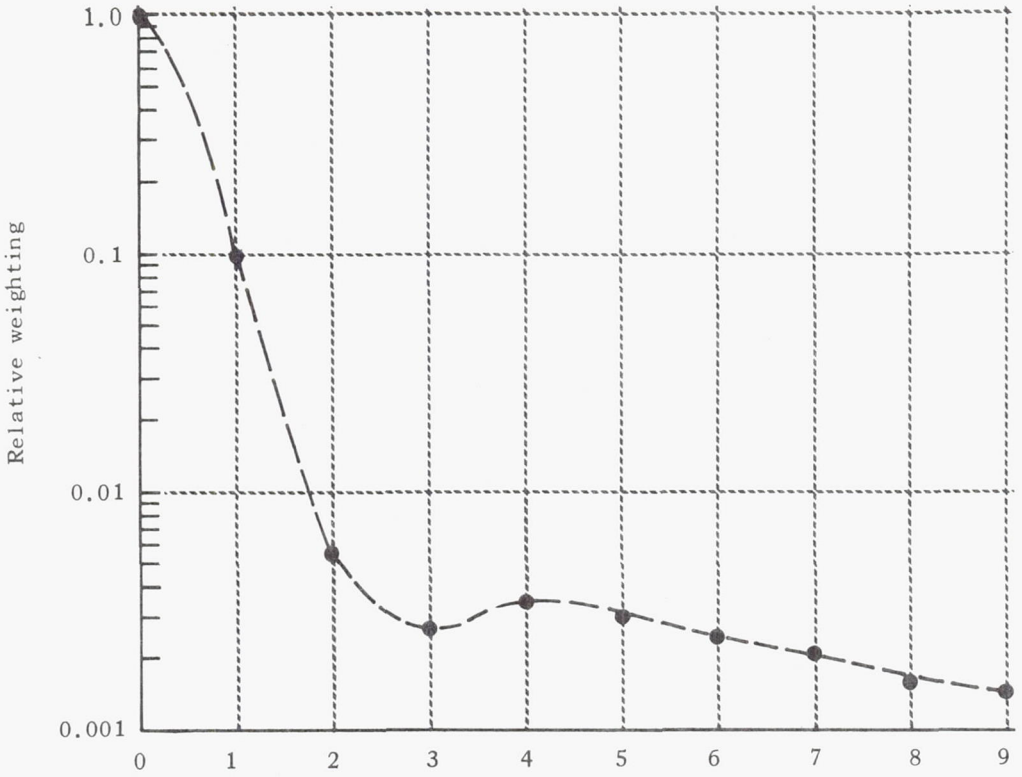

Fig. A1. Character of numerical filter used in spectrum calculations

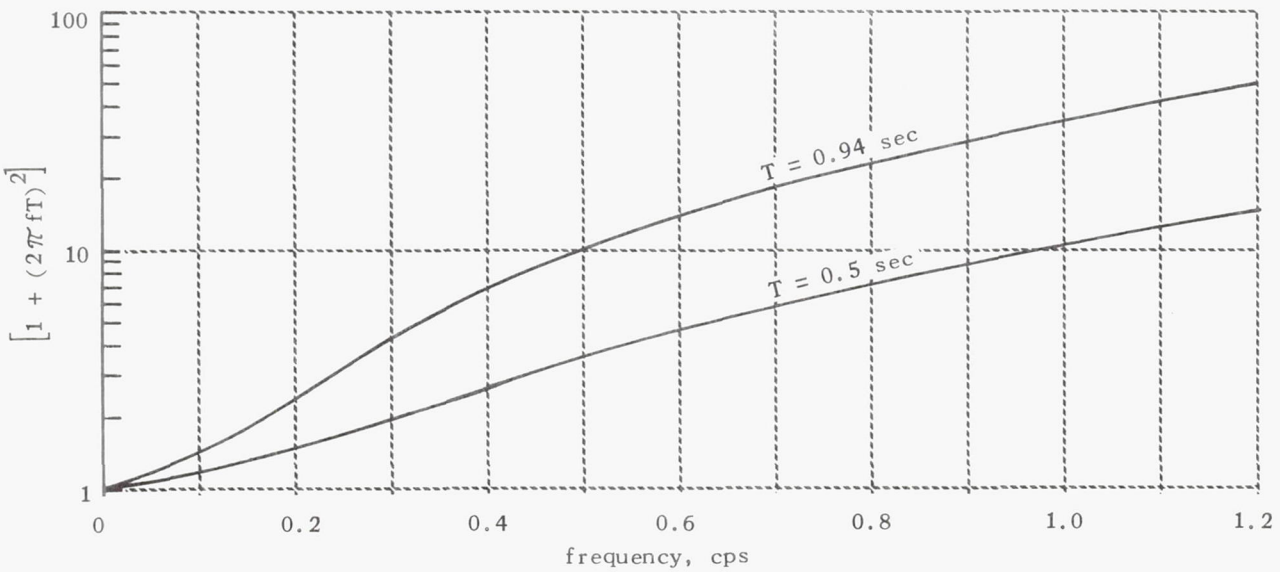

Fig. A2. Reciprocal of weighting factor T(f) for RC filtering

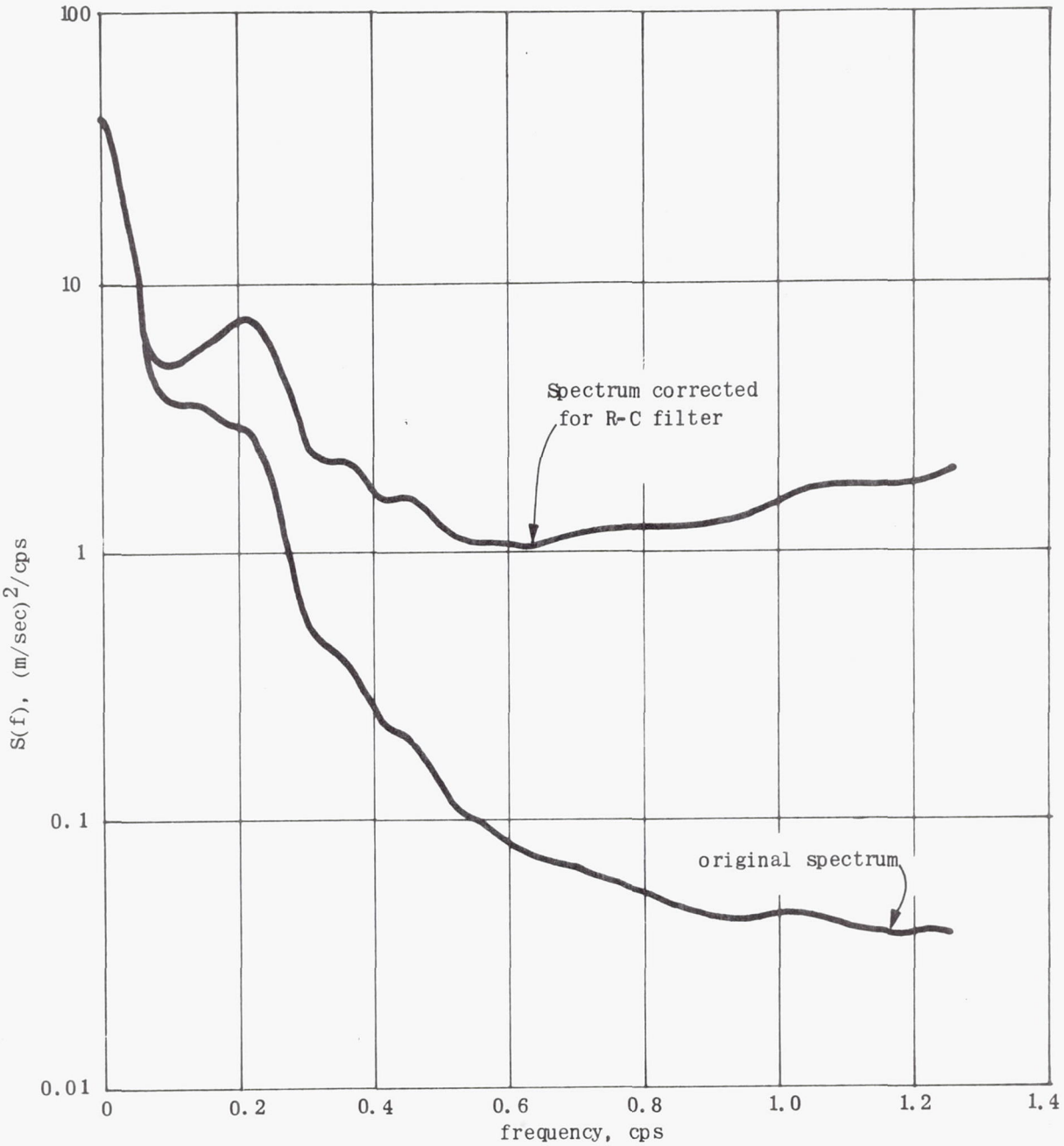

Fig. A3 Example spectrum corrected for the effect of smoothing

APPENDIX 4

The Proof of a Fundamental Relation*

A logical generalization of the equality of the ensemble average and infinite time average which is applicable to nonstationary time functions is the relation

$$\langle f \rangle = \langle \bar{f} \rangle \tag{4.1}$$

where f denotes a random function of the time, the overbar denotes an ensemble average, and the bent brackets $\langle\ \rangle$ denote an infinite time average. Sufficient conditions will be given for the validity of the realtion (4.1).

The relation (4.1) will be correct (except possibly on a set of measure zero) if

$$\overline{\left(\langle f \rangle - \langle \bar{f} \rangle\right)^2} = 0 \tag{4.2}$$

We have, putting

$$\delta f = f - \bar{f}, \tag{4.3}$$

$$\overline{\left(\langle f \rangle - \langle \bar{f} \rangle\right)^2} = \overline{\langle \delta f \rangle^2}$$

Now

$$\overline{\langle \delta f \rangle^2} = \lim_{T, T_1 \to \infty} \frac{1}{4TT_1} \int_{-T}^{T} \int_{-T_1}^{T_1} \overline{\delta f(t) \delta f(t_1)}\, dt_1\, dt$$

---

*The proof presented here was originally prepared under effort for Project Spectrum, a CAL project under Contract NAS 1-3485 (NASA Langley).

Changing variables from t_1 to α with $t_1 = t+\alpha$ we have

$$\overline{\langle \delta f \rangle^2} = \lim_{T, T_1 \to \infty} \frac{1}{4TT_1} \int_{-T}^{T} \int_{-t_1-t}^{T_1-t} \overline{\delta f(t)\delta f(t+\alpha)}\, d\alpha\, dt$$

$$\overline{\langle \delta f \rangle^2} = \lim_{T, T_1 \to \infty} \frac{1}{4TT_1} \int_{-T}^{T} \int_{-T_1}^{T_1} \overline{\delta f(t)\delta f(t+\alpha)}\, d\alpha\, dt \qquad (4.4)$$

$$+ \lim_{T, T_1 \to \infty} \frac{1}{4TT_1} \int_{-T}^{T} \left[\int_{-T_1-t}^{-T_1} \overline{\delta f(t)\delta f(t+\alpha)}\, d\alpha - \int_{T_1-t}^{T_1} \delta f(t)\delta f(t+\alpha)\, d\alpha \right] dt$$

Now

$$\int_{-T_1-t}^{-T_1} \overline{\delta f(t)\delta f(t+\alpha)}\, d\alpha = \int_{-t}^{0} \overline{\delta f(t)\delta f(t-T_1+\beta)}\, d\beta$$

Substituting into the second term on the right in (4.4) we obtain for this term:

$$\lim_{T \to \infty} \lim_{T_1 \to \infty} \frac{1}{4TT_1} \int_{-T}^{T} \int_{-t}^{0} \overline{\delta f(t)\delta f(t-T_1+\beta)}\, d\beta\, dt \qquad (4.5)$$

We now assume

$$\lim_{T_1 \to \infty} \frac{\overline{\delta f(t)\, \delta f(t - T_1 + \beta)}}{T_1} = 0 \qquad \text{uniformly in } |\beta| < |t| < \infty \tag{4.6}$$

With this condition the limit with respect to T_1 in (4.5) may be taken under the integral sign, so (4.5) vanishes. By the same argument the third integral on the right in (4.4) vanishes. The relation (4.6) will be satisfied if the correlation function

$$\overline{\delta f(t)\, \delta f(t+\gamma)}$$

is bounded uniformly for all t and γ that is, if

$$\left| \delta f(t)\, \delta f(t+\gamma) \right| < B \tag{4.7}$$

for some positive constant B independent of t and γ. Consider the first integral on the right in (4.4). We assume

$$\lim_{T \to \infty} \frac{1}{2T} \int_{-T}^{T} \overline{\delta f(t)\, \delta f(t+\alpha)}\, dt = \left\langle \overline{\delta f(t)\, \delta f(t+\alpha)} \right\rangle \tag{4.8}$$

Then in the first integral on the right in (4.4) we switch the order of integration and may take the limit with respect to T under the integral sign, obtaining

$$\begin{aligned} \overline{\langle \delta f \rangle^2} &= \lim_{T_1 \to \infty} \frac{1}{2T_1} \int_{-T_1}^{T_1} \overline{\left\langle \delta f(t)\, \delta f(t+\alpha) \right\rangle}\, d\alpha \\ &= \lim_{T_1 \to \infty} \frac{1}{T_1} \int_{0}^{T_1} \overline{\left\langle \delta f(t)\, \delta f(t+\alpha) \right\rangle}\, d\alpha \end{aligned} \tag{4.9}$$

We now assume

$$\lim_{T_1 \to \infty} \frac{1}{T_1} \int_0^{T_1} \overline{\langle \delta f(t)\, \delta f(t+\alpha) \rangle}\, d\alpha = 0 \qquad (4.10)$$

then from (4.9) $\overline{\langle \delta f \rangle^2} = 0$. It is thus apparent that (4.7), (4.8) and (4.10) are sufficient conditions for the equality (4.1). Clearly, none of these conditions are particularly stringent for functions encountered in physical situations so there is no reason for believing that they will not be satisfied by the functions of interest in this report.